UNIVERSITÉ DE GENÈVE

Archive ouverte UNIGE
https://archive-ouverte.unige.ch

Thèse 2019

Open Access

This version of the publication is provided by the author(s) and made available in accordance with the copyright holder(s).

Histological characterization and the role of biomechanical forces in intracranial aneurysm disease

Diagbouga, Mannekomba Roxane

How to cite

DIAGBOUGA, Mannekomba Roxane. Histological characterization and the role of biomechanical forces in intracranial aneurysm disease. Doctoral Thesis, 2019. doi: 10.13097/archive-ouverte/unige:129927

This publication URL: https://archive-ouverte.unige.ch/unige:129927
Publication DOI: 10.13097/archive-ouverte/unige:129927

© This document is protected by copyright. Please refer to copyright holder(s) for terms of use.

UNIVERSITÉ DE GENÈVE

Section de Médecine Fondamentale
Département de Pathologie et Immunologie

FACULTÉ DE MÉDECINE
Professeur Brenda Kwak

HISTOLOGICAL CHARACTERIZATION AND THE ROLE OF BIOMECHANICAL FORCES IN INTRACRANIAL ANEURYSM DISEASE

THÈSE

présentée aux Facultés de Médecine et des Sciences de l'Université de Genève
pour obtenir le grade de Docteur ès Sciences en Sciences de la vie,
mention Sciences biomédicales

par

Mannekomba Roxane DIAGBOUGA

de

Ouagadougou, Burkina Faso

Thèse Nº 34

GENÈVE

Repromail

2019

LIFE SCIENCES PhD SCHOOL GENEVA

DOCTORAT ÈS SCIENCES EN SCIENCES DE LA VIE DES
FACULTÉS DE MÉDECINE ET DES SCIENCES
MENTION SCIENCES BIOMÉDICALES

Thèse de Madame Mannekomba Roxane DIAGBOUGA

intitulée:

« Histological characterization and the role of biomechanical forces in intracranial aneurysm disease »

Les Facultés de médecine et des sciences, sur le préavis de Madame Brenda KWAK, professeure ordinaire et directrice de thèse (Département de Pathologie et Immunologie), Monsieur Eric FERAILLE, professeur associé (Département de Physiologie Cellulaire et Métabolisme), Monsieur Philippe BULENGA, professeur (Département des Neurosciences Cliniques, HUG), Monsieur Paul EVANS, professeur (Département des Maladies Infectieuses, Immunitaires et Cardiovasculaires, Université de Sheffield, Angleterre) autorisent l'impression de la présente thèse, sans exprimer d'opinion sur les propositions qui y sont énoncées.

Genève, le 6 Décembre 2019

Thèse - 34 -

Le Doyen
Faculté de médecine

Le Doyen
Faculté des sciences

N.B. - La thèse doit porter la déclaration précédente et remplir les conditions énumérées dans les "Informations relatives aux thèses de doctorat à l'Université de Genève".

« Goutte après goutte, l’eau finit par creuser le marbre »

Proverbe grec; Les maximes de la Grèce antique (1855)

Acknowledgments

I would like to acknowledge with deep gratitude the people who made this work possible.

First, I thank my thesis director and mentor, Prof. Brenda Kwak for hosting me into her lab and for her excellent supervision. I am grateful for the patient guidance, encouragement and advice she provided throughout my studies.

Thanks to Prof. Philippe Bijlenga, for initiating the nice project my thesis has been part of. I thank him also for being always available, for the support and invaluable advices.

I give my special thanks to Sandrine Morel, who has always been there to help and guide me in my work, I have been extremely lucky to have her. I have learnt a lot from her and I thank her also for all the ideas and critical discussions.

I would like to thank the present and former members of the lab: Filippo Molica, Olga Rusiecka, Aurélie Hautefort, Avigail Ehrlich, Bernard Foglia, Graziano Pelli, Anne Cayron, Christophe Montessuit, Ettore Vanni, Esther Sutter, Jean-Francois Denis, Merlijn Meens, Viviane Rochemont, for the good time in the lab, all the technical help and scientific input. Thanks for the pleasant working atmosphere.

To my committee members; Prof. Paul Evans, Prof. Eric Feraille, Prof. Philippe Bijlenga and Prof. Brenda Kwak, thank you for being my jury committee.

I would like to thank Dr. Marie-Luce Piallat and Prof. Marc Chanson and their lab members, for keeping their doors opened, for their scientific input and advices. I thank specially my friends Aderonke Sofoluwe and Antonija Sakic for sharing the moments of stress, doubt but also joy. Thanks for the countless laughs, and invigorating coffee breaks.

I would like to thank my dear parents Serge and Benoîte who are continuously fighting for the happiness and success of their children. They have always encouraged me to pursue my studies

and to go as far as possible. If I am here today and accomplished this PhD, it is at the price of many sacrifices, and there is no word to describe how grateful I am. I Thanks them for the constant support, for always believing in me. I hope that I make them proud, and I want to tell them that the best is yet to come. “Aw ni tié, Baarka”.

Thanks to my brother Brice and to my sister Corinne, for all the love, words of encouragement and support. If am here today, it is also thanks to the. They are always there for me and are the best gifts from our parents.

No word of thanks will be enough to express my gratitude to my beloved Christel, for his thoughtfulness, love and care. He lived all the emotions of this PhD journey except being in the lab. I thank him for being the most supportive partner, and for all the efforts and sacrifices, he made to help me to get to this point. I thank him for his patience, compassion and for cheering me up all those times when I doubted.

To our beautiful son, Mensie, I say thank you for the happiness he brings to me every day. He has made me stronger than I could imagine. I thank him for being a cool baby, patient and understanding for all the time I have been in the lab and not at home with him.

To all my friends, especially Gisèle, and to all the people, near and far, who encouraged me, I express my utmost gratitude.

Résumé

La prévalence des anévrismes intracrâniens (AIs) est d'environ 2 à 3% dans la population générale, avec une prédilection pour des patients jeunes, d'un âge moyen d'environ 50 ans. Bien que rare, la rupture des AIs entraîne la mort dans environ 15% des cas, et plus de 30% des survivants présentent un handicap sévère. Les mécanismes sous-jacents à la pathologie des AIs ne sont pas complètement compris. D'une part, il est généralement admis que le remodelage de la paroi vasculaire induit par les forces hémodynamiques précède la croissance ou la rupture des AIs. D'autre part, une forte prévalence des AIs a été mise en évidence chez les patients atteints de la polykystose rénale (PKD), ce qui pourrait s'expliquer par l'absence de fonctionnalité des cils primaires des cellules endothéliales (CEs). De ce fait, il apparait crucial de comprendre l'interaction entre les forces hémodynamiques et les cellules composant la paroi vasculaire ainsi que les effets résultants sur l'organisation de la paroi vasculaire.

Le premier objectif de mon travail de thèse consistait à identifier des marqueurs de rupture des AIs. Pour ce faire, nous avons caractérisé, au moyen d'analyses histologiques, des dômes d'AIs provenant de patients traités par voie chirurgicale. Chez les AIs à risque de rupture, nos observations ont révélé une diminution du taux de cellules musculaires lisses (CML) et de collagène, ainsi qu'une augmentation du taux de macrophages. Nous avons également constaté que la paroi des AIs rompus était généralement plus fine que celle des AIs non-rompus. De plus, nous avons mis en évidence des corrélations entre certains facteurs de risque cliniques favorisant la rupture et les caractéristiques histologiques du dôme des AIs. Ainsi, il est apparu qu'une grande taille des AIs était associée à une teneur plus élevée en collagène total, en collagène de type III et en macrophages. De même, la morphologie irrégulière du dôme des AIs était associée à une teneur plus élevée en collagène de type III. Enfin, la paroi des AIs provenant de patients fumeurs présentait une faible teneur en CMLs comparativement à celui des patients non-fumeurs.

Le second objectif de ma thèse consistait à étudier l'impact d'une faible contrainte de cisaillement sur la fonction des CEs, ainsi que le rôle que pourrait jouer le cil primaire dans la réponse endothéliale. Pour ce faire, des CEs isolées d'un modèle murin PKD défaillant en cil primaire ou isolées de souris contrôles ont été exposées soit à des conditions physiologiques de flux, soit à des conditions de flux observées dans les dômes d'anévrisme. Ces expériences ont été complétées par un séquençage d'ARN. Nous avons pu observer que dans des conditions pathologiques de forces de cisaillement faible, l'absence de cils sur les CEs induit une perturbation de l'expression des gènes 5 fois plus importante que dans les cellules contrôles exprimant les cils primaires. Les gènes exprimés de manière différentielle par les CEs entre conditions pathologiques et physiologiques sont distribués selon leurs fonctions dans des processus contrôlant la prolifération cellulaire, la transition endothélio-mésenchymateuse, la réponse au stress ainsi que la régulation des CMLs et de la pression artérielle. En outre, nous avons pu démontrer que les CEs ne possédant pas de cils présentaient des jonctions intercellulaires perturbées, ceci en accord avec la hausse de perméabilité endothéliale observée. Plus spécifiquement, la protéine de jonction ZO-1 a pu être identifiée comme régulatrice centrale de l'organisation des jonctions intercellulaires avec une expression plus faible dans les CEs des dômes d'AIs isolés de patients PKD.

Le troisième objectif de ma thèse consistait à étudier l'impact de l'étirement circonférentiel cyclique sur le fonctionnement des CEs. Pour ce faire, nous avons exploré le transcriptome des CEs, soumises à des étirements cycliques physiologiques ou pathologiques, par séquençage d'ARN. L'analyse d'enrichissement basée sur l'ensemble de gènes a permis de mettre en évidence l'enrichissement des voies de signalisation liées au stress oxydatif, à l'inflammation, à la régulation de la matrice extracellulaire et à la prolifération cellulaire en condition d'étirement cyclique pathologique. Ces résultats sont cohérents avec l'hypothèse selon laquelle l'étirement cyclique influencerait également le remodelage de la paroi des AIs.

Les observations faites au cours de ma thèse de doctorat offrent de nouvelles perspectives pour l'amélioration de la prédiction du risque de rupture des AIs, ceci à travers l'utilisation des paramètres histologiques identifiés. De même, des recherches futures sur l'importance des gènes perturbés en conditions de flux et d'étirements pathologiques pourraient conduire à l'identification de nouveaux marqueurs de risque de rupture, mais également à l'identification de cibles thérapeutiques potentielles.

Abstract

Intracranial aneurysm (IA) disease affects about 2 to 3% of the general population and generally young patients with a median age of 50 years. Although the rupture of IAs is rare, it leads to death in about 15% of cases, and more than 30% of survivors are left with severe disabilities. The mechanisms underlying IA pathology are not fully understood. It is generally assumed that vascular wall remodeling induced by hemodynamic forces precedes IA growth or rupture. A high prevalence of IA in polycystic kidney disease (PKD) patients has been reported and attributed to endothelial primary cilia dysfunction. It is thus crucial to understand the interaction between hemodynamic forces and the cells composing the vascular wall as well as the resulting effects on vessel wall organization.

In this thesis, I first seek to identify markers of IA rupture. We characterized, by the means of histological analysis, the vascular walls of human IA domes that were collected after surgery. We found that IA walls prone to rupture have a lower content in smooth muscle cells (SMCs) and collagen, and a higher content in macrophages. We also observed that ruptured IAs had generally thinner walls than non-ruptured ones. Interestingly, we noticed some correlations between clinical risk factors and IA wall histological features. First, large size IAs had higher total collagen, type III collagen and macrophage contents. Secondly, high content of type III collagen was associated with increased IA dome roughness. Finally, SMC content was lower in unruptured IA walls of smokers.

Then, I investigated how aneurysmal low wall shear stress (WSS) could affect endothelial cell (EC) function and how primary cilia would impact on the EC response. We performed RNA sequencing on ECs from PKD mice or control (wild-type) mice that were exposed to either a physiological or aneurysmal low WSS. We found that PKD ECs exhibit much greater disturbance (5-fold) in the number of WSS responsive genes in response to aneurysmal low WSS. The differentially expressed genes in aneurysmal low compared to

physiological high WSS generated an enrichment in gene ontology terms that are known to be linked with EC function such as cell cycle proliferation, endothelial to mesenchymal transition, response to stress, SMC and blood pressure regulation. In addition, we showed that PKD ECs displayed perturbed intercellular junctions, correlating with higher endothelial permeability. We identified ZO-1 as central regulator in junctional organization and a low expression of ZO-1 was observed in ECs of IA domes from PKD patients.

Lastly, I investigated how cyclic circumferential stretch (CCS) would affect ECs function. We explored transcriptomic profiles of ECs under physiological or aneurysmal (absence of) CCS. The gene set enrichment analysis identified signaling pathways related to oxidative stress, inflammation, extracellular matrix regulation and cell proliferation as being enriched under aneurysmal CCS. This was consistent with the hypothesis that CCS can also influence IA wall remodeling.

The overall findings of this thesis open new avenues on the use of histological features to improve the prediction of IA rupture. In addition, future research on the significance of disturbed genes under aneurysmal flow conditions could lead to the identification of new markers to identify IA under risk of rupture, but also to the identification of potential therapeutic targets.

Table of Contents

List of abbreviations **..... 1**

Chapter 1*: Introduction* **..... 5**

I. Structure and composition of arteries **..... 6**

1. Cellular components **..... 6**
2. Extracellular matrix components **..... 8**

II. Physiology of the vascular endothelium **..... 10**

1. Structural organization of the endothelium **..... 10**
2. Function of the endothelium: barrier, vascular tone, hemostasis and host defense **.. 12**

III. Biomechanical forces and vascular physiology **..... 13**

1. Wall shear stress and cyclic circumferential stretch **..... 13**
2. Mechano-sensors of biomechanical forces **..... 15**
3. Biological response of endothelial cells to wall shear stress and intracellular signalling **18**
4. Biological response of endothelial cells to cyclic circumferential stretch and intracellular signalling **..... 20**

IV. Aneurysm disease **..... 22**

1. Intracranial aneurysm generalities **..... 23**
2. Pathogenesis of intracranial aneurysms **..... 25**
   a. Intracranial aneurysm initiation 25
   b. Intracranial aneurysm growth 26
   c. Intracranial aneurysm rupture 28
3. Intracranial aneurysm risk factors and associated diseases **..... 29**
4. Primary cilia: role in polycystic kidney disease and in intracranial aneurysms **..... 31**
5. Animal models to study intracranial aneurysm **..... 33**
6. Aims and chapter outline of this thesis **..... 37**

Chapter 2*: Correlating Clinical Risk Factors and Histological Features in Ruptured and Unruptured Human Intracranial Aneurysms: The Swiss AneuX Study* **..... 47**

Chapter 3*: Primary cilia control endothelial permeability by regulating expression and location of junction proteins.* **..... 60**

Chapter 4*: Endothelial cells display a unique transcriptional profile due to lack of cyclic stretch as observed in saccular intracranial aneurysms* **.....107**

Chapter 5*: General discussion* **.....141**

Curriculum vitae **.....157**

List of abbreviations

AAA	abdominal aortic aneurysm
ADPKD	autosomal polycystic kidney disease
AJ	adherens junction
Akt	protein kinase B
AMPK	AMP-activated protein kinase
AP-1	activator protein-1
AT1R	angiotensin II receptor 1
ATF2	activating transcription factor 2
ATP	adenosine triphosphate
AVM	arteriovenous malformation
Bcl6	B-cell lymphoma 6 protein
BMP	bone morphogenetic protein
cAMP	cyclic adenosine monophosphate
CCS	cyclic circumferential stretch
CDKN2B	cyclin-dependent kinase inhibitor 2B
CFD	computational fluid dynamics
cGMP	cyclic guanosine monophosphate
COX	Cyclooxygenase
CTA	computed tomographic angiography
Cx	Connexin
CXCL	chemokine (C-X-C motif) ligand
EC	endothelial cell
ECM	extracellular matrix

EDHF	endothelium-derived hyperpolarizing factor
EEL	external elastic lamina
eNOS	endothelial nitric oxide synthase
ERK	extracellular signal-regulated kinase
ET-1	endothelin-1
FAK	focal adhesion kinase
GJ	gap junction
GTPase	nucleotide guanosine triphosphate (GTP) hydrolase
GUK	guanylate kinase
HDAC	histone deacetylase
Hsp	heat shock protein
HWSS	high wall shear stress
IA	intracranial aneurysm
ICAM	intercellular adhesion molecule
IEL	internal elastic lamina
IFN	Interferon
IKK2	nuclear factor kappa-B kinase subunit beta
IL	Interleukin
iNOS	inducible nitric oxide synthase
IP3	inositol trisphosphate
JAK	janus kinase
JNK1	c-Jun N-terminal kinase 1
KLF	Krüppel-like family of transcription factors
LWSS	low wall shear stress
MAGUK	membrane-associated guanylate kinase

MAPK	mitogen-activated protein kinase
MEF	myocyte enhancer factor
MMP	Metalloproteinase
MRA	magnetic resonance angiography
MRI	magnetic resonance imaging
mTOR	mammalian target of rapamycin
NF-κB	nuclear factor kappa-light-chain-enhancer of activated B cells
NLRP3	NACHT, LRR and PYD domains-containing 3
NO	nitric oxide
Nrf2	nuclear factor erythroid 2 related factor-2
OWSS	oscillatory wall shear stress
Pa	Pascal
PARP-1	poly(ADP-ribose) polymerase-1
PC1	polycystin-1
PC2	polycystin-2
PDGF-BB	platelet-derived growth factor beta homodimers
PDZ	discs-large homologous regions (DHR) or GLGF
PECAM-1	platelet endothelial cell adhesion molecule
PGI2	prostaglandin I2
PI3K	phosphoinositide 3-kinases
PPARα	peroxisome proliferator-activated receptor α
R-IA	ruptured intracranial aneurysm
Rho	ras homologous protein family
ROS	reactive oxygen species
SH3	src homology 3

SHP	src homology 2 domain-containing phosphatase
SOX17	transcription regulator gene SRY-box 17
STAT	signal transducers and activators of transcription
SWSS	supra-physiological wall shear stress
TGF	transforming growth factor
TIMP	tissue inhibitor of metalloproteinase
TJ	tight junction
TLR	toll-like receptor
TNF-α	tumour necrosis factor-α
tPA	tissue plasminogen activator
TRPV	transient receptor potential cation channel
uPA	plasminogen activator, urokinase
UR-IA	unruptured intracranial aneurysm
VCAM	vascular cell adhesion molecule
VE-cadherin	vascular endothelial cadherin
VEGFR	vascular endothelial growth factor receptor
VSMC	vascular smooth muscle cell
WSS	wall shear stress
WSSG	wall shear stress gradient
ZO	zonula occludens

Chapter 1: Introduction

Adapted from: Diagbouga, M.R., Morel S., Bijlenga P., Kwak B.R.. Role of hemodynamics in initiation/growth of intracranial aneurysms. Eur J Clin Invest, 2018. ***48****(9): p. e12992.*

I. Structure and composition of arteries

Arteries are components of the circulatory system **(Figure 1)** and are responsible for the transport of blood containing oxygen and nutrients through all the body. The structure of arteries is such that they can withstand the highly pressurized and pulsatile blood flow ejected from the heart. The histological structure of arteries is defined by three main layers: the *tunica intima* is the innermost layer and consist of an endothelium (a monolayer of endothelial cells (ECs)) and a supportive basement membrane; the *tunica media* is the middle layer that contains vascular smooth muscle cells (VSMCs), elastin and collagen fibers; the external *tunica adventitia* is a connective tissue mostly composed of collagen fibers, VSMCs and fibroblasts. The medial layer is separated from the intima by an internal elastic lamina (IEL) and from the adventitia by an external elastic lamina (EEL) and its thickness varies depending on the artery size. Large arteries (diameter >10 mm) that are closest to the heart contain a high percentage of elastic fibers in their media that allows the vessel to stretch in response to a large volume of blood and to ascertain that blood flows to tissues during diastole. This type of arteries, also called conducting arteries, divide into distributing arteries that contain more VSMCs and less elastic fibers in their tunica media compared to elastic arteries. Some muscular arteries like cerebral arteries have a well-developed IEL but lack the EEL **(Figure 2)** [1, 2].

1. Cellular components

Along the vascular tree, EC thickness varies between 0.1-1μm and they cover a surface estimated as more than 1000m^2 in human [3, 4]. ECs are elongated and aligned in the straight part of arteries, while they have a cobblestone-shape in areas of disturbed flow such as bifurcations [5-7]. ECs organize in a single cell layer that lines all blood vessels and regulate exchanges between the bloodstream and the surrounding tissues. Depending on the environmental cues, ECs in small arteries and arterioles regulate vascular tone by secreting

vasoactive molecules that cause VSMCs to contract or to relax, thereby regulating tissue irrigation [8]. ECs are joined together by junctions and thus form a semi-permeable barrier that regulates fluids, macromolecules and leukocytes movement into the arterial wall [9, 10]. In addition, they regulate the local inflammatory response by modulating the expression of adhesion molecules at their surface [11]. In direct contact with blood, the endothelium has a smooth surface, which minimizes friction of the blood and prevents coagulation [12]. More details on endothelium physiology are found in section II.

VSMC is the most abundant cell type in a healthy arterial wall. They organize circularly around the vascular lumen and form multiple layers. They are interconnected through gap junctions, which facilitate the transmission of signaling molecules and action potentials between cells [13]. The principal function of VSMCs is to regulate vessel lumen diameter by vasoconstriction or vasodilatation [1, 8]. This is controlled by autonomic nerves present in the adventitia but also by factors produced locally or present in the blood. In healthy arteries, VSMCs have a contractile phenotype characterized by a spindle shape and a quiescent state and they express differentiation markers such as myosin heavy chain 1 and 2, smoothelin, desmin and calponin [14]. In injured arteries, VSMCs can switch to a synthetic phenotype characterized by an high proliferative and migratory activity and an increased production of extracellular matrix (ECM) components and metalloproteinases (MMPs) [1]. Even though this phenotypic adaptation is important for vascular repair, in a long term the high turnover of VSMCs and ECM affect the structural integrity of the vessel wall and contribute to the development of vascular disease [15].

Communication between ECs and VSMCs is essential for vascular development [16] and also for homeostasis and repair of mature blood vessels [17]. EC-VSMC interactions are mediated through direct contact (gap junctions) [13, 18] or paracrine signaling (vasoactive molecules, extracellular vesicles, micro-RNAs) [17]. ECs and VSMCs are sensitive to chemical and

mechanical stimuli through receptors and sensors present at their surface and the nature of the stimuli can drive pathological changes [19-21].

Other cell types can be found in an arterial vessel wall such as fibroblasts, nerves fibers, resident inflammatory cells and progenitor cells. These cells are often located in the adventitial tissue and they also participate in blood vessels' adaptation to changing conditions. Fibroblasts constitute the primary cell type in the adventitia of arteries where they express ECM components and other regulatory molecules [1]. Under certain conditions, fibroblasts can start expressing markers of VSMCs such as α-smooth muscle actin and myosin and switch to a contractile myofibroblast phenotype. However, the myofibroblasts do not express markers of differentiated VSMCs like desmin and smoothelin [22].

2. Extracellular matrix components

The subendothelial ECM called basement membrane or basal lamina is composed of numerous molecules including laminin isoforms, types IV, V, VI and XVIII collagen, fibronectin, perlecan, nidogens and von Willebrand factor synthesized by ECs [22, 23]. The basement membrane is separated from the endothelium by fibrillin-containing microfibrils and collagen fibers [22, 23]. The Medial ECM is also composed of a fundamental substance comprising diverse proteoglycan, glycosaminoglycan, glycoprotein and fibers. Elastin fibers are abundant in vessels close to the heart and reduced in peripheral in arteries. Type I and III collagens are the major collagen types in the media and provide tensile strength mechanical properties [24]. It has been shown that type III collagen is important for type I collagen fibrillogenesis [25]. While type III collagen is thought to contribute to extensibility of the blood vessel, type I collagen may confer arterial stiffness [24]. ECM composition varies along the vascular tree and is also determining the ECs and VSMCs adaptability to physiological or pathophysiological changes. Cell-ECM contacts through integrins regulate cellular processes such as cell cycle

transition, survival, differentiation and migration [22, 23]. Thus, ECM is a key contributor in major vascular pathological processes.

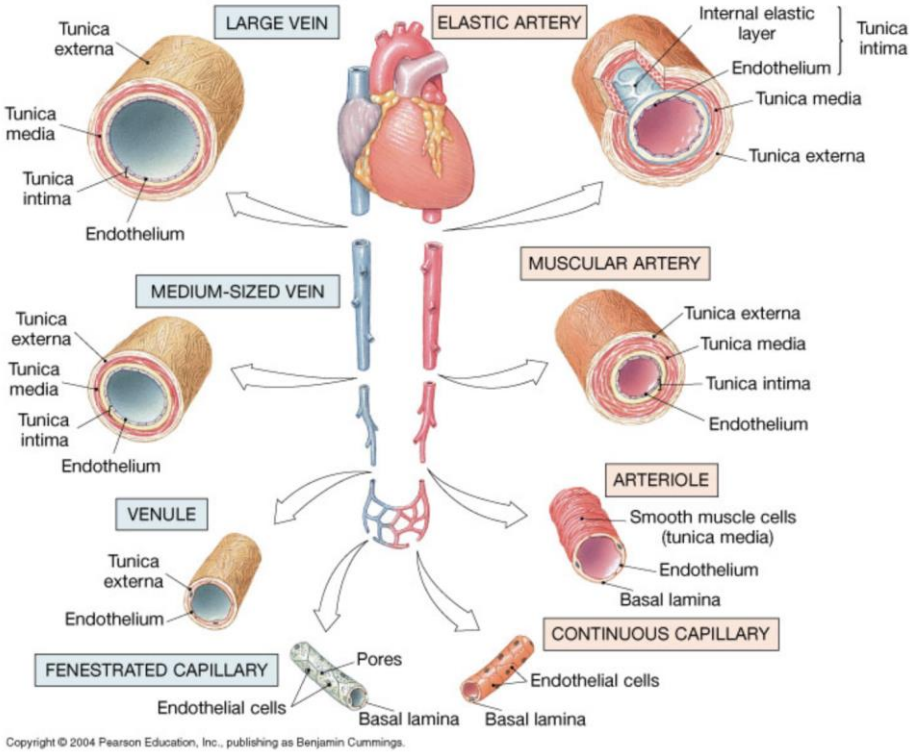

Figure 1: Schematic representation of blood vessel types in the circulatory system. From Marieb, E.N [26].

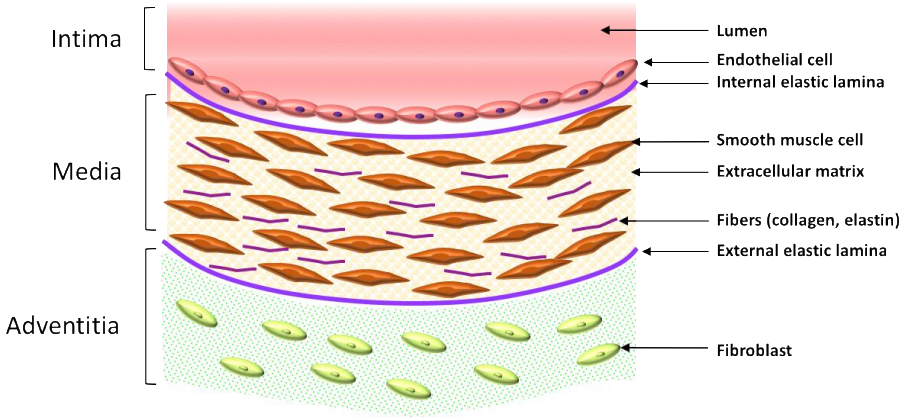

Figure 2: Schematic representation of the general structure of an arterial wall.

II. Physiology of the vascular endothelium

The structure of ECs and their function are important for the maintenance of the vessel wall and circulatory function. The endothelium is not an inert barrier but rather acts as a signaling platform that can respond to stimuli and exert autocrine, paracrine or endocrine actions, and influence diverse types of cells [16, 17, 27]. ECs derive from hemangioblasts [28], and depending on their location in the vasculature, they acquire specific properties and thus can respond differently to the same stimulus [29].

1. Structural organization of the endothelium

ECs are linked together by junctional complexes, which general organization comprises transmembrane proteins that form homophilic bonds through their extracellular domains [30]. The intracellular domains are associated with partners that mediate anchorage with the actin cytoskeleton or can mediate functions as diverse as establishment of cell polarity, membrane trafficking, cell signaling and the control of gene expression [30]. Three major types of junctions are found in the endothelium: tight junctions (TJs) and adherens junctions (AJs) that mediate cell-to-cell adhesion and gap junction (GJ) that mediate cell-to-cell communication **(Figure 3)** [10, 30].

Members of the claudin (*i.e* Claudin-5 specific of ECs) and junctional adhesion molecule (JAM) family, occludin and endothelial cell-selective adhesion molecule (ESAM) compose TJs. The cytoplasmic partners of TJs are zonula occludens (ZO-1, ZO-2, ZO-3) proteins, cingulin, ZO-associated nucleic acid binding protein (ZONAB) and others. The ZO proteins belong to the family of membrane-associated guanylate kinases (MAGUK) defined by their inclusion of PDZ, Src Homology 3 (SH3) domain and guanylate kinase (GUK) domains [30].

Members of the cadherin family principally mediate AJ complexes. ECs express a specific cadherin called vascular endothelial (VE)-cadherin. AJ intracellular interacting proteins components comprises α-, β-, γ-catenins, p120 and α-actinin.

ECs express other adhesive proteins outside of the TJ and AJ. Among these molecules are platelet endothelial cell adhesion molecule-1 (PECAM-1), S-endo 1 and Nectin-afadin complex [30].

The core proteins of GJ channels are connexins (Cx). The assembly of six Cxs forms a connexon also called hemichannel. When two hemichannels dock together they form a GJ channel. ECs on arteries express four types of Cxs (Cx37, Cx40, Cx43 and Cx45) [31]. The pore size of GJ channels ranges around 10-20 Å and the channels allow the passage of ions such as K^+, Na^+ or Ca^{2+}, and small molecules below 1.5 kDa like ATP, glucose, ascorbic acid, glutathione, cAMP, cGMP or inositol trisphosphate (IP3) [13, 30].

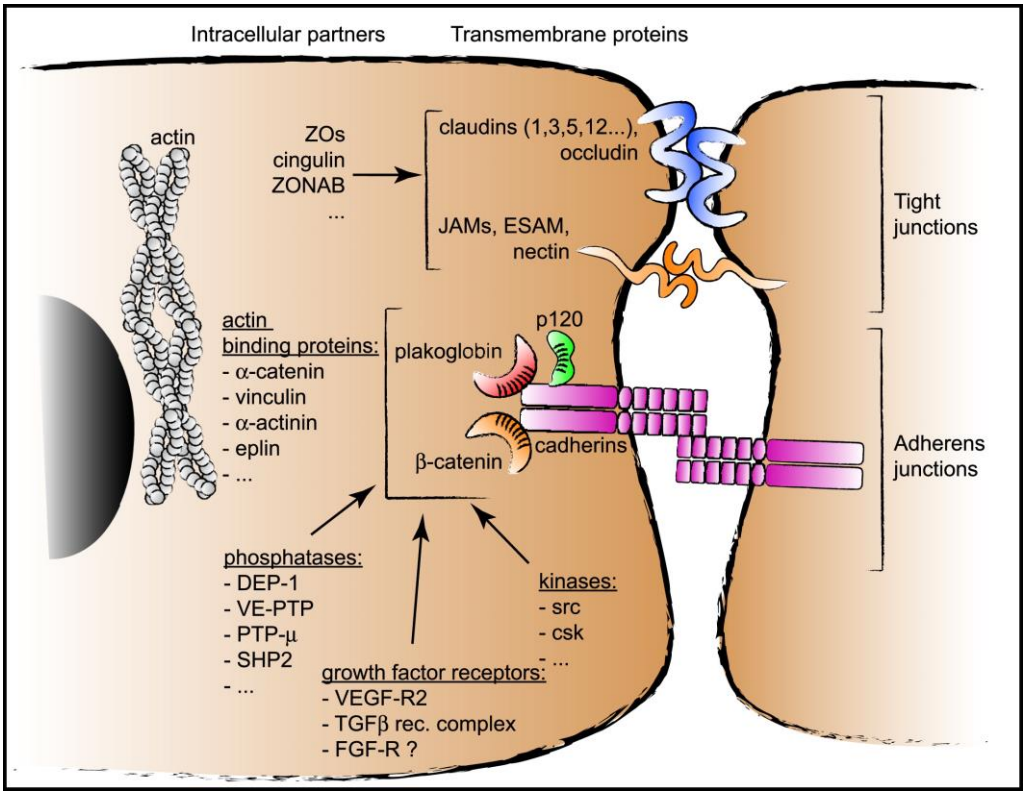

Figure 3: Schematic representation of TJ and AJ organization in the endothelium. From Dejana *et al.* [10].

2. Function of the endothelium: barrier, vascular tone, hemostasis and host defense

Transport of fluids, macromolecules and leukocytes through the vessel wall is regulated by the EC barrier and involves 2 different mechanisms: the transcellular and paracellular pathways [32]. Channels and vesicular transport (endocytosis, transcytosis and exocytosis) mediate the transcellular pathway. It allows passage of selective macromolecules like albumin and albumin-bound ligands, insulin, lipids and hormones through their receptors localized in caveolae at the surface of the endothelium. The paracellular pathway is regulated by intercellular junctions. AJs are impermeant to large molecules like albumin (69 kDa; molecular radius 3.6 nm) [32]. TJs instead prevent the passage of small molecules (<1 kDa) [32]. The paracellular infiltration of leukocytes into the vascular wall is also regulated by intercellular junctions, involving for instance JAM and PECAM-1. The integrity of endothelial junctions can be assessed by measuring the passage of solutes or macromolecules across the intercellular junctions [30]. The permeability is not only dependent on the amount, but also on the type of junctional proteins present at the cell membrane [30].

ECs are involved in the regulation of the diameter of muscular arteries followed by an increase or decrease of blood flow to the irrigated tissues. One of the principal molecules involved in vasodilation is nitric oxide (NO), synthetized from L-arginine by endothelial nitric oxide synthase (eNOS). The release of NO is stimulated by biomechanical forces, but also by some endogenous substances such as catecholamines, histamine and thrombin. Prostaglandin I_2 is another vasodilator produced by ECs. Molecules such as endothelin-1 (ET-1) and thromboxane A_2 trigger vasoconstriction [29].

One of the essential functions of the endothelium is to maintain blood fluidity and thus to present a surface in a quiescent state that inhibits platelet activation and initiation of the coagulation cascade. However, under the effect of different physical or chemical factors, ECs

can also direct their genetic program to a procoagulant phenotype to limit the damage created by infection, trauma or inflammation. There is therefore a permanent balance between an anticoagulant state and a procoagulant phenotype. ECs also play a key role in host defense and inflammation. They produce diverse cytokines like interferons (IFN), interleukins (IL) and adhesion molecules such as intercellular adhesion molecules (ICAM), vascular cell adhesion molecules (VCAM) and P- and E-selectin to regulate leukocyte recruitment and transmigration [29].

III. Biomechanical forces and vascular physiology

1. Wall shear stress and cyclic circumferential stretch

The viscous and pulsatile nature of blood flow exposes arteries to different mechanical forces, such as wall shear stress (WSS). WSS represents the drag force per unit area imposed by the flowing blood on the vessel wall, parallel to the flow direction **(Figure 4)**. In the healthy human aorta, WSS forces range between 10 and 20 dynes/cm^2 (1 Pa = 1 N/m^2 = 10 dynes/cm^2) [19] and this value slightly increases in arteries with smaller diameters like cerebral arteries [33]. WSS calculation is obtained using the Hagen-Poiseuille formula: $\tau = 4\mu Q/\pi r^3$; in which τ is the shear stress, μ is the blood viscosity, Q is the volumetric flow rate and r is the lumen radius [5]. Using this formula implies that the vessel is a straight, uniform and stiff tube; that blood is an incompressible Newtonian fluid (constant viscosity) and flow is constant and laminar. These compromises are acceptable for WSS measurement in large and straight arteries where blood flow approximates Newtonian fluid behaviour [5]. However, in reality, blood flow is unsteady and indeed a non-Newtonian fluid. Moreover, the arterial system is a network of branched and curved vessels where blood flow patterns become complex due to flow separation and reversal, and to spatial and temporal variations. Thus, WSS calculation should include additional

parameters among which: the Reynolds number (Re) describing the ratio between inertial and viscous forces and representing the stability of the flow; the Womersley Number (α) that is the expression of the pulsatile flow frequency in relation to viscous effects; the Dean number (Dn) depicting the effect of curvature of a vessel on the flow profile [34]. The WSS complex calculation in the circle of Willis can thus be achieved by using computational fluid dynamics (CFD).

The cyclic circumferential stretch (CCS) is the vascular wall distension induced by pulsatile blood pressure **(Figure 4)**. During the systole, large arteries, for instance the aorta, experience ≈10% circumferential stretch and this strain reduces to lower extent in peripheral arteries (≈5%) [20].

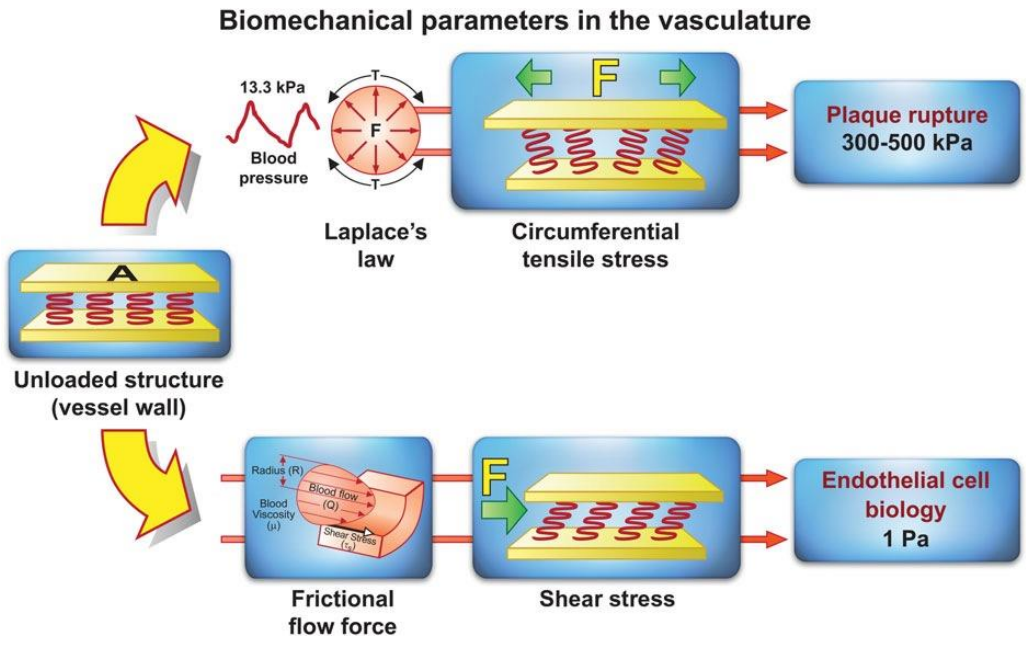

Figure 4: Biomechanical forces acting on the arterial wall. Blood pressure and blood flow induce forces in the vascular system that deforms the vessel wall and trigger intracellular signaling. From Kwak *et al.* [19].

Already in the 1960s, the idea emerged that blood flow could induce a vascular remodelling similar to the remodelling of bone trabeculae by mechanical load [35]. Surgically created arteriovenous shunt sustained the idea of flow-induced structural remodelling as observed in veins exposed to unusual high flow [36, 37]. WSS and CCS regulate vascular wall structure and function in a different manner. Increased blood flow leads to vessel vasodilation by release of NO or vasoactive molecules, whereas high blood pressure induces stretching of the vessel accompanied by compensatory remodelling mechanisms [38]. ECs and VSMCs are able to respond to chemical or mechanical stimuli through various sensors present at their surface or through their interaction with ECM [21, 39-43]. Under physiological conditions, vascular cells generate biochemical signals to maintain homeostatic conditions. Perturbation of blood flow conditions with lower or higher mechanical stimuli leads to adaptation, that in case of excessive remodelling can favour vascular disease development (e.g. atherosclerosis, aneurysms). The mechanism by which ECs and VSMCs sense mechanical stimuli and convert it into intracellular biochemical responses is called mechano-transduction. Both cell types respond to changes in blood flow by structural adaptation, involving numerous signalling molecules [19, 21, 39-43]). ECs are primarily exposed to WSS, however both ECs and VSMCs are submitted to CCS [20, 44, 45]. My PhD work has focused on biological response and intracellular signalling initiated by the two biomechanical forces in ECs.

2. Mechano-sensors of biomechanical forces

The force transmission to the cell is mediated by several cellular components **(Figure 5)**. The cell membrane itself has been shown to be sensitive to WSS. Remodelling of the phospholipid bilayer is a fast process (seconds) after exposure to shear stress. This leads to changes in the organization and activity of the proteins, consequently affecting downstream intracellular signalling pathways [39]. Several ion channels including K^+, Na^+, Ca^{2+}, TRPV (transient

receptor potential cation channel) and Piezo 1/2 channels mediate the endothelial response to WSS. For instance, expressing K^+ channels into *Xenopus laevis* oocytes turns them sensitive to shear stress [40]. The glycocalyx, a polycarbonate coat that covers the cell membrane, is also regulated by WSS. It has been shown that knock-down of some core proteins of the glycocalyx leads to failure of WSS-induced NO, and cytoskeleton remodelling [40, 46, 47]. Caveolae are cholesterol- and sphingolipid-rich microdomains that contain high levels of caveolin and cavin family proteins. Caveolae are cup-like invaginations containing many receptors and signalling molecules that may function as a signalling platform. The flattening of these structures by WSS or stretch would activate caveolin and induce responses through extracellular signal-regulated kinase (ERK), Rho GTPases, eNOS, Src family kinase and protein kinase B (Akt) activation [40]. Primary cilia are microtubule-based organelles that protrude at the apical side of most differentiated cells (*i.e*. kidney, retina, liver epithelial cells, neuronal and vascular cells) and have numerous functions (chemosensing, mechanosensing, olfaction, photoreception). Their role in WSS sensing on the one hand and in aneurysm development on the other hand has been well established in the past years [41-43] (see section IV-4), however the molecular link between primary cilia, aneurysmal WSS and vascular remodelling remains to be established. Integrins, the proteins connecting the cell to the ECM can also mediate WSS-induced responses. WSS induces activation of integrins, which undergo conformational changes and modulate their affinity for cytoskeleton or ECM proteins. AJ proteins, principally VE-cadherin can also transmit extracellular force. In association with PECAM-1 and vascular endothelial growth factor receptor (VEGFR) 2/3, VE-cadherin forms a mechanoresponsive complex, stimulation of which leads to activation of the pro-inflammatory nuclear factor kappa-light-chain-enhancer of activated B cells (NF-κB) pathway [40]. A central core of WSS responsive elements is the cytoskeleton, which remodelling is part of the early changes induced by flow. Indeed, the cytoskeleton binds to most of the sensors cited above and therefore ties them

together. This configuration helps the transmission of a force applied locally at one site of the membrane to a distant site allowing for an efficient and complete adaptive response to stress [40]. Finally, another fundamental player in mechano-transduction is the nucleus. Disruption of nucleus envelope proteins leads to impaired mechano-transduction signalling. Even if the nucleus is not a direct sensor of WSS, it establishes the link between force transmission and biochemical signalling [48]. Much less is known about CCS mechano-transduction in ECs; it seems to implicate stretch activated channels (TRPV), integrins and PECAM-1 [45].

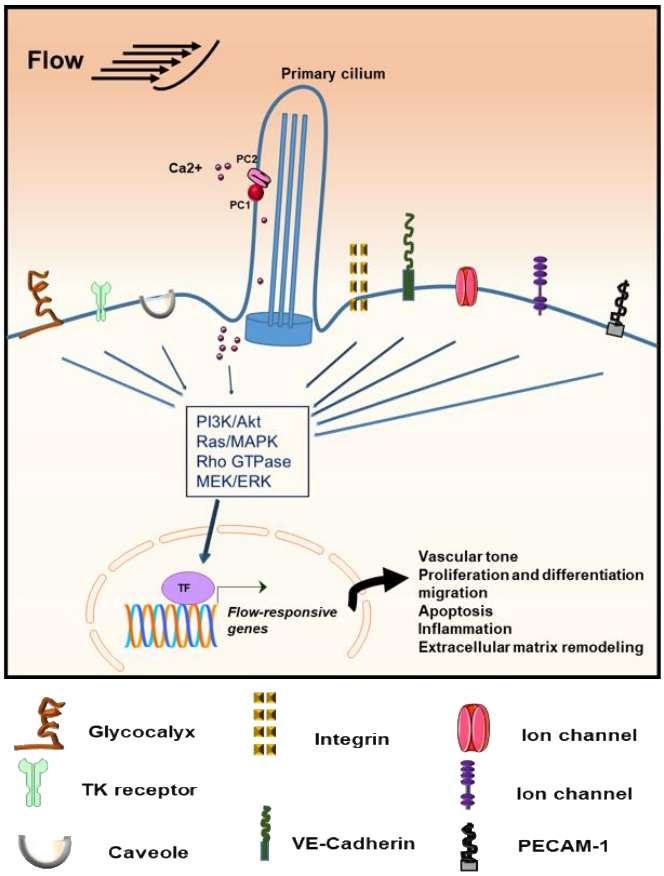

Figure 5: **Schematic representation of WSS mechano-sensors at endothelial cell surface. The activation of mechano-sensors by shear stress triggers a cascade of signaling pathways and modulates gene expression. From Diagbouga *et al.* [49].**

3. Biological response of endothelial cells to wall shear stress and intracellular signalling

In healthy arteries, straight parts experience a unidirectional laminar high WSS (HWSS), which is associated with a quiescent state. ECs in these areas are elongated and aligned in the direction of the flow, and they express genes such as Krüppel-like family of transcription factors (KLF2/4), nuclear factor erythroid 2 related factor-2 (Nrf2) and eNOS, involved in anti-inflammatory, anti-thrombotic and anti-proliferative processes [50-53]. eNOS activation is fundamental for regulating of blood flow and for maintaining of vascular homeostasis [21, 54]. Under physiological HWSS, eNOS expression is regulated by a delicate balance between Akt phosphorylation-mediated activation [55] and protein tyrosine kinase 2 beta (PYK2)-mediated repression [56]. KLF2, which positively regulates eNOS, has a sustained expression, involving the ERK5 - myocyte enhancer factor (MEF2) signalling cascade [57] and miR-92a repression, which is a negative regulator of KLF2 [58]. NO production dampens angiotensin II receptor 1 (AT1R) activity and results in downregulation of NADPH oxidase activity, which is a major source of superoxide ions [59]. Another important regulatory pathway of blood flow involves cyclooxygenase (COX) 2 and prostaglandin I_2 (PGI_2) [60-62]. PGI_2 is a vasodilator induced by HWSS, that can suppress tumour necrosis factor-α (TNF-α) and prevent platelet aggregation [63]. In addition, physiological HWSS has a negative regulation of Ras GTPase/mitogen-activated protein kinases (MAPK) signalling, thus repressing inflammatory gene expression. Indeed, NO production inhibits protein kinase C (PKC)-ε and ERK 1/2 leading to the repression of monocyte chemoattractant protein 1 (MCP-1) [64]. In addition, AMP-activated protein kinase (AMPK), poly(ADP-ribose) polymerase 1 (PARP-1) and B-cell lymphoma 6 protein (Bcl6) signalling inhibits VCAM-1, MCP-1 and MCP-3 expression [65]. Finally, physiological HWSS sustains quiescence of ECs by activating genes that promote growth arrest such as growth arrest and DNA-damage-inducible protein 45 (GADD45) and cyclin-dependent kinase

inhibitor 1 (p21) [66, 67], and abrogate apoptosis via activation of signalling pathways involving superoxide dismutase and eNOS [19, 68].

Arterial bifurcations and curvatures experience low (LWSS) and oscillatory WSS (OWSS), which is characterized by the reversal of blood flow directionality, and present dysfunctional ECs [69]. ECs bearing LWSS and OWSS exhibit an altered morphology (cobblestone instead of elongated shape), an increased permeability and migratory activity, and a high turnover (increased proliferation and increased apoptosis) [5-7]. LWSS triggers the expression of the pro-inflammatory transcription factor NF-κB through c-Jun N-terminal kinases 1 (JNK1) and activating transcription factor 2 (ATF2) signalling [70], and promotes the induction of NF-κB positive regulators (Toll-like receptors (TLR), bone morphogenetic proteins (BMP), nuclear factor kappa-B kinase subunit beta (IKK2) and reactive oxygen species (ROS)) [71-78]. MCP-1 and VCAM-1 activation by OWSS is mediated by miR-21/peroxisome proliferator-activated receptor alpha (PPARα)/activator protein 1 (AP-1) signalling cascade [79]. OWSS also induces histone deacetylases (HDAC)-3/5/7 [80] and NLR Family Pyrin Domain Containing 3 (NLRP3)-mediated inflammation [71]. Furthermore, disturbed flow promotes cell cycle progression via a sustained phosphorylation of Smad1/5 through integrin/BMP receptor association and the focal adhesion kinase (FAK)/ERK cascade [81]. Apoptosis is also increased through PKC-ζ [82], JNK - MAPK and p53 signalling [19, 83, 84]. Enhanced proliferation and apoptosis are typical signs of endothelial dysfunction.

Comparably to LWSS, an abnormal increase in WSS, designated as supra-physiological WSS (SWSS>HWSS), can cause EC dysfunction [85-90]. Vascular walls experiencing a sustained SWSS undergo remodelling to increase lumen diameter such that the mean WSS returns to its baseline level. This is mediated by MMPs production that leads to ECM degeneration,

temporary fragmentation of the IEL, vascular cell proliferation and migration into the enlarged area [91]. At the same time, changes induced by SWSS make the vessel wall vulnerable and prone to diseases [69, 85, 87-90, 92-94]. *In vitro* studies revealed that SWSS impaired EC alignment, increased cell turnover and reduced cell density [85]. Transcriptomic profile of cells exposed to SWSS revealed an induction of genes essential for an active remodelling process including *Plasminogen Activator, Urokinase (uPA), tissue plasminogen activator (tPA), metalloproteinase ADAMTS1/6* and *tissue inhibitor of metalloproteinase (TIMP) 3* [95]. The effect of SWSS on ECs is exacerbated when combined with a steep increasing WSS gradient (WSSG) or attenuated by negative WSSG [85, 96]. Increasing WSS can cause platelet activation [97], while in contrast, it has been shown that SWSS can upregulate anti-coagulant, anti-inflammatory genes expression and downregulate expression of proinflammatory cytokines genes such as *IL-8*, chemokine genes (C-X-C motif) ligand (*CXCL)-2, -5* [95]. It has been proposed that the anti-inflammatory and anti-coagulation effects of SWSS may protect the endothelium and the vessel wall from inflammatory cell-associated damage [95]. Disease may occur when there is an imbalance in the protective response as a result of EC dysfunction or loss. Indeed, SWSS leads to reduced production of eNOS, which has been linked to increased oxidative stress molecules, loss of intercellular contacts and consequently to the loss of ECs [92].

4. Biological response of endothelial cells to cyclic circumferential stretch and intracellular signalling

The effect of CCS on VSMCs function has been extensively studied whereas only a small amount of studies explored at CCS and its pathological implication in ECs. CCS is critical for vessel formation (sprouting, migration, tube formation) and also for the regulation of mature vessel functions [45]. However, excessive stretch, as observed in hypertension, can lead to

atypical responses [45]. Under physiological CCS ECs change their shape from polygonal (under static condition) to elongated. Subsequently, stress fibres organise perpendicularly to the stretch direction in order to reduce tension load, which involves Ca^{2+} influx and Rho kinase-induced activation of phosphoinositide 3-kinases (PI3K) [98-100]. In addition, it has been reported that under CCS, PECAM-1 gets phosphorylated and activates ERK1/2 through p21ras and Raf-1 [101, 102]. PECAM-1 phosphorylation also triggers cytosolic protein tyrosine phosphatase (SHP)-2 binding to activate MAPK and ERK1/2 thus promoting cellular reorientation [103]. CCS is also implicated in ECM remodelling as both physiological and pathological CCS increases expression of MMPs through TNF-α and JNK [104, 105]. Even though MMP activity is important for vascular adaptation, angiogenesis and repair, in pathological conditions, increased MMP activity would facilitate VSMC migration into the intima. Vasoactive molecules such as ET-1, endothelium-derived hyperpolarizing factor (EDHF) and NO are stimulated as well by CCS [106-110]. Cellular processes like proliferation and apoptosis are influenced by CCS, not only by the magnitude of the mechanical force but also by the duration of the stretch [45].

The principle of structural changes initiated by blood flow variation is to revert to baseline flow conditions and to maintain proper function of the vessel. When cells cannot adapt any longer, it gives rise to disorders. In general, hemodynamic forces alone are not sufficient for vascular disease development and progression. They are usually associated with additional factors like ageing or genetic diseases that change the mechanical and the structural properties of vessels. At high doses some substances like caffeine, nicotine, alcohol or cholesterol can be harmful and participate in disease onset. Hemodynamic forces, however, play a crucial role in several vascular pathologies such as arteriovenous malformation (AVM), atherosclerosis and intracranial aneurysms.

IV. Aneurysm disease

An aneurysm is a disease characterized by a focal dilatation of >50% of the normal vessel diameter [111]. When only one side of the vascular wall is affected, it leads to a saccular (spherical shape) aneurysm while a fusiform (spindle shape) aneurysm affects the entire circumference of the wall **(Figure 6A)**. We can distinguish true aneurysms that involve all three layers of the wall or false/pseudo aneurysms that are induced by a dissection and blood accumulation between the different layers. Aneurysm disease can affect all vessels of the circulatory system and are thus classified by their location. Venous aneurysms are very uncommon [112] while arterial aneurysms have an increasing prevalence. Arterial aneurysms are for the most part cerebral or intracranial aneurysms (IAs), thoracic and abdominal aortic aneurysms (AAA). IA and AAA are considered as different pathologies even though they share some similarities **(Table 1)**. My thesis will focus only on saccular IAs.

Table 1: Comparison of hemodynamic and cellular factors that play a role in IA and AAA initiation. Adapted from Tanweer *et al.* [69].

	IA	AAA
WSS	High	Low
WSSG	High	High
EC dysfunction	Yes	Yes
Destruction of elastin	Yes	Yes
VSMC apoptosis	Yes	Yes
MMPs and other proteinases	Yes	Yes
ROS	Yes	Yes
Increased cell adhesion	No	Yes
Inflammation	No	Yes

1. Intracranial aneurysm generalities

IA prevalence ranges between 2-3% in the general adult population, it affects middle age (>50 years old) persons [113]. IAs are in 90% of cases saccular aneurysms and they develop mostly at or near bifurcations in the circle of Willis **(Figure 6B)** [114]. This is a circle of arteries that supplies blood to the brain. It comprises the left and right internal carotid artery, the anterior and posterior cerebral artery, the anterior and posterior communicating artery. The interconnected arrangement of arteries in the circle of Willis ensures provision of blood to the brain in case of an obstruction or diminished flow through one of its feeding arteries. On the other hand, the atypical organization of the circle of Willis exposes its arteries to multiform irregular blood flow patterns like impinging, converging, dividing, swirling and secondary flows [49].

IA disease is often asymptomatic until the aneurysm ruptures. Unruptured intracranial aneurysms (UR-IA) are in general discovered incidentally either when the aneurysm increases in size and compresses adjacent tissues causing pain, troubles with vision, numbness of one side of the face or when thromboembolic events occur. The rupture of an IA leads to bleeding in the subarachnoid space causing an hemorrhagic stroke. A sudden severe headache is the primary symptom of a ruptured aneurysm (R-IA). Common signs of rupture also include nausea, vomiting, stiffness of the neck, blurred vision, sensitivity to light, seizure, drooping eyelid, loss of consciousness and confusion [114].

Early detection of IA is crucial for a good management of the disease. Imaging is an essential tool for IA diagnosis. Computed tomographic angiography (CTA), magnetic resonance angiography/imaging (MRA, MRI) and cerebral angiograms are commonly used to detect aneurysms [115]. There is not yet a blood test for IA detection. However, in a recent study, different transcriptomic signatures of circulating neutrophils have been found between patients

with and without IA. These observations reinforce venture towards developing a blood-based test for IA diagnostic [116].

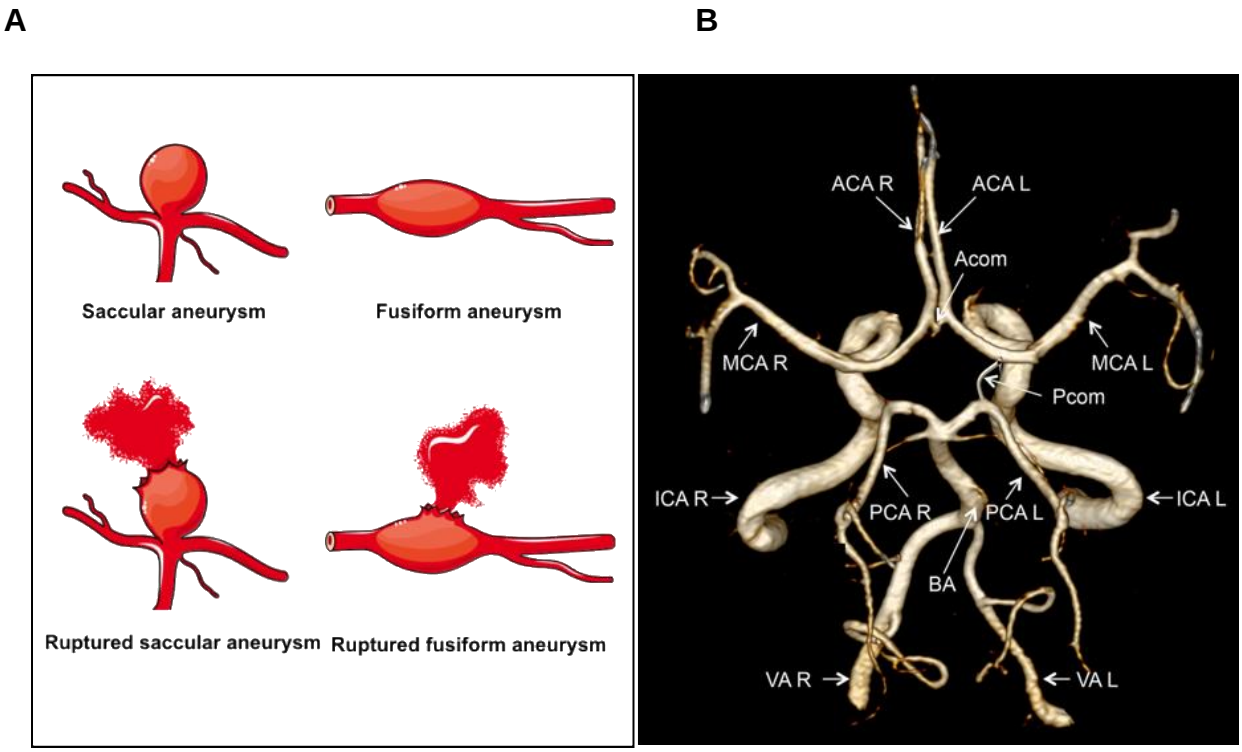

Figure 6: (A) Schematic representation of saccular, fusiform and ruptured aneurysms. (B) Angiographic image of a human circle of Willis. Indicated are: vertebral arteries (VA), right (R) and left (L), basilar artery (BA), internal carotid arteries (ICA R, ICA L), posterior cerebral arteries (PCA R, PCA L), anterior cerebral arteries (ACA R, ACA L), middle cerebral arteries (MCA R, MCA L), posterior communicating artery (Pcom) and anterior communicating artery (Acom). From Diagbouga *et al.* [49].

2. Pathogenesis of intracranial aneurysms

a. Intracranial aneurysm initiation

For a long time IA has been thought to be a congenital disease. Another theory has evolved and it is commonly accepted that IA are acquired lesions that take years to develop [117]. The role of hemodynamic forces in IA development is certain. IAs develop principally nearby or at bifurcations in the circle of Willis that experience complex blood flow pattern [85-90, 93, 118]. The histological features of nascent IAs were first obtained through autopsy analyzes, and then through IA animal models. Disruption of the IEL and media thinning are characteristic of developing IAs [69, 85, 87, 89, 90, 94, 118]. Studies conducted in IA animal models indicated that the histological changes characteristic of nascent IAs take place at regions experiencing SWSS and positive WSSG **(Figure 7)** [86-90, 118]. Meta-analysis in patients correlating hemodynamic forces and IA development support the fact that IAs are triggered by SWSS and positive WSSG [86]. It appears that aneurysmal remodeling starts only when WSS and WSSG go beyond a certain threshold [90]. This could explain why IAs are more frequently found at specific bifurcations in the circle of Willis and why certain individuals are more susceptible than others to develop IAs. Because the anatomy/geometry of the artery (angle of the bifurcation, size of the parental and daughter artery) influences the resulting forces, some arteries are more prone to reach the threshold. Moreover, a damaged vascular wall caused by ageing, smoking, high blood pressure, high blood cholesterol level or genetic diseases would have a lower tolerance than a healthy vessel for the same magnitude of WSS.

Endothelial dysfunction triggered by SWSS and positive WSSG is one of the earliest events of IA initiation, followed by IEL and ECM disruption [27, 89, 92-94]. Experiments in a rodent model of IA indicate that inflammatory cells, for instance macrophages, participate in IA disease [27, 119, 120]. Inflammatory cell recruitment leads to proteolytic destruction of IEL and ECM content by MMPs and consequently to IA formation [121, 122]. In a canine model,

IA aneurysm wall remodeling was associated with IL-1β and MMP expression as well as a reduced eNOS expression [92] that will incite inflammatory gene expression. Along these lines, again in a rodent model of IA, macrophage infiltration in the arterial wall was observed, and migration through the wall was mediated by MCP-1 expression by fibroblasts present in the adventitia [123]. Macrophages in the aneurysmal wall secrete MMP2 and MMP9 and inducible nitric oxide synthase (iNOS). iNOS activity results in excessive production of NO which increases superoxide derivatives such as peroxynitrite [92, 94, 119]. This peroxynitrite is toxic for cells and can trigger SMC apoptosis. The combination of ECM degradation and SMC death result in thinning of the media. It is important to note that in some studies early aneurysmal changes were devoid of inflammatory cell infiltration until 2 months after IA induction [89, 92, 94]. However, an increased expression of MMPs, IL-1β, iNOS and peroxynitrite, and reduced expression of eNOS were observed in the aneurysmal region. [92, 94]. These results suggest that destructive remodeling at the initial state is mediated by SMCs since a co-localization with MMPs has been observed [94]. Together, these results point to the complexity of IA disease involving various mechanisms.

b. Intracranial aneurysm growth

In the IA wall, collagen fibers principally bear the mechanical load as the IEL is lost. Collagen fibers limit the expansion of the aneurysm as they have lower extensibility properties compared to elastin [124]. For an aneurysm to grow, an active remodeling process is required. ECM degradation and renewal as well as SMC proliferation provoke IA growth, and biomechanical stresses play a critical role in this process [88]. Blood flow conditions have been associated with vascular wall remodeling **(Figure 7)** [88, 125]. When an IA bulges out it may lead to a progressive lowering of WSS in cases of wide neck IAs for example, or a high impinging flow can subsist in aneurysms with narrowed neck or with high-curvature parent vessels, high

aneurysm angle or high inflow angle [88]. LWSS being associated with a pro-inflammatory state of ECs, as discussed above, it will typically incite leukocyte recruitment and transmigration into the IA wall. Consequently, this will further enhance ECM degradation, and increase SMC matrix synthesis and proliferation by secreting growth factor like transforming growth factor (TGF)-β, platelet-derived growth factor (PDGF)-BB and increase VSMC apoptosis through iNOS signaling [126]. Impinging flow and SWSS would drive same remodeling as in IA initiation generating sometimes secondary IAs called blebs that are more inclined to rupture [127]. SMCs can also switch their contractile phenotype to a more synthetic one [15].

Human IAs have heterogeneous phenotypes [128-130]. Small IAs (<4 mm) commonly have thin, smooth hypocellular walls with low number of inflammatory cells. Small IAs seems to develop relatively fast [131] and their wall remodeling converge with SWSS-induced remodeling. Large aneurysms (>10 mm), instead, more frequently have thick and hyperplastic walls with inflammation corresponding to LWSS-derived remodeling. Intermediate phenotypes exist with thin and thick walls in different regions [88]. Biomechanical forces and morphological characteristics (size, shape) of IAs are interconnected. WSS across the IA dome is heterogeneous and affects IA morphology. In the same way, growing aneurysms result in changing WSS. The time and spatial variation of WSS in an IA result in a wide range of IAs with diverse morphological, size, vascular remodeling, and growth rate characteristics.

Increased mechanical stretch may also participate in the IA disease progression. As the aneurysm grows, it is subjected to increasing wall tension, which will trigger remodeling similar to changes associated with hypertension [124]. One the other hand, IAs with atherosclerotic plaques and calcification have reduced or no stretch capacity [132, 133]. The large gaps in our understanding of the role of CCS in IA disease urgently need to be filled.

c. Intracranial aneurysm rupture

IA rupture occurs when the vascular wall is too weak to resist to the tension applied by a high blood pressure **(Figure 7)**. Rupture occurs most of the time during physical exercise or high emotional stress that abruptly increases blood pressure [113, 134]. The risk of rupture of IAs has been evaluated to 0.3-15% per 5 years [135]. A rupture of an aneurysm leads in 50% of the cases to death if there is no intervention. This percentage reduces to 15% after treatment. One-third of the patients suffer from life-long disabilities [136]. So far, no pharmaceutical treatment can prevent IAs from rupture. IAs are treated by endovascular coiling which consist on the insertion of a platinum coil to seal off the aneurysm from the artery or by open surgery and the fixation of a clip at the neck of the aneurysm to stop blood flow into it. A tubular stent implant can also be used to divert blood flow away from the aneurysm [115]. IA treatment is invasive and not devoid of risk. Surgical clipping or endovascular coiling is associated with 6.7% and 4.8% unfavorable outcomes, respectively [137, 138]. Due to the high risk of complications, surgeons and patients face a hard decision to treat or not UR-IAs since the risk of rupture of an aneurysm during its natural course is usually low [139]. To improve decision-making, many parameters associated with IA ruptures have been described [139-141]. It is essential to identify IAs with a high risk of rupture and to evaluate the balance between risk and benefit of treatment. Therefore, groups of clinicians have made an attempt to estimate the risk of rupture of an aneurysm based on individual patient data and aneurysm characteristics. PHASES [139] and UIATS [141] scores for clinical decision-making are based on aneurysm characteristics and clinical risk factors. However, most, if not all, biological reactions of the vessel wall are mediated by the flowing blood and cyclic stretching of the wall, and thus are the main actors responsible for the disease progression. More knowledge on the natural history of aneurysms and how these mechanical conditions transduce into biological effects in aneurysm wall morphology in a spatio-temporal manner would help for therapeutic decisions.

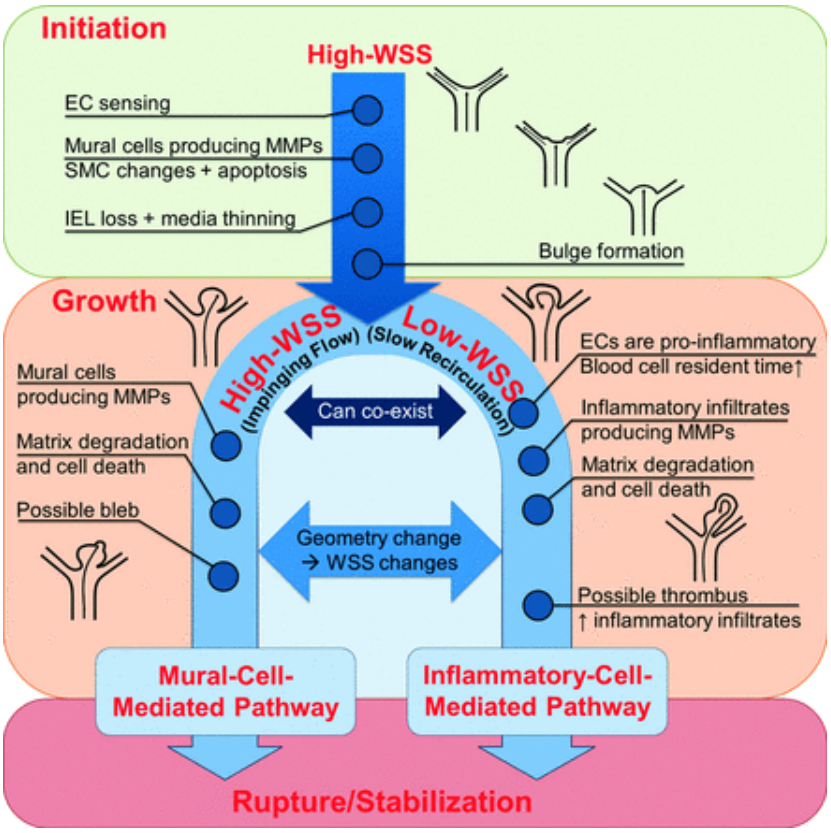

Figure 7: Schematic description of the implication of WSS in the pathogenesis of IAs. From Meng *et al.* [88].

3. Intracranial aneurysm risk factors and associated diseases

Several conditions and diseases are associated with high prevalence of IA. Female sex, hypertension and cigarette smoking are strong risk factors for IA growth and rupture. IA growth rate seems higher for IAs at posterior location in the circle of Willis, at larger initial size and when having an irregular shape. Diabetes, hyperlipidemia and excessive alcohol use have also been associated with increased risk of aneurysm growth [142].

Brain AVMs, which is a non-standard connection of arteries to veins without capillary bed, are associated with high frequency of IAs. This abnormal shunt results in atypical high flow and pressure in the venous vessels inducing aneurysmal remodeling [143]. IA is not a hereditary

disease, but when two or more first-degree relatives have a history of IAs we talk about "familial aneurysms." Available evidence suggests that specific genetic polymorphisms associate with IA formation or subarachnoid hemorrhage [143]. The strongest associations from different cohorts and populations are found for the cyclin dependent kinase inhibitor 2B (CDKN2B) gene, the transcription regulator gene SRY-box 17 (SOX17) and the endothelin receptor A (EDNRA) genes. Interestingly, SMC-specific inactivation of the EDNRA gene in mice induces abnormal vascular development [143].

Some genetic disorders have also been associated with high risk of IA formation. For example, diseases affecting connective tissue related genes such as Ehlers–Danlos syndrome (abnormal collagen production or organization) and Marfan syndrome (mutation in fibrillin-1) have an instable fragile vascular wall. The most common disease that has been associated with IA formation is autosomal dominant polycystic kidney disease (ADPKD) with a relative risk ≈ 6.9%. Between 5-40% of ADPKD patients develop IAs and one-third develop multiple IAs [144]. In addition to increased prevalence, IAs rupture more frequently in these patients [145]. ADPKD disease is caused by mutations in PKD1 and PKD2 genes [146]. The two genes encode for polycystin-1 and -2 (PC1 and PC2), respectively, which are proteins essential for primary cilium function [147]. ADPKD patients primarily develop cysts in their kidneys leading to kidney failure. ADPKD patients can also suffer from various extra-renal complications including hepatic and pancreatic cysts, hypertension, left ventricular hypertrophy, valvular heart disease, atherosclerosis and aneurysms [146, 148].

Since renal therapy has improved, cardiovascular diseases are becoming the leading cause of death in ADPKD patients [146]. EC dysfunction is a common feature in ADPKD patients even with preserved kidney function. It is known that ADPKD ECs have reduced NO availability, increased ROS and increased expression of inflammatory genes, which may all promote IA formation [149-151]. Evidence of primary cilia acting as mechano-sensors and mechanical

forces being important for IA pathogenesis, support the idea that IAs in ADPKD would result from abnormal flow sensing and vascular remodeling.

4. Primary cilia: role in polycystic kidney disease and in intracranial aneurysms

Primary cilia, by opposition to motile cilia, are organelles that exists as a single structure at the cell surface **(Figure 8)**. A primary cilium length ranges from 1 to 9μm [152]. A so-called "9+0" arrangement defines the structure of their axonemes, where nine doublets of microtubules organise in a circumferential way, and the central part lacks the additional pair of microtubules, present in motile cilia (9+2). Primary cilia have gained importance in biomedical research since Pazour and colleagues revealed that the *Tg737* gene, whose mutation leads to renal polycystic disease in mice, encodes for a protein necessary for primary cilium assembly [153]. Additional studies clearly confirmed that ADPKD is a ciliopathy. PC1 and PC2 are localized at the ciliary membrane and they form a complex that mediates Ca^{2+} influx into the cells [154, 155]. The PC1 C-terminal tail can act as an activator of heterotrimeric G_i/G_o proteins. PC1 C-terminal tail can also be cleaved and translocate into the nucleus where it activates transcription factors. These processes are restrained when the PC1/PC2 complex is assembled [156, 157]. PC2 is a transient cation channel that requires PC1 for its correct localisation and function [158]. Differences in cilium size, composition and morphology between cell types or organs testify the versatility of primary cilia and their ability to recruit multiple different receptors to serve specific functions inherent to each cell type or organ. Primary cilia regulate diverse cellular processes mediated by Wnt, Src, JNK, mammalian target of rapamycin (mTOR), Janus kinase (JAK)/signal transducers and activators of transcription (STAT) signalling pathway [147]. Primary cilia are more frequently found in arterial areas experiencing low and complex flow, and increasing evidence suggests that they play a critical role in the functions of ECs [42, 159-

161]. Furthermore, it has been demonstrated that endothelial primary cilia are essential for vascular contractility as they mediate WSS-induced Ca^{2+} influx and NO synthesis [155, 162].

A **B**

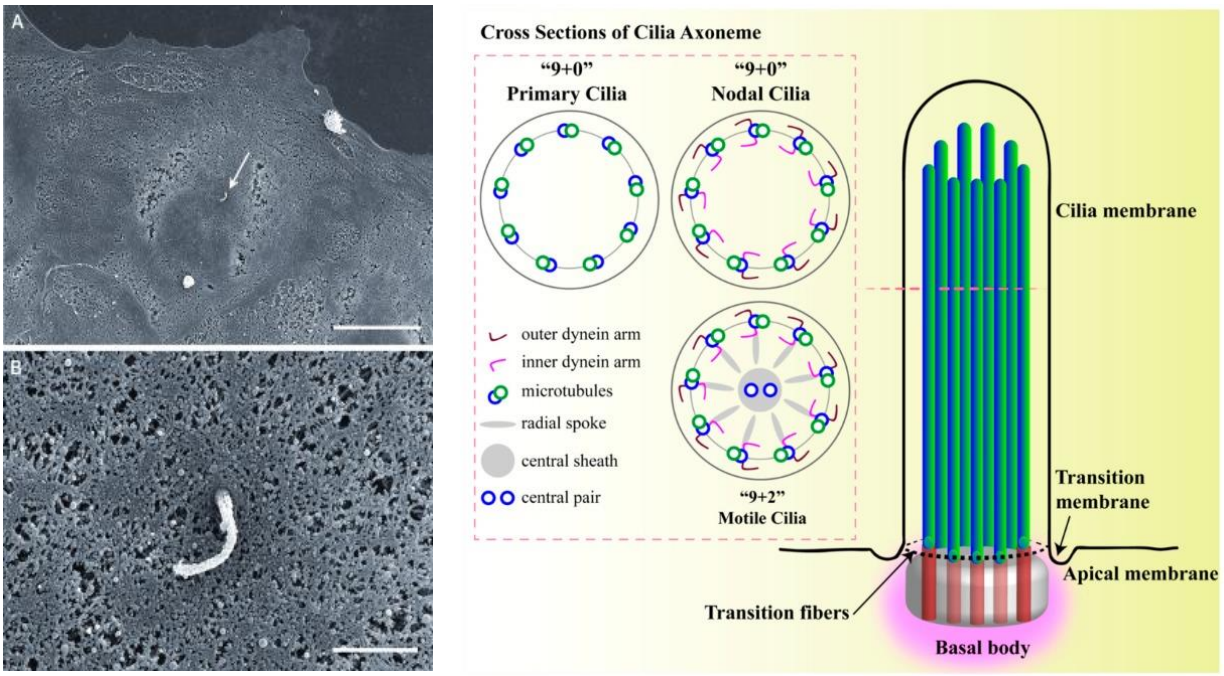

Figure 8: (A) Electron microscopy image of an endothelial primary cilium. Scale bar represents 10μm (top image) and 1μm (bottom image). From Van der Heiden *et al.* [163]. (B) Structure of primary cilium. From Pala *et al.* [164].

During vascular development, primary cilia can also mediate SMCs recruitment by ECs through the activation of the Notch/foxc1b signalling pathway [41]. Assuming that this process also occurs in adult blood vessels, it might be relevant for vascular repair and remodelling, notably in IAs. Moreover, loss of endothelial primary cilia has been associated with decreased level of heat shock protein (hsp) 27 and reduced FAK phosphorylation leading to weaker stress fibres, impaired migration and reduced cellular barrier integrity [165]. The affected junctional proteins in this process still need to be unveiled. Actually, loss of endothelial integrity is observed in

IAs and is typical for instable vascular walls since it promotes inflammatory cell infiltration [166]. Moreover, absence of primary cilia has been associated with increase in inflammatory gene expression [164, 167]. Finally, mouse and human ECs lacking primary cilia have been shown to be more sensitive to BMP-induced osteogenic differentiation, as a result of β-catenin and transcription factor Slug activation [168]. Interestingly, calcification has been reported in histological analyses of IAs as a marker of adverse outcome [169].

5. Animal models to study intracranial aneurysm

To get more insight into IA disease, good animal models are essential to address a variety of questions from basic science to clinical aspects. Even if *in vitro* cellular models help to decrypt mechanistic events, *in vivo* models reproducing morphological, histological and hemodynamic characteristics provide integrative phenotypic clues onto the disease, indispensable for the development of diagnostic or therapeutic strategies. **Table 2** displays a comprehensive overview of some of the animal models currently used to study the relationship between WSS and IAs. In brief, IAs rarely occur spontaneously in animals, therefore induced IAs have been designed for experimental studies. IA induction relies on the principle that hemodynamic stress imposed on a fragile arterial wall will induce an aneurysmal out-pouching of the wall [170]. Hemodynamic stress is frequently increased by the induction of hypertension through renal artery ligation, angiotensin II infusion or high salt diet for example. Ligation of one common carotid artery would also increase the hemodynamic stress in the other common carotid artery **(Table 2).** The arterial wall is in general weakened by chemical treatment such as elastase, an enzyme that breaks-down elastin, or β-aminopropionitrile, which inhibits the cross-linking of collagen and elastin **(Table 2)**. Various animal species can be used (mouse, rat, rabbit, dog and primate) and the choice relies on the experimental purpose. Although rodent models are easy to handle and relatively low-cost, the small size of their arteries is challenging for IA induction.

Moreover, the small size of their cerebral arteries and IAs limits the possibility of radiological imaging or testing endovascular devices. The use of larger animals such as dogs and primates would overcome these hurdles, but are more difficult to handle and thus restrict the number of animals that can be used. Rabbits seem to be a good compromise, and the diameter of their extracranial carotid arteries is similar to humans [171]. Another frequently used technique for experimental IAs is the surgically created model, where an arterial or venous pouch from a donor animal is end-to-side or side-to-side grafted to an arterial wall of a recipient animal [172]. The main advantage of this technique is that it gives more freedom onto the choice of the IA size, orientation and localisation. It is therefore very suitable for testing of endovascular devices. The recent development of CRISPR/Cas9-induced genetic modifications in multiple animal species will certainly be helpful to further unravel the pathophysiology of IA growth and rupture in relation to hemodynamic forces in experimental IA models.

Table 2: Intracranial aneurysm models

Study	Species	Genetic Background	Methods for IA formation	Application
Hashimoto N, *et al*. [170]	Rat	Wild-type	β-aminopropionitrile and elastase treatments + hypertension induced by deoxycorticosterone acetate or by ligation of the posterior branches of the renal arteries + high salt diet	IA initiation
Hashimoto N, *et al*. [173]	Monkey	Wild-type	Ligation of the posterior branch of left and right renal arteries, and ligation of the left common carotid artery + diet containing NaCl and β-aminopropionitrile fumarate for > 1 year	IA incidence rate: 2/7 develop IA at 1 year. 5/7 with no IA detectable at the end of the study Model for pharmacotherapy test Limitation: restricted number of animal, small size of IA (0.5-0.9mm)
Coutard M, *et al.* [174]	Mouse	Blotchy mice (C57BL/6 J moblo)	Ligation of the left common carotid artery + induced hypertension by ligation of renal arteries during 6-12 months	17-38% incidence with small and large size IA Testing of endovascular devices Model for pharmacotherapy test Limitation: High percentage of death due to surgical procedure (30–40%)
Altes TA, *et al.* [171] Wang S, *et al*. [118]	Rabbit	Wild-type	Elastase treatment and ligation of the common carotid artery for 2-24 weeks	89% IA incidence rate Study of unorganized thrombus Testing of endovascular devices Limitation: Big size aneurysm but risk of elastase intoxication
Morimoto M, *et al*. [175]	Mouse	Wild-type	Ligations of the left common carotid artery and posterior branches of bilateral renal arteries + high salt diet during 4 weeks	77% IA incidence rate Limitation: Early aneurysm changes observed only in microscopic studies

Study	Species	Genetic Background	Methods for IA formation	Application
Frosen J, *et al.* [172]	Mouse and Rat	Wild-type	Microsurgical grafts on the lateral wall of the abdominal aorta during 3 days to 3 months	100% success Testing of endovascular device IA growth
Moriwaki T, *et al*. [176]	Mouse	Wild-type	Ligation of the left common carotid artery and the posterior branch of the left and right renal arteries + high salt diet containing β-aminopropionitrile during 3–5 months	23-31% IA incidence rate 30% early aneurysm changes + 30% advanced stage aneurysm
Abruzzo T, *et al*. [177]	Mouse	$eNOS^{-/-}$	Ligation of the left common carotid artery for 13 months	30% IA incidence rate
Meng H, *et al*. [89]	Dog	Wild-type	Surgically created bifurcation between left and right common carotid arteries + high salt diet and renal artery ligation during 2 weeks to 2 months	100% IA incidence rate of early aneurysm change
Nuki Y, *et al.* [178]	Mouse	Wild-type	Angiotensin II and elastase treatments for 2 weeks	77% IA incidence rate Limitation: Small size IA, early aneurysm changes
Metaxa E, *et al*. [90] Gao L, *et al.* [93]	Rabbit	Wild-type	Bilateral common carotid arteries ligation for 5 days to 12 weeks	100% IA incidence rate of early aneurysm changes
Makino H, *et al.* [179]	Mouse	Wild-type	Deoxycorticosterone acetate-salt hypertension and elastase treatments for 7-28 days	63% incidence rate within 7 days 40% rupture rate after 28 days Model for pharmacotherapy test
Hosaka K, *et al*. [180]	Mouse	Wild-type	Ligation of the right renal artery and the left common carotid artery + angiotensin II and elastase treatment + hypertensive diet containing β-aminopropionitrile during 3 weeks	90-100% IA incidence rate 20-60% IA rupture rate
Liu M, *et al*. [43]	Mouse	EC specific knockout of PKD1, PKD2 or IFT88	Angiotensin II and elastase treatments during 20 days, 4 weeks after gene excision	60-100% incidence and 60-100% rupture rate Model for pharmacotherapy test

6. Aims and chapter outline of this thesis

Rationale: There is a growing number of asymptomatic IAs detected as a result of increasing screening with modern imaging modalities. IA rupture is a hazardous event that can be fatal or results in devastating neurologic outcomes and is associated with a high socio-economic impact. Criteria nowadays used to recommend surgical intervention for IAs are principally based on aneurysm location and size together with empirical patient characteristics such as age, ethnicity and presence of hypertension. These criteria are subject to controversies as they remain unsatisfying to predict the risk of rupture accurately. Hence, more factors signifying the biological processes leading to growth and rupture should be considered for decisions onto elective treatment of unruptured IAs. For my PhD thesis, the first goal was to characterize the human IA wall histologically and to correlate the histological characteristics with clinical and radiological parameters that are presently used in clinics to estimate the risk of rupture (**Chapter 2**). In addition, I investigated the effects of biomechanical forces on vascular ECs with the aim to understand how these effects could be involved in aneurysm growth and rupture. ADPKD patients lack or have abnormal primary cilia and are more prone to develop IAs. The dysfunction or absence of the primary cilium may alter the endothelial response to WSS and affect the pathogenesis of IA. I sought to understand how primary cilia would influence ECs response to physiological or pathological WSS (**Chapter 3**). Finally, I compare the effects of physiological arterial CCS (6%) *vs.* the lack of stretch (0%) as found in IAs on ECs behavior (**Chapter 4**).

- **Chapter 2:** Histological characterization of human IA domes obtained after surgical clipping
- **Chapter 3:** The effects of wall shear stress on ECs: role of primary cilium
- **Chapter 4:** The effect of cyclic circumferential stretch on ECs

References

1. Alberts B, J.A., Lewis J, Morgan D, Raff M, Roberts K, Walter P, *Blood Vessels and Endothelial Cells*. 2002, Molecular biology of the cell.
2. Liebeskind, D.S. and L.R. Caplan, *Intracranial Arteries - Anatomy and Collaterals.* Front Neurol Neurosci, 2016. **40**: p. 1-20.
3. Bibi S Van Thiel , I.v.d.P., Roland Kanaar, A.H. Jan Danser and Jeroen Essers, *Structure and cell biology of the vessel wall*. ESC textbook of vascular biology. 2017.
4. Wolinsky, H., *A proposal linking clearance of circulating lipoproteins to tissue metabolic activity as a basis for understanding atherogenesis.* Circ Res, 1980. **47**(3): p. 301-11.
5. Davies, P.F., *Hemodynamic shear stress and the endothelium in cardiovascular pathophysiology.* Nat Clin Pract Cardiovasc Med, 2009. **6**(1): p. 16-26.
6. Davies, P.F., et al., *The atherosusceptible endothelium: endothelial phenotypes in complex haemodynamic shear stress regions in vivo.* Cardiovasc Res, 2013. **99**(2): p. 315-27.
7. Davies, P.F., et al., *Turbulent fluid shear stress induces vascular endothelial cell turnover in vitro.* Proc Natl Acad Sci U S A, 1986. **83**(7): p. 2114-7.
8. Sandoo, A., et al., *The endothelium and its role in regulating vascular tone.* Open Cardiovasc Med J, 2010. **4**: p. 302-12.
9. Dejana, E. and C. Giampietro, *Vascular endothelial-cadherin and vascular stability.* Curr Opin Hematol, 2012. **19**(3): p. 218-23.
10. Dejana, E., E. Tournier-Lasserve, and B.M. Weinstein, *The control of vascular integrity by endothelial cell junctions: molecular basis and pathological implications.* Dev Cell, 2009. **16**(2): p. 209-21.
11. Pober, J.S. and W.C. Sessa, *Evolving functions of endothelial cells in inflammation.* Nat Rev Immunol, 2007. **7**(10): p. 803-15.
12. Yau, J.W., H. Teoh, and S. Verma, *Endothelial cell control of thrombosis.* BMC Cardiovasc Disord, 2015. **15**: p. 130.
13. Leybaert, L., et al., *Connexins in Cardiovascular and Neurovascular Health and Disease: Pharmacological Implications.* Pharmacol Rev, 2017. **69**(4): p. 396-478.
14. Duband, J.L., et al., *Calponin and SM 22 as differentiation markers of smooth muscle: spatiotemporal distribution during avian embryonic development.* Differentiation, 1993. **55**(1): p. 1-11.
15. Hao, H., G. Gabbiani, and M.L. Bochaton-Piallat, *Arterial smooth muscle cell heterogeneity: implications for atherosclerosis and restenosis development.* Arterioscler Thromb Vasc Biol, 2003. **23**(9): p. 1510-20.
16. Hungerford, J.E. and C.D. Little, *Developmental biology of the vascular smooth muscle cell: building a multilayered vessel wall.* J Vasc Res, 1999. **36**(1): p. 2-27.
17. Li, M., et al., *Endothelial-Vascular Smooth Muscle Cells Interactions in Atherosclerosis.* Front Cardiovasc Med, 2018. **5**: p. 151.
18. Emerson, G.G. and S.S. Segal, *Electrical coupling between endothelial cells and smooth muscle cells in hamster feed arteries: role in vasomotor control.* Circ Res, 2000. **87**(6): p. 474-9.
19. Kwak, B.R., et al., *Biomechanical factors in atherosclerosis: mechanisms and clinical implications.* Eur Heart J, 2014. **35**(43): p. 3013-20, 3020a-3020d.
20. Anwar, M.A., et al., *The effect of pressure-induced mechanical stretch on vascular wall differential gene expression.* J Vasc Res, 2012. **49**(6): p. 463-78.
21. Lu, D. and G.S. Kassab, *Role of shear stress and stretch in vascular mechanobiology.* J R Soc Interface, 2011. **8**(63): p. 1379-85.

22. Halper, J., *Basic Components of Vascular Connective Tissue and Extracellular Matrix.* Adv Pharmacol, 2018. **81**: p. 95-127.
23. Eble, J.A. and S. Niland, *The extracellular matrix of blood vessels.* Curr Pharm Des, 2009. **15**(12): p. 1385-400.
24. Barnes, M.J. and R.W. Farndale, *Collagens and atherosclerosis.* Exp Gerontol, 1999. **34**(4): p. 513-25.
25. Liu, X., et al., *Type III collagen is crucial for collagen I fibrillogenesis and for normal cardiovascular development.* Proc Natl Acad Sci U S A, 1997. **94**(5): p. 1852-6.
26. Marieb, E.N., *Essentials of human anatomy and physiology*. 7th edition ed. 2004.
27. Aoki, T., et al., *NF-kappaB is a key mediator of cerebral aneurysm formation.* Circulation, 2007. **116**(24): p. 2830-40.
28. Choi, K., et al., *A common precursor for hematopoietic and endothelial cells.* Development, 1998. **125**(4): p. 725-32.
29. Galley, H.F. and N.R. Webster, *Physiology of the endothelium.* Br J Anaesth, 2004. **93**(1): p. 105-13.
30. Bazzoni, G. and E. Dejana, *Endothelial cell-to-cell junctions: molecular organization and role in vascular homeostasis.* Physiol Rev, 2004. **84**(3): p. 869-901.
31. Molica, F., et al., *Connexins and Pannexins in Vascular Function and Disease.* Int J Mol Sci, 2018. **19**(6).
32. Yuan, S.Y. and R.R. Rigor, in *Regulation of Endothelial Barrier Function*. 2010: San Rafael (CA).
33. Zhao, X., et al., *Wall shear stress in major cerebral arteries as a function of age and gender--a study of 301 healthy volunteers.* J Neuroimaging, 2015. **25**(3): p. 403-7.
34. Ku, D.N., *BLOOD FLOW IN ARTERIES.* Annual Review of Fluid Mechanics, 1997. **29**(1): p. 399-434.
35. Langille, B.L., *Arterial remodeling: relation to hemodynamics.* Can J Physiol Pharmacol, 1996. **74**(7): p. 834-41.
36. Franzoni, M. and M.T. Walsh, *Towards the Identification of Hemodynamic Parameters Involved in Arteriovenous Fistula Maturation and Failure: A Review.* Cardiovasc Eng Technol, 2017. **8**(3): p. 342-356.
37. Sigovan, M., et al., *Vascular remodeling in autogenous arterio-venous fistulas by MRI and CFD.* Ann Biomed Eng, 2013. **41**(4): p. 657-68.
38. Langille, B.L. and F. O'Donnell, *Reductions in arterial diameter produced by chronic decreases in blood flow are endothelium-dependent.* Science, 1986. **231**(4736): p. 405-7.
39. White, C.R. and J.A. Frangos, *The shear stress of it all: the cell membrane and mechanochemical transduction.* Philos Trans R Soc Lond B Biol Sci, 2007. **362**(1484): p. 1459-67.
40. Givens, C. and E. Tzima, *Endothelial Mechanosignaling: Does One Sensor Fit All?* Antioxid Redox Signal, 2016. **25**(7): p. 373-88.
41. Chen, X., et al., *Cilia Control Vascular Mural Cell Recruitment in Vertebrates.* Cell Rep, 2017. **18**(4): p. 1033-1047.
42. Nauli, S.M., et al., *Endothelial cilia are fluid shear sensors that regulate calcium signaling and nitric oxide production through polycystin-1.* Circulation, 2008. **117**(9): p. 1161-71.
43. Liu, M., et al., *Primary Cilia Deficiency Induces Intracranial Aneurysm.* Shock, 2018. **49**(5): p. 604-611.
44. Lacolley, P., *Mechanical influence of cyclic stretch on vascular endothelial cells.* Cardiovasc Res, 2004. **63**(4): p. 577-9.

45. Jufri, N.F., et al., *Mechanical stretch: physiological and pathological implications for human vascular endothelial cells.* Vasc Cell, 2015. **7**: p. 8.
46. Florian, J.A., et al., *Heparan sulfate proteoglycan is a mechanosensor on endothelial cells.* Circ Res, 2003. **93**(10): p. e136-42.
47. Thi, M.M., et al., *The role of the glycocalyx in reorganization of the actin cytoskeleton under fluid shear stress: a "bumper-car" model.* Proc Natl Acad Sci U S A, 2004. **101**(47): p. 16483-8.
48. Wang, N., J.D. Tytell, and D.E. Ingber, *Mechanotransduction at a distance: mechanically coupling the extracellular matrix with the nucleus.* Nat Rev Mol Cell Biol, 2009. **10**(1): p. 75-82.
49. Diagbouga, M.R., et al., *Role of hemodynamics in initiation/growth of intracranial aneurysms.* Eur J Clin Invest, 2018. **48**(9): p. e12992.
50. Ortiz, P.A., N.J. Hong, and J.L. Garvin, *Luminal flow induces eNOS activation and translocation in the rat thick ascending limb.* Am J Physiol Renal Physiol, 2004. **287**(2): p. F274-80.
51. Partovian, C., et al., *PKCalpha activates eNOS and increases arterial blood flow in vivo.* Circ Res, 2005. **97**(5): p. 482-7.
52. Sangwung, P., et al., *KLF2 and KLF4 control endothelial identity and vascular integrity.* JCI Insight, 2017. **2**(4): p. e91700.
53. Satta, S., et al., *The Role of Nrf2 in Cardiovascular Function and Disease.* Oxid Med Cell Longev, 2017. **2017**: p. 9237263.
54. Zhou, J., Y.S. Li, and S. Chien, *Shear stress-initiated signaling and its regulation of endothelial function.* Arterioscler Thromb Vasc Biol, 2014. **34**(10): p. 2191-8.
55. Dimmeler, S., et al., *Activation of nitric oxide synthase in endothelial cells by Akt-dependent phosphorylation.* Nature, 1999. **399**(6736): p. 601-5.
56. Fisslthaler, B., et al., *Inhibition of endothelial nitric oxide synthase activity by proline-rich tyrosine kinase 2 in response to fluid shear stress and insulin.* Circ Res, 2008. **102**(12): p. 1520-8.
57. Young, A., et al., *Flow activation of AMP-activated protein kinase in vascular endothelium leads to Kruppel-like factor 2 expression.* Arterioscler Thromb Vasc Biol, 2009. **29**(11): p. 1902-8.
58. Wu, W., et al., *Flow-Dependent Regulation of Kruppel-Like Factor 2 Is Mediated by MicroRNA-92a.* Circulation, 2011. **124**(5): p. 633-41.
59. Ramkhelawon, B., et al., *Shear stress regulates angiotensin type 1 receptor expression in endothelial cells.* Circ Res, 2009. **105**(9): p. 869-75.
60. Koller, A. and G. Kaley, *Prostaglandins mediate arteriolar dilation to increased blood flow velocity in skeletal muscle microcirculation.* Circ Res, 1990. **67**(2): p. 529-34.
61. Sun, D., et al., *Enhanced release of prostaglandins contributes to flow-induced arteriolar dilation in eNOS knockout mice.* Circ Res, 1999. **85**(3): p. 288-93.
62. Sun, D., et al., *COX-2 contributes to the maintenance of flow-induced dilation in arterioles of eNOS-knockout mice.* Am J Physiol Heart Circ Physiol, 2006. **291**(3): p. H1429-35.
63. Bergh, N., et al., *Influence of TNF-alpha and biomechanical stress on endothelial anti- and prothrombotic genes.* Biochem Biophys Res Commun, 2009. **385**(3): p. 314-8.
64. Ni, C.W., et al., *Activation of PKC-epsilon and ERK1/2 participates in shear-induced endothelial MCP-1 expression that is repressed by nitric oxide.* J Cell Physiol, 2003. **195**(3): p. 428-34.
65. Gongol, B., et al., *AMPKalpha2 exerts its anti-inflammatory effects through PARP-1 and Bcl-6.* Proc Natl Acad Sci U S A, 2013. **110**(8): p. 3161-6.

66. Lin, K., et al., *Molecular mechanism of endothelial growth arrest by laminar shear stress.* Proc Natl Acad Sci U S A, 2000. **97**(17): p. 9385-9.
67. Akimoto, S., et al., *Laminar shear stress inhibits vascular endothelial cell proliferation by inducing cyclin-dependent kinase inhibitor p21(Sdi1/Cip1/Waf1).* Circ Res, 2000. **86**(2): p. 185-90.
68. Dimmeler, S., et al., *Upregulation of superoxide dismutase and nitric oxide synthase mediates the apoptosis-suppressive effects of shear stress on endothelial cells.* Arterioscler Thromb Vasc Biol, 1999. **19**(3): p. 656-64.
69. Tanweer, O., et al., *A comparative review of the hemodynamics and pathogenesis of cerebral and abdominal aortic aneurysms: lessons to learn from each other.* J Cerebrovasc Endovasc Neurosurg, 2014. **16**(4): p. 335-49.
70. Cuhlmann, S., et al., *Disturbed blood flow induces RelA expression via c-Jun N-terminal kinase 1: a novel mode of NF-kappaB regulation that promotes arterial inflammation.* Circ Res, 2011. **108**(8): p. 950-9.
71. Xiao, H., et al., *Sterol regulatory element binding protein 2 activation of NLRP3 inflammasome in endothelium mediates hemodynamic-induced atherosclerosis susceptibility.* Circulation, 2013. **128**(6): p. 632-42.
72. Wang, C., et al., *Endothelial cell sensing of flow direction.* Arterioscler Thromb Vasc Biol, 2013. **33**(9): p. 2130-6.
73. Ni, C.W., et al., *Discovery of novel mechanosensitive genes in vivo using mouse carotid artery endothelium exposed to disturbed flow.* Blood, 2010. **116**(15): p. e66-73.
74. Mullick, A.E., et al., *Increased endothelial expression of Toll-like receptor 2 at sites of disturbed blood flow exacerbates early atherogenic events.* J Exp Med, 2008. **205**(2): p. 373-83.
75. Chang, K., et al., *Bone morphogenic protein antagonists are coexpressed with bone morphogenic protein 4 in endothelial cells exposed to unstable flow in vitro in mouse aortas and in human coronary arteries: role of bone morphogenic protein antagonists in inflammation and atherosclerosis.* Circulation, 2007. **116**(11): p. 1258-66.
76. Mohan, S., et al., *Low shear stress preferentially enhances IKK activity through selective sources of ROS for persistent activation of NF-kappaB in endothelial cells.* Am J Physiol Cell Physiol, 2007. **292**(1): p. C362-71.
77. Passerini, A.G., et al., *Coexisting proinflammatory and antioxidative endothelial transcription profiles in a disturbed flow region of the adult porcine aorta.* Proc Natl Acad Sci U S A, 2004. **101**(8): p. 2482-7.
78. Sorescu, G.P., et al., *Bone morphogenic protein 4 produced in endothelial cells by oscillatory shear stress stimulates an inflammatory response.* J Biol Chem, 2003. **278**(33): p. 31128-35.
79. Zhou, J., et al., *MicroRNA-21 targets peroxisome proliferators-activated receptor-alpha in an autoregulatory loop to modulate flow-induced endothelial inflammation.* Proc Natl Acad Sci U S A, 2011. **108**(25): p. 10355-60.
80. Lee, D.Y., et al., *Role of histone deacetylases in transcription factor regulation and cell cycle modulation in endothelial cells in response to disturbed flow.* Proc Natl Acad Sci U S A, 2012. **109**(6): p. 1967-72.
81. Zhou, J., et al., *BMP receptor-integrin interaction mediates responses of vascular endothelial Smad1/5 and proliferation to disturbed flow.* J Thromb Haemost, 2013. **11**(4): p. 741-55.
82. Magid, R. and P.F. Davies, *Endothelial protein kinase C isoform identity and differential activity of PKCzeta in an athero-susceptible region of porcine aorta.* Circ Res, 2005. **97**(5): p. 443-9.

83. Heo, K.S., et al., *PKCzeta mediates disturbed flow-induced endothelial apoptosis via p53 SUMOylation.* J Cell Biol, 2011. **193**(5): p. 867-84.
84. Garin, G., et al., *Flow antagonizes TNF-alpha signaling in endothelial cells by inhibiting caspase-dependent PKC zeta processing.* Circ Res, 2007. **101**(1): p. 97-105.
85. Dolan, J.M., et al., *High fluid shear stress and spatial shear stress gradients affect endothelial proliferation, survival, and alignment.* Ann Biomed Eng, 2011. **39**(6): p. 1620-31.
86. Alfano, J.M., et al., *Intracranial aneurysms occur more frequently at bifurcation sites that typically experience higher hemodynamic stresses.* Neurosurgery, 2013. **73**(3): p. 497-505.
87. Meng, H., et al., *A model system for mapping vascular responses to complex hemodynamics at arterial bifurcations in vivo.* Neurosurgery, 2006. **59**(5): p. 1094-100; discussion 1100-1.
88. Meng, H., et al., *High WSS or low WSS? Complex interactions of hemodynamics with intracranial aneurysm initiation, growth, and rupture: toward a unifying hypothesis.* AJNR Am J Neuroradiol, 2014. **35**(7): p. 1254-62.
89. Meng, H., et al., *Complex hemodynamics at the apex of an arterial bifurcation induces vascular remodeling resembling cerebral aneurysm initiation.* Stroke, 2007. **38**(6): p. 1924-31.
90. Metaxa, E., et al., *Characterization of critical hemodynamics contributing to aneurysmal remodeling at the basilar terminus in a rabbit model.* Stroke, 2010. **41**(8): p. 1774-82.
91. Staarmann, B., M. Smith, and C.J. Prestigiacomo, *Shear stress and aneurysms: a review.* Neurosurg Focus, 2019. **47**(1): p. E2.
92. Wang, Z., et al., *Molecular alterations associated with aneurysmal remodeling are localized in the high hemodynamic stress region of a created carotid bifurcation.* Neurosurgery, 2009. **65**(1): p. 169-77; discussion 177-8.
93. Gao, L., et al., *Nascent aneurysm formation at the basilar terminus induced by hemodynamics.* Stroke, 2008. **39**(7): p. 2085-90.
94. Kolega, J., et al., *Cellular and molecular responses of the basilar terminus to hemodynamics during intracranial aneurysm initiation in a rabbit model.* J Vasc Res, 2011. **48**(5): p. 429-42.
95. Dolan, J.M., et al., *Endothelial cells express a unique transcriptional profile under very high wall shear stress known to induce expansive arterial remodeling.* Am J Physiol Cell Physiol, 2012. **302**(8): p. C1109-18.
96. Dolan, J.M., et al., *Differential gene expression by endothelial cells under positive and negative streamwise gradients of high wall shear stress.* Am J Physiol Cell Physiol, 2013. **305**(8): p. C854-66.
97. Moake, J.L., et al., *Involvement of large plasma von Willebrand factor (vWF) multimers and unusually large vWF forms derived from endothelial cells in shear stress-induced platelet aggregation.* J Clin Invest, 1986. **78**(6): p. 1456-61.
98. Huang, W., et al., *Role of paxillin in the early phase of orientation of the vascular endothelial cells exposed to cyclic stretching.* Biochem Biophys Res Commun, 2012. **418**(4): p. 708-13.
99. Yoshigi, M., E.B. Clark, and H.J. Yost, *Quantification of stretch-induced cytoskeletal remodeling in vascular endothelial cells by image processing.* Cytometry A, 2003. **55**(2): p. 109-18.
100. Naruse, K., T. Yamada, and M. Sokabe, *Involvement of SA channels in orienting response of cultured endothelial cells to cyclic stretch.* Am J Physiol, 1998. **274**(5): p. H1532-8.

101. Shi, F., et al., *Down-regulation of ERK but not MEK phosphorylation in cultured endothelial cells by repeated changes in cyclic stretch.* Cardiovasc Res, 2007. **73**(4): p. 813-22.
102. Osawa, M., et al., *Evidence for a role of platelet endothelial cell adhesion molecule-1 in endothelial cell mechanosignal transduction: is it a mechanoresponsive molecule?* J Cell Biol, 2002. **158**(4): p. 773-85.
103. Ueki , Y.S., Naoya. Ohashi, Toshiro. Sato, Masaaki., *Morphological Responses of Vascular Endothelial Cells Induced by Local Stretch Transmitted Through Intercellular Junctions.* Experimental Mechanics, 2009. **49** p. 125–134.
104. Michel, J.B., *Anoikis in the cardiovascular system: known and unknown extracellular mediators.* Arterioscler Thromb Vasc Biol, 2003. **23**(12): p. 2146-54.
105. Wang, B.W., et al., *Induction of matrix metalloproteinases-14 and -2 by cyclical mechanical stretch is mediated by tumor necrosis factor-alpha in cultured human umbilical vein endothelial cells.* Cardiovasc Res, 2003. **59**(2): p. 460-9.
106. Hu, Z., et al., *Acute mechanical stretch promotes eNOS activation in venous endothelial cells mainly via PKA and Akt pathways.* PLoS One, 2013. **8**(8): p. e71359.
107. Toda, M., et al., *Differential gene responses in endothelial cells exposed to a combination of shear stress and cyclic stretch.* J Biotechnol, 2008. **133**(2): p. 239-44.
108. Fisslthaler, B., et al., *Cyclic stretch enhances the expression and activity of coronary endothelium-derived hyperpolarizing factor synthase.* Hypertension, 2001. **38**(6): p. 1427-32.
109. Cheng, T.H., et al., *Reactive oxygen species mediate cyclic strain-induced endothelin-1 gene expression via Ras/Raf/extracellular signal-regulated kinase pathway in endothelial cells.* J Mol Cell Cardiol, 2001. **33**(10): p. 1805-14.
110. Takeda, H., et al., *Bi-phasic activation of eNOS in response to uni-axial cyclic stretch is mediated by differential mechanisms in BAECs.* Life Sci, 2006. **79**(3): p. 233-9.
111. Thompson, M.M. and P.R. Bell, *ABC of arterial and venous disease. Arterial aneurysms.* BMJ, 2000. **320**(7243): p. 1193-6.
112. Vermeer, N.C., J.W. Elshof, and P.W. Vriens, *Clinical presentation, diagnosis, and treatment of venous aneurysms.* J Vasc Surg Venous Lymphat Disord, 2014. **2**(3): p. 349-353 e3.
113. Vlak, M.H., et al., *Trigger factors for rupture of intracranial aneurysms in relation to patient and aneurysm characteristics.* J Neurol, 2012. **259**(7): p. 1298-302.
114. Brisman, J.L., J.K. Song, and D.W. Newell, *Cerebral aneurysms.* N Engl J Med, 2006. **355**(9): p. 928-39.
115. Seibert, B., et al., *Intracranial aneurysms: review of current treatment options and outcomes.* Front Neurol, 2011. **2**: p. 45.
116. Tutino, V.M., et al., *Circulating neutrophil transcriptome may reveal intracranial aneurysm signature.* PLoS One, 2018. **13**(1): p. e0191407.
117. Stehbens, W.E., *Histopathology of cerebral aneurysms.* Arch Neurol, 1963. **8**: p. 272-85.
118. Wang, S., et al., *Rabbit aneurysm models mimic histologic wall types identified in human intracranial aneurysms.* J Neurointerv Surg, 2018. **10**(4): p. 411-415.
119. Aoki, T., et al., *Macrophage-derived matrix metalloproteinase-2 and -9 promote the progression of cerebral aneurysms in rats.* Stroke, 2007. **38**(1): p. 162-9.
120. Aoki, T., et al., *Impact of monocyte chemoattractant protein-1 deficiency on cerebral aneurysm formation.* Stroke, 2009. **40**(3): p. 942-51.
121. Jamous, M.A., et al., *Endothelial injury and inflammatory response induced by hemodynamic changes preceding intracranial aneurysm formation: experimental study in rats.* J Neurosurg, 2007. **107**(2): p. 405-11.

122. Jamous, M.A., et al., *Vascular corrosion casts mirroring early morphological changes that lead to the formation of saccular cerebral aneurysm: an experimental study in rats.* J Neurosurg, 2005. **102**(3): p. 532-5.
123. Koseki, H., et al., *Two Diverse Hemodynamic Forces, a Mechanical Stretch and a High Wall Shear Stress, Determine Intracranial Aneurysm Formation.* Transl Stroke Res, 2019.
124. Frosen, J., et al., *Flow-induced, inflammation-mediated arterial wall remodeling in the formation and progression of intracranial aneurysms.* Neurosurg Focus, 2019. **47**(1): p. E21.
125. Cebral, J., et al., *Flow Conditions in the Intracranial Aneurysm Lumen Are Associated with Inflammation and Degenerative Changes of the Aneurysm Wall.* AJNR Am J Neuroradiol, 2017. **38**(1): p. 119-126.
126. Shirai, T., et al., *Macrophages in vascular inflammation--From atherosclerosis to vasculitis.* Autoimmunity, 2015. **48**(3): p. 139-51.
127. Cebral, J.R., M. Sheridan, and C.M. Putman, *Hemodynamics and bleb formation in intracranial aneurysms.* AJNR Am J Neuroradiol, 2010. **31**(2): p. 304-10.
128. Mizoi, K., T. Yoshimoto, and Y. Nagamine, *Types of unruptured cerebral aneurysms reviewed from operation video-recordings.* Acta Neurochir (Wien), 1996. **138**(8): p. 965-9.
129. Asari, S. and T. Ohmoto, *Long-term outcome of surgically treated unruptured cerebral aneurysms.* Clin Neurol Neurosurg, 1994. **96**(3): p. 230-5.
130. Inagawa, T. and A. Hirano, *Autopsy study of unruptured incidental intracranial aneurysms.* Surg Neurol, 1990. **34**(6): p. 361-5.
131. Horie, N., et al., *Detection of blood blister-like aneurysm and intramural hematoma with high-resolution magnetic resonance imaging.* J Neurosurg, 2011. **115**(6): p. 1206-9.
132. Barrett, H.E., et al., *Calcification Volume Reduces Stretch Capability and Predisposes Plaque to Rupture in an in vitro Model of Carotid Artery Stenting.* Eur J Vasc Endovasc Surg, 2017. **54**(4): p. 431-438.
133. Ramella, M., et al., *Effect of Cyclic Stretch on Vascular Endothelial Cells and Abdominal Aortic Aneurysm (AAA): Role in the Inflammatory Response.* Int J Mol Sci, 2019. **20**(2).
134. Schievink, W.I., et al., *Circumstances surrounding aneurysmal subarachnoid hemorrhage.* Surg Neurol, 1989. **32**(4): p. 266-72.
135. Etminan, N. and G.J. Rinkel, *Unruptured intracranial aneurysms: development, rupture and preventive management.* Nat Rev Neurol, 2016. **12**(12): p. 699-713.
136. Schatlo, B., et al., *Introducing a nationwide registry: the Swiss study on aneurysmal subarachnoid haemorrhage (Swiss SOS).* Acta Neurochir (Wien), 2012. **154**(12): p. 2173-8; discussion 2178.
137. Kotowski, M., et al., *Safety and occlusion rates of surgical treatment of unruptured intracranial aneurysms: a systematic review and meta-analysis of the literature from 1990 to 2011.* J Neurol Neurosurg Psychiatry, 2013. **84**(1): p. 42-8.
138. Naggara, O.N., et al., *Endovascular treatment of intracranial unruptured aneurysms: systematic review and meta-analysis of the literature on safety and efficacy.* Radiology, 2010. **256**(3): p. 887-97.
139. Greving, J.P., et al., *Development of the PHASES score for prediction of risk of rupture of intracranial aneurysms: a pooled analysis of six prospective cohort studies.* Lancet Neurol, 2014. **13**(1): p. 59-66.

140. Bijlenga, P., et al., *PHASES Score for the Management of Intracranial Aneurysm: A Cross-Sectional Population-Based Retrospective Study.* Stroke, 2017. **48**(8): p. 2105-2112.
141. Etminan, N., et al., *The unruptured intracranial aneurysm treatment score: a multidisciplinary consensus.* Neurology, 2015. **85**(10): p. 881-9.
142. Backes, D., et al., *Patient- and Aneurysm-Specific Risk Factors for Intracranial Aneurysm Growth: A Systematic Review and Meta-Analysis.* Stroke, 2016. **47**(4): p. 951-7.
143. Frosen, J. and A. Joutel, *Smooth muscle cells of intracranial vessels: from development to disease.* Cardiovasc Res, 2018. **114**(4): p. 501-512.
144. Zhou, S., P.A. Dion, and G.A. Rouleau, *Genetics of Intracranial Aneurysms.* Stroke, 2018. **49**(3): p. 780-787.
145. Sanchis, I.M., et al., *Presymptomatic Screening for Intracranial Aneurysms in Patients with Autosomal Dominant Polycystic Kidney Disease.* Clin J Am Soc Nephrol, 2019. **14**(8): p. 1151-1160.
146. Krishnappa, V., et al., *Autosomal dominant polycystic kidney disease and the heart and brain.* Cleve Clin J Med, 2017. **84**(6): p. 471-481.
147. Lemos, F.O. and B.E. Ehrlich, *Polycystin and calcium signaling in cell death and survival.* Cell Calcium, 2018. **69**: p. 37-45.
148. Luciano, R.L. and N.K. Dahl, *Extra-renal manifestations of autosomal dominant polycystic kidney disease (ADPKD): considerations for routine screening and management.* Nephrol Dial Transplant, 2014. **29**(2): p. 247-54.
149. Raptis, V., C. Loutradis, and P.A. Sarafidis, *Renal injury progression in autosomal dominant polycystic kidney disease: a look beyond the cysts.* Nephrol Dial Transplant, 2018. **33**(11): p. 1887-1895.
150. Klawitter, J., et al., *Endothelial dysfunction and oxidative stress in polycystic kidney disease.* Am J Physiol Renal Physiol, 2014. **307**(11): p. F1198-206.
151. Kuo, I.Y. and A. Chapman, *Intracranial Aneurysms in ADPKD How Far Have We Come?* Clinical Journal of American Society of Nephrology, 2019. **14**: p. 1119–1121.
152. Dummer, A., et al., *Measuring the primary cilium length: improved method for unbiased high-throughput analysis.* Cilia, 2016. **5**: p. 7.
153. Pazour, G.J., et al., *Chlamydomonas IFT88 and its mouse homologue, polycystic kidney disease gene tg737, are required for assembly of cilia and flagella.* J Cell Biol, 2000. **151**(3): p. 709-18.
154. Su, Q., et al., *Structure of the human PKD1-PKD2 complex.* Science, 2018. **361**(6406).
155. AbouAlaiwi, W.A., et al., *Ciliary polycystin-2 is a mechanosensitive calcium channel involved in nitric oxide signaling cascades.* Circ Res, 2009. **104**(7): p. 860-9.
156. Chauvet, V., et al., *Mechanical stimuli induce cleavage and nuclear translocation of the polycystin-1 C terminus.* J Clin Invest, 2004. **114**(10): p. 1433-43.
157. Delmas, P., et al., *Constitutive activation of G-proteins by polycystin-1 is antagonized by polycystin-2.* J Biol Chem, 2002. **277**(13): p. 11276-83.
158. Hanaoka, K., et al., *Co-assembly of polycystin-1 and -2 produces unique cation-permeable currents.* Nature, 2000. **408**(6815): p. 990-4.
159. Iomini, C., et al., *Primary cilia of human endothelial cells disassemble under laminar shear stress.* J Cell Biol, 2004. **164**(6): p. 811-7.
160. Van der Heiden, K., et al., *Monocilia on chicken embryonic endocardium in low shear stress areas.* Dev Dyn, 2006. **235**(1): p. 19-28.
161. Aboualaiwi, W.A., et al., *Survivin-induced abnormal ploidy contributes to cystic kidney and aneurysm formation.* Circulation, 2014. **129**(6): p. 660-72.

162. Nauli, S.M., et al., *Polycystins 1 and 2 mediate mechanosensation in the primary cilium of kidney cells.* Nat Genet, 2003. **33**(2): p. 129-37.
163. Van der Heiden, K., et al., *Role for primary cilia as flow detectors in the cardiovascular system.* Int Rev Cell Mol Biol, 2011. **290**: p. 87-119.
164. Pala, R., et al., *The Roles of Primary Cilia in Cardiovascular Diseases.* Cells, 2018. **7**(12).
165. Jones, T.J., et al., *Primary cilia regulates the directional migration and barrier integrity of endothelial cells through the modulation of hsp27 dependent actin cytoskeletal organization.* J Cell Physiol, 2012. **227**(1): p. 70-6.
166. Yamamoto, R., et al., *A sphingosine-1-phosphate receptor type 1 agonist, ASP4058, suppresses intracranial aneurysm through promoting endothelial integrity and blocking macrophage transmigration.* Br J Pharmacol, 2017. **174**(13): p. 2085-2101.
167. Dinsmore, C. and J.F. Reiter, *Endothelial primary cilia inhibit atherosclerosis.* EMBO Rep, 2016. **17**(2): p. 156-66.
168. Sanchez-Duffhues, G., et al., *SLUG is expressed in endothelial cells lacking primary cilia to promote cellular calcification.* Arterioscler Thromb Vasc Biol, 2015. **35**(3): p. 616-27.
169. Frosen, J., et al., *Remodeling of saccular cerebral artery aneurysm wall is associated with rupture: histological analysis of 24 unruptured and 42 ruptured cases.* Stroke, 2004. **35**(10): p. 2287-93.
170. Hashimoto, N., H. Handa, and F. Hazama, *Experimentally induced cerebral aneurysms in rats.* Surg Neurol, 1978. **10**(1): p. 3-8.
171. Altes, T.A., et al., *1999 ARRS Executive Council Award. Creation of saccular aneurysms in the rabbit: a model suitable for testing endovascular devices. American Roentgen Ray Society.* AJR Am J Roentgenol, 2000. **174**(2): p. 349-54.
172. Frosen, J., et al., *Contribution of mural and bone marrow-derived neointimal cells to thrombus organization and wall remodeling in a microsurgical murine saccular aneurysm model.* Neurosurgery, 2006. **58**(5): p. 936-44; discussion 936-44.
173. Hashimoto, N., et al., *Experimental induction of cerebral aneurysms in monkeys.* J Neurosurg, 1987. **67**(6): p. 903-5.
174. Coutard, M., *Experimental cerebral aneurysms in the female heterozygous Blotchy mouse.* Int J Exp Pathol, 1999. **80**(6): p. 357-67.
175. Morimoto, M., et al., *Mouse model of cerebral aneurysm: experimental induction by renal hypertension and local hemodynamic changes.* Stroke, 2002. **33**(7): p. 1911-5.
176. Moriwaki, T., et al., *Impaired progression of cerebral aneurysms in interleukin-1beta-deficient mice.* Stroke, 2006. **37**(3): p. 900-5.
177. Abruzzo, T., et al., *Cerebral aneurysm formation in nitric oxide synthase-3 knockout mice.* Curr Neurovasc Res, 2007. **4**(3): p. 161-9.
178. Nuki, Y., et al., *Elastase-induced intracranial aneurysms in hypertensive mice.* Hypertension, 2009. **54**(6): p. 1337-44.
179. Makino, H., et al., *Pharmacological stabilization of intracranial aneurysms in mice: a feasibility study.* Stroke, 2012. **43**(9): p. 2450-6.
180. Hosaka, K., et al., *Modified murine intracranial aneurysm model: aneurysm formation and rupture by elastase and hypertension.* J Neurointerv Surg, 2014. **6**(6): p. 474-9.

Chapter 2: Correlating Clinical Risk Factors and Histological Features in Ruptured and Unruptured Human Intracranial Aneurysms: The Swiss AneuX Study

 # Original manuscript 1

Many studies have put efforts on the understanding of the course of IA disease. The combination of clinical observations, computational approaches and biological analyzes has highlighted some key factors in IA disease, which allows the establishment of guidelines for decision of treatment (or not) of IAs. However, the large number of confounding variables (yet probably not all known) that can influence IA progression challenge the decryption of the pathophysiology. The aneurysm wall histological characteristics show explicitly the state of vascular remodeling. We hypothesized that histological features may serve as a biomarker and may contribute to the stratification of the risk of rupture. In this second chapter, I present patient and aneurysm characteristics from the AneuX biobank. We compared ruptured IAs against unruptured IAs to determine the different aspects that may drain towards the rupture. Histological features were then correlated to clinical risk factors.

Personal contribution: In the framework of the AneuX project, I have helped to establish a biobank of human IA. I participated to setting up the logistics of IA dome collection during/after surgery, the optimization of sample handling and processing into paraffin sections. In addition, I help to optimize (immuno-)histochemical protocols and have performed a number of the immunostainings on the samples presented in the publication (Figures 2,4,5). Lastly, I helped in the editing of the manuscript, under the supervision of Prof. Brenda KWAK.

Manuscript Status: The manuscript has been published in the Journal of Neuropathology & Experimental Neurology https://doi.org/10.1093/jnen/nly031

J Neuropathol Exp Neurol
Vol. 77, No. 7, July 2018, pp. 555–566
doi: 10.1093/jnen/nly031

ORIGINAL ARTICLE

Correlating Clinical Risk Factors and Histological Features in Ruptured and Unruptured Human Intracranial Aneurysms: The Swiss AneuX Study

Sandrine Morel, PhD, Mannekomba R. Diagbouga, MSc, Nicolas Dupuy, Esther Sutter, Vincent Braunersreuther, PhD, Graziano Pelli, Marco Corniola, MD, Renato Gondar, MD, Max Jägersberg, MD, Nathalie Isidor, Karl Schaller, MD, Marie-Luce Bochaton-Piallat, PhD, Philippe Bijlenga, MD-PhD, and Brenda R. Kwak, PhD

Abstract

Pathogenesis of intracranial aneurysm is complex and the precise biomechanical processes leading to their rupture are uncertain. The goal of our study was to characterize the aneurysmal wall histologically and to correlate histological characteristics with clinical and radiological factors used to estimate the risk of rupture. A new biobank of aneurysm domes resected at the Geneva University Hospitals (Switzerland) was used. Histological analysis revealed that unruptured aneurysms have a higher smooth muscle cell (SMC) content and a lower macrophage content than ruptured domes. These differences were associated with more collagen in unruptured samples, whereas the elastin content was not affected. Collagen content and type distribution were different between thick and thin walls of unruptured aneurysms. Classification of aneurysm domes based on histological characteristics showed that unruptured samples present organized wall rich in endothelial and SMCs compared with ruptured samples. Finally, aneurysm wall composition was altered in unruptured domes of patients presenting specific clinical factors used to predict rupture such as large dome diameter, dome irregularities, and smoking. Our study shows that the wall of aneurysm suspected to be at risk for rupture undergoes structural alterations relatively well associated with clinical and radiological factors currently used to predict this risk.

From the Department of Pathology and Immunology, Faculty of Medicine, University of Geneva, Geneva, Switzerland (SM, MRD, ND, ES, GP, MLBP, BRK); Neurosurgery Division, Department of Clinical Neurosciences, Faculty of Medicine, Geneva University Hospitals, Geneva, Switzerland (SM, ND, MC, RG, MJ, NI, KS, PB); Department of Clinical Pathology, Faculty of Medicine, University of Geneva and Geneva University Hospitals, Geneva, Switzerland (VB); Clinical Trial Unit, Faculty of Medicine, Geneva University Hospitals, Geneva, Switzerland (NI); and Department of Medical Specializations – Cardiology, Faculty of Medicine, University of Geneva, Geneva, Switzerland (BRK).

Send correspondence to: Sandrine Morel, PhD, Department of Pathology and Immunology, Centre Médical Universitaire, Rue Michel-Servet, 1 F06.2767.a, 1211 Geneva, Switzerland; E-mail: sandrine.morel@unige.ch

This study was supported by grants from the Swiss SystemsX.ch initiative, evaluated by the Swiss National Science Foundation (to PB and BRK) and the Foundation Carlos et Elsie De Reuter (to BRK and PB).

The authors have no duality or conflicts of interest to declare.

Key Words: Collagen, Endothelial cells, Intracranial aneurysm, Risk factors, Smooth muscle cells, Wall thickness.

INTRODUCTION

Intracranial aneurysm (IA) formation results from the deformation and the enlargement of the arterial lumen. IAs are mostly quiescent and asymptomatic but their rupture induces severe brain damage and death. The prevalence of IAs is high (2%–5%) and they most frequently affect middle-aged females (median at 50 years). The incidence of IA rupture is estimated at 9/100 000 inhabitants per year in western populations (1). In Switzerland, IA rupture results in 13.3% patients recovering with no residual symptoms, 54% patients getting back to an independent life, 31% severely disabled patients, and 15% death (2). One third of the patients suffer from multiple IAs. The risk of rupture is associated with factors of the IA itself such as location, size or presence of dome irregularities, and patient-related factors including ethnicity, age, hypertension, or smoking (3–7).

As may be predicted from the discrepancy between the high prevalence of IAs and the low incidence of IA rupture, subarachnoid hemorrhage (SAH) will not occur during the lifetime of 50% of the patients diagnosed with an IA (1). Treatment of unruptured IAs requires a perilous intervention that induces patient's disability for several months (5%–7% morbidity) and also death in the worst case (1%–4% mortality) (8–10). As an increasing number of patients face the need to decide whether or not to risk an intervention, it is extremely important to better define the characteristics of rupture-prone IAs, and to find appropriate clinical and radiological markers to determine IA rupture risk.

The pathogenesis of IA formation and growth is complex and the precise biomechanical processes leading to IA wall rupture are not yet known. Several studies have shown that lack of internal elastic lamina, erosion of luminal endothelium, infiltration of inflammatory cells, loss of smooth muscle cells (SMCs), destruction of the extracellular matrix (ECM),

© 2018 American Association of Neuropathologists, Inc.
This is an Open Access article distributed under the terms of the Creative Commons Attribution Non-Commercial License (http://creativecommons.org/licenses/by-nc/4.0/), which permits non-commercial re-use, distribution, and reproduction in any medium, provided the original work is properly cited. For commercial re-use, please contactjournals.permissions@oup.com

activation of the innate immunity, calcification, or lipid accumulation are associated with IA wall degeneration and rupture (11–16). Although these studies have increased our knowledge on aneurysm wall characteristics, these isolated postsurgical observations have been of limited help for the clinician to predict whether an IA should be treated or not. There remains an urgent need for diagnostic markers to estimate the risk of IA rupture. The goal of our study was to characterize the aneurysmal wall histologically and to directly correlate histological features with clinical and radiological factors classically used to estimate the risk of IA rupture. In the context of the AneuX project (17), a new biobank of ruptured IA (R-IA) and unruptured IA (UR-IA) domes resected during neurosurgical clipping at the Geneva University Hospitals in Switzerland was used.

MATERIALS AND METHODS

Clinical and Radiological Data

Patients have been recruited at the Geneva University Hospitals. The inclusion criteria were as follows: 1) IA identified on the basis of angiographic appearance (3D-Digital Subtraction Angiography [3D-DSA], 3D-Magnetic Resonance Angiogram [3D-MRA], or 3D-Computed Tomography Angiogram [3D-CTA]) as well as availability of surgical documentation; 2) age older than 18 years; and 3) patient to provide informed consent. The exclusion criteria were as follows: 1) lack of angiographically proven IA on 3D-DSA, 3D-MRA, or 3D-CTA; 2) failure to contribute to clinical data; 3) age younger than 18 years; and 4) refusal to provide informed consent. The study was approved by the Ethical Committee of the Geneva University Hospitals, Geneva, Switzerland (Geneva Local Ethical Authorization reference CER 07-056 [NAC 07-020, @neurIST (18)]). All patients consented their data and biological samples to be used for research in the field of cerebrovascular diseases according to the information and consent forms. Procedures were in accordance with the Helsinki Declaration of the World Medical Association.

For all recruited patients, available baseline characteristics were collected including: 1) Age of the patient when IA was discovered or when IA ruptured; 2) Sex of the patient; 3) Clinical history for IA: (i) presence of multiple IAs; (ii) previous aneurysmal SAH from another IA or from the same IA; (iii) positive familial history for IA: one or more 1st degree relative(s) with IA; 4) Risk factors for IA: smoking status defined as (i) never smoked: never smoked >300 cigarettes ever; (ii) current smoker: smoked >300 cigarettes and continues current smoking; (iii) former smoker: smoked >300 cigarettes and stopped at least 6 months ago. Arterial hypertension is defined as blood pressure >140/90 mmHg independently of the existence or not of a treatment against hypertension; 5) For patients with SAH, the time between the first signs of rupture and the resection of the IA has been estimated as precisely as possible, and 2 periods were defined, that is, <2 days and >2 days.

On the basis of images obtained from 3D-MRA, 3D-CTA, and 3D-DSA, IA location was determined, IA morphological information such as presence of submillimetric irregularities (roughness), single or multiple blebs or lobules were obtained, and neck size and maximal dome diameter were measured, as previously described (19, 20).

Human Saccular IA Samples

Human saccular IA samples were obtained during microsurgery by resecting the aneurysmal dome after clipping of the aneurysmal neck (Fig. 1A–C). All samples were collected at the neurosurgery division of the Geneva University Hospitals and were stored following 2 different routines depending on the timing of IA resection. Four R-IAs and 8 UR-IAs stored in RNAlater stabilization solution (Qiagen, Hombrechtikon, Switzerland) at −80°C for several months were gently thawed on ice, fixed for 2 hours in formol and embedded in paraffin. Thirteen R-IAs and 23 UR-IAs were directly fixed in formol and stored at room temperature until embedding in paraffin. The percentage of samples stored in RNAlater stabilization solution was 24% in the ruptured group and 26% in the unruptured group. Detailed histological assessment of the tissue integrity associated with both routines showed that samples from both groups were similar. For example, intact nuclei were readily observed by hematoxylin and eosin staining in samples conserved in RNAlater stabilization solution (Fig. 1D, G) and in samples directly fixed in formol (Fig. 1J, M). Moreover, antibody-based immunohistological staining (see below) resulted in similar positive labeling between the 2 protocols (Fig. 1E, H, K, N as examples for α-smooth muscle actin [α-SMA] staining). Finally, histological staining performed to reveal the ECM showed equivalent patterns between the 2 methods (Fig. 1F, I, L, O as examples for Masson-trichrome staining).

Histology and Immunohistochemistry

IA domes were embedded in paraffin, sectioned at 5 µm and conserved at 4°C. For histology, aneurysmal dome sections were stained routinely with hematoxylin and eosin, Masson-trichrome (total collagen), Victoria blue (elastin) and with Picrosirius Red (type I and III collagen; Sigma–Aldrich, Buchs, Switzerland). For immunohistochemistry, sections were immunolabeled with antibodies recognizing α-SMA (mouse IgG2a antibody, clone 1A4 (21, 22); a general marker of SMCs), smooth muscle myosin heavy chains (SMMHC) types 1 and 2 (rabbit polyclonal antibody, BT-562, Biomedical Technologies, Inc., Stoughton, MA; a marker of well-differentiated SMCs), CD68 (mouse IgG1 antibody, clone KP1, Dako, Glostrup, Denmark; marker of macrophages), or CD31 (rabbit polyclonal antibody, clone pAK, Dianova, Hamburg, Germany; a marker of endothelial cells). Before using the first antibody, immunoreactivity was retrieved by microwave treatment (600 W, 5 minutes) in citrate buffer (10 mM, pH 6.0) for α-SMA and CD68, and by pressure cooker treatment (3 minutes) in citrate buffer for SMMHCs and CD31. Goat antimouse- or antirabbit-biotinylated IgGs (Dako) were used as secondary antibodies and the streptavidin-biotin peroxidase complex and 3, 3′-diamino-benzidine chromophore were used for visualization (EnVision system; Dako).

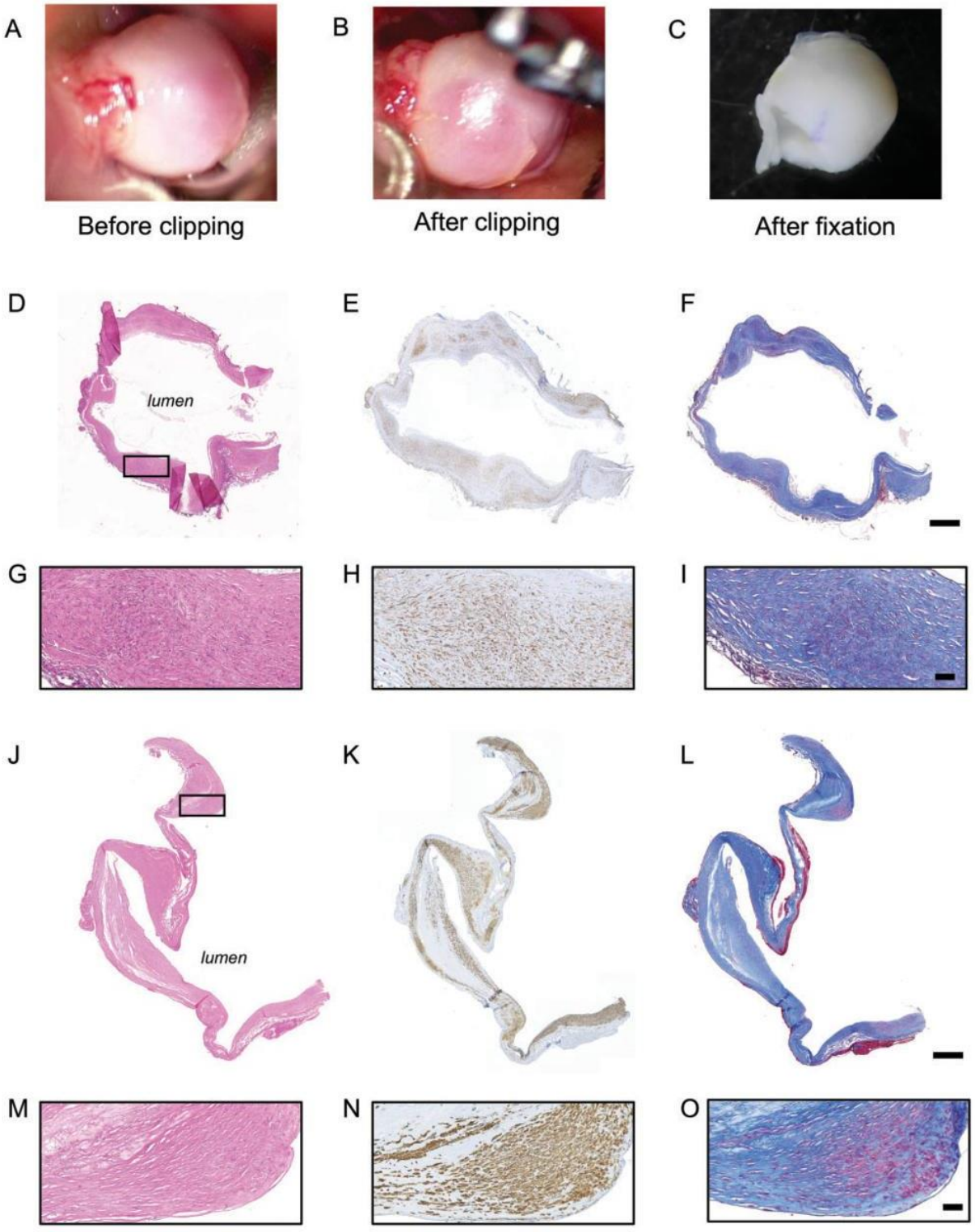

FIGURE 1. Sample preparation. Examples of intracranial aneurysm (IA) dome obtained during the surgery (before **[A]** and after **[B]** the clipping of the IA neck) and just before paraffin embedding **(C)**. Representative examples of H&E **(D, G, J, M)**, α-SMA (SMCs in brown, **E**, **H**, **K**, **N**) and Masson-trichrome (collagen in blue, **F**, **I**, **L**, **O**) stainings performed on IA domes stored in RNA latter solution **(D–I)** or directly fixed in formol **(J–O)**. The black rectangle in panels **D** and **J** represent the region of magnification for panels **G–I** and **M–O**. Scale bars: **D-F**, **J-L** = 500 μm; **G-I**, **M-O** = 50 μm.

Hemalun (Merck, Darmstadt, Germany) was used as counterstaining. All stainings were performed on consecutive sections.

Image Analyses

Sections were scanned at 10× magnification and high resolution using the fully automated slide scanner Axioscan.Z1 (Carl Zeiss Microscopy, Oberkochen, Germany) and images were processed using the software ZEN 2 (Carl Zeiss Microscopy). Depending on the size of the sample, 3–5 regions of interest (ROI) were manually determined for all aneurysms to cover almost the entire surface of the sample. The size of these ROIs was always identical (0.48 μm^2) and the ROI was placed at the same regions inside each aneurysm for the different stainings. Total tissue area and positive area in each ROI were quantified using the NIH Image software (NIH AutoExtractor 1.51; National Institutes of Health, Bethesda, MD) and the positive staining was expressed as a percentage of the total area. Results were calculated as the mean of the 3–5 ROIs for each staining.

To evaluate the relative contribution of type I and type III collagen in the aneurysm wall, sections stained with Picrosirius red were examined using polarized light on a Zeiss Axioskop 2 plus microscope and images were processed using the software AxioVision 4.8.10. Yellow-red birefringence and green birefringence were used to discriminate between type I and type III collagen fibers, respectively. As for all other stainings, total tissue area and positive area were quantified using the NIH Image software and the positive staining was expressed as a percentage of the total area. Results were calculated as the mean of the 3–5 ROIs.

To quantify endothelial cell coverage, using the NIH Image software, we determined the length of the intraluminal part positively stained for CD31 as a percentage of the total length of the intraluminal part of the resected dome.

Statistical Analyses

We calculated that a minimum of 16 IAs/group were needed to see a significant difference of 40% between the 2 groups with a significance level of 5% and a power of 90%. Results are shown in median (interquartile range), in percentage or in correlation. Comparisons of medians have been performed using a nonparametric Mann-Whitney *U* test. Comparisons of distributions have been performed using the Fisher exact test or Chi-square test. Spearman correlations were performed to examine association between variables. Differences were considered statistically significant at values of $p \leq 0.05$.

RESULTS

Patient and IA Characteristics

Patients with ruptured (n = 17) and unruptured (n = 30) IAs did not differ in age, sex, ethnicity, presence of multiple IAs, existence of a previous aneurysmal SAH, positive familial history for IA or SAH, smoking status or hypertension (Table 1). IA characteristics just before the surgery, that is, location, presence of irregularities (roughness, blebs, and lobules), neck size, and maximal dome diameter, were not different between R-IAs and UR-IAs (Table 2).

TABLE 1. Patient Characteristics at the Time of the Inclusion in the Study

	Ruptured IAs	Unruptured IAs	p value
Patients	n = 17	n = 30	
Age, years: median (IQR)	55 (44–64)	53 (44–64)	0.83
Sex, female: n (%)	14 (82)	22 (73)	0.72
Ethnicity: Eurasian: n (%)	15 (88)	30 (100)	0.13
Multiple aneurysms: n (%)	7 (41)	19 (63)	0.35
Previous aSAH: n (%)	1 (6)	4 (26)	0.64
Positive familial history for IA: n (%)	2 (12)	6 (23)	0.69
Smoker (former and current): n (%)	10 (59)	20 (67)	0.31
Hypertension: n (%)	5 (29)	15 (50)	0.35

Comparisons of medians and percentages have been performed using nonparametric Mann-Whitney *U* test or Fisher exact test, respectively.

Positive familial history for IA is defined as one or more 1st degree relative(s) with IA.

A current smoker is a patient currently smoking >300 cigarettes and a former smoker is a patient who smoked >300 cigarettes and who stopped at least 6 months ago.

Arterial hypertension is defined as blood pressure >140/90 mmHg independently of the existence or not of a treatment against hypertension.

ECM Content

Collagen content in IA wall was determined using 2 different staining protocols: Masson-trichrome allowing us to visualize total collagen in blue as well as Picrosirius red followed by polarized light examination to distinguish type I collagen fibers (in yellow-red) and type III collagen fibers (in green). We found that R-IAs contained less collagen (total, type I and type III) than UR-IAs (Fig. 2A–E). The relative contribution of type I and III collagens was similar between the 2 groups (Fig. 2F). In contrast to collagen content, the elastin content was not different between R-IAs and UR-IAs (Fig. 2G–H).

To determine whether the content in ECM was influenced by the thickness of the IA wall, we compared thick (tissue area >0.31 μm^2 in the defined ROI) to thin (tissue area <0.31 μm^2 in the defined ROI) aneurysmal wall regions. The cut-off of 0.31 μm^2 was chosen based on the mean tissue area in the defined ROI of all samples. Thick regions had similar mean area values between R-IAs and UR-IAs ($0.41 \pm 0.03\ \mu m^2$ and $0.39 \pm 0.06\ \mu m^2$, respectively). Similarly, mean areas of thin regions were also not different between R-IAs and UR-IAs ($0.21 \pm 0.08\ \mu m^2$ and $0.18 \pm 0.06\ \mu m^2$, respectively). Thin regions of UR-IAs appeared to contain less total collagen than thicker regions (Fig. 3A), whereas total collagen content was not affected by the thickness of the IA wall in the ruptured group (Fig. 3F). The relative contribution of type I and type III collagens between thin and thick regions in UR-IAs was significantly different (Fig. 3B) due to a higher content of type I collagen (Fig. 3C) and a lower content of type III collagen in the thin IA wall regions (Fig. 3D). In R-IAs, type I and type III collagen contents (Fig. 3H, I) and relative contribution (Fig. 3G) were not

TABLE 2. Intracranial Aneurysm Characteristics Before Surgery

	Ruptured IAs	Unruptured IAs	p value
Intracranial aneurysm	n = 17	n = 31	
Location: n (%)	MCA: 11 (65) ACA: 4 (23) ICA: 1 (6) Unknown: 1 (6)	MCA: 24 (77.5) ACA: 6 (19.5) ICA: 1 (3)	0.75
Rough appearance: n (%)	4 (22)	14 (45)	0.33
Presence of blebs or lobules: n (%)	9 (53)	18 (58)	0.75
Neck size, mm: median (IQR)	3.8 (2.4–4.4)	3.6 (3.0–5.0)	0.54
Maximal diameter, mm: median (IQR)	7.5 (6.2–10.5)	6.2 (4.5–9.3)	0.27
Time from rupture to resection: n	<2 days: 10 >2 days: 6 Unknown: 1	NA	–

Comparisons of medians and percentages have been performed using nonparametric Mann-Whitney *U* test or Fisher exact test, respectively.

Rough appearance is defined as the presence of submillimetric irregularities.

IQR = interquartile range; ICA = internal carotid artery; MCA = middle cerebral artery; ACA = anterior cerebral arteries, including: anterior cerebral artery, anterior communicating artery (Acom) and pericallosal artery (A2); n, number; NA: not applicable.

different between thin and thick regions. Total, type I and type III collagen contents were significantly lower in thick regions of R-IAs in comparison to thick regions of UR-IAs ($p < 0.001$, $p < 0.05$, and $p < 0.01$, respectively). Thin regions of R-IAs had a lower content of type I collagen ($p < 0.01$) whereas the content in type III collagen was not different between the 2 groups. Finally, elastin content was similar between thick and thin regions of UR-IAs (Fig. 3E) or R-IAs (Fig. 3J).

Cellular Content

Presence of endothelial cells (CD31-positive cells) was found in 9 R-IAs out of the 17 samples harvested for this group, and in 26 UR-IAs over the 31 harvested for this group ($p < 0.05$). The percentage of endothelial coverage of the IA wall varied from 7.1% to 52.8% in the ruptured group and from 2.2% to 91.1% in the unruptured group. The wall of UR-IAs contained more total and differentiated SMCs (α-SMA and SMMHCs staining, respectively) than the wall of R-IAs (Fig. 4A–D) but the proportion of differentiated SMCs was not different between the 2 groups (32% and 35% in R-IAs and UR-IAs, respectively, ns). Moreover, the UR-IA walls presented a significantly lower content of inflammatory CD68-positive cells in comparison to R-IAs (Fig. 4E, F). Subsequently, 2 subgroups have been compared in the ruptured group; a first subgroup in which the time between the first signs of rupture and the resection of the aneurysm has been estimated lower than 2 days (n = 10) and a second group in which this time has been estimated longer than 2 days (n = 6) (Table 2). The time between the first signs of rupture and the resection was unknown for 1 patient. The percentage of CD68-positive cells was not different between the 2 subgroups (median [interquartile range]: <2 days = 2.2 (0.3–3.6); >2 days = 5.2 (1.1–7.2), ns). However, the percentage of CD68-positive cells present in recently ruptured domes (<2 days) was significantly higher in comparison to UR-IA domes (0.4 [0–1.1], $p < 0.01$, nonparametric Mann-Whitney *U* test). Finally, we found no correlations between cellular content (CD68-positive cells or α-SMA-positive cells) and collagen content within the walls of ruptured (Fig. 4G, H) or unruptured (Fig. 4I, J) IAs. In contrast to collagen content, α-SMA, SMMHCs, and CD68 contents were not different between thick and thin regions in the UR-IAs (Fig. 4K–M). Moreover, we observed no difference with respect to these 3 markers between thick and thin regions in R-IAs (data not shown).

IA Wall Classification

IA domes obtained after surgical clipping in Finland have been elegantly classified according to histological severity grades based on the following definitions (12): (a) Endothelialized wall with linearly organized SMCs; (b) Thickened wall with disorganized SMCs; (c) Hypocellular wall with either intimal hyperplasia or organizing luminal thrombosis; and (d) An extremely thin thrombosis-lined hypocellular wall.

We classified the 48 Swiss IA domes according the above criteria (see Fig. 5A for examples). Using the dominant wall type observed in the resected sample (i.e. the wall type covering the vast majority of the dome surface), 16%, 55%, 26%, and 3% of UR-IA domes were classified as a, b, c, and d, respectively (Fig. 5B). Interestingly, the percentage of R-IA domes for each histological severity grade was 0%, 18%, 70%, and 12%, respectively, demonstrating a significant difference in the distribution of histological severity grades between both groups (Fig. 5B). Thus, the group of UR-IAs was populated with a majority of a and b grades representing the relatively organized IA wall types, whereas the ruptured group contained mainly c and d wall severity grades. When we based our classification of the IA domes on the most severe focal histological grade observed within the IA dome sample, 26%, 42%, and 32% of UR-IA domes were graded b, c, and d, respectively, which is significantly different from the distribution obtained in R-IAs (b: 12%, c: 76%, d: 12%) (Fig. 5C). Finally, a direct comparison of the 2 grading methods showed that in the ruptured group, the classification of IA wall based on the dominant wall type or in the most pathological score was not different, whereas the distribution was significantly different in the unruptured group (Fisher exact test, $p < 0.001$).

Aneurysmal Wall Composition and Clinical Risk Factors for Rupture

IA Size

Increased size of UR-IAs correlated with a higher content of CD68-positive cells (Fig. 6A) and total collagen (Fig. 6B), more particularly with type III collagen (Fig. 6C).

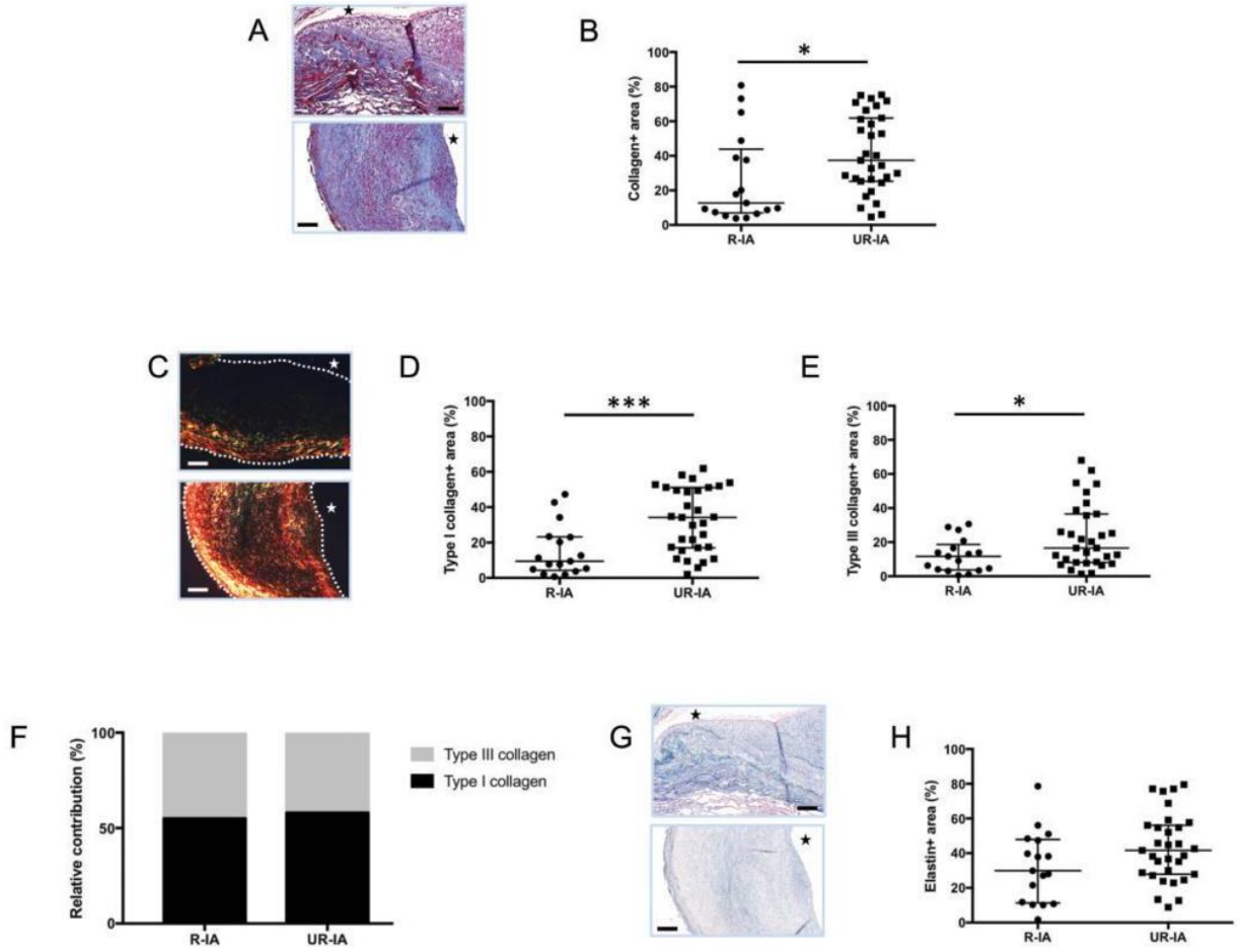

FIGURE 2. Extracellular matrix composition in ruptured and unruptured intracranial aneurysms (IAs). Representative examples and quantification of total collagen (Masson-trichrome staining: collagen in blue, **A, B**), type I collagen (Picrosirius red staining: type I collagen in yellow-red, **C, D**) and type III collagen (Picrosirius red staining: type III collagen in green, **C, E**) in ruptured (R-IA) and unruptured (UR-IA) IA domes. The relative contribution of type I (black) and type III (grey) collagen is not different between the 2 groups **(F)**. Representative examples and quantification of elastin (Victoria blue staining: elastin in blue, **G, H**) in ruptured and unruptured IA domes. The lumen of the vessel is indicated by a star. Scale bars in panels **A**, **C**, and **G** represent 100 μm. Dotted lines on the images of panel C represent the borders of the samples. Results are shown as individual values and as median ± interquartile range **(B, D, E,** and **H)** or in percentage **(F)**. *$p < 0.05$, ***$p < 0.001$, nonparametric Mann-Whitney *U* test.

However, we found no correlation between the size of UR-IAs and SMC or elastin content (data not shown).

Dome Irregularity

UR-IA domes with submillimetric irregularities (rough) contained more type III collagen in comparison to IAs with a smooth appearance (Fig. 6D). The amount of type I collagen was not different between rough and smooth domes, which led to a significantly lower ratio type I collagen/type III collagen for rough domes (Fig. 6E). Presence or absence of irregularities (roughness, blebs or lobules) was not significantly associated with any other aneurysmal wall characteristic (data not shown).

Smoking Status

Analysis of the association of clinical risk factors for IA rupture and histological characteristics of UR-IAs wall revealed that the aneurysmal wall of smokers contains less SMCs in comparison to the wall of nonsmokers (Fig. 6F). Intriguingly, the reduced SMC content in the IA wall of smokers was similar to that measured in R-IAs (Fig. 6F). Finally, classification of UR-IA domes per most severe focal histological grades for smokers and nonsmokers resulted in 19% (b), 48% (c), and 33% (d) versus 40%, 30%, and 30%, respectively (Chi-square test, $p < 0.01$). Smoking status was not correlated with others histological characteristics of the IA wall (data not shown). Finally, we found no association

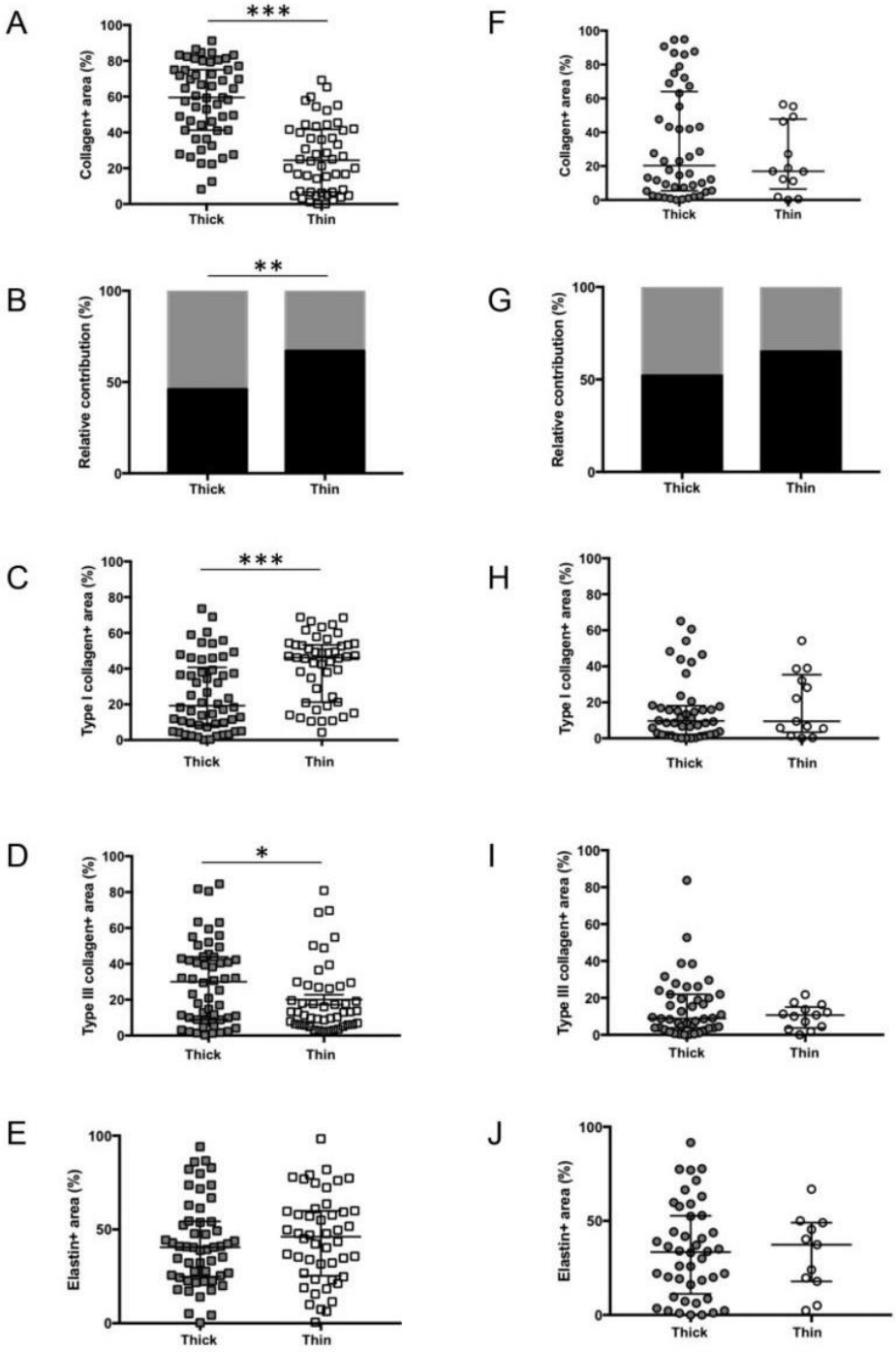

FIGURE 3. Extracellular matrix composition and thickness of intracranial aneurysm (IA) wall. Thin regions of UR-IAs contain less total collagen than thicker regions **(A)**, whereas total collagen content is not affected by the thickness of the IA wall in the ruptured group **(F)**. Type I (black) and III (grey) collagen relative contributions are significantly different between thick and thin regions of UR-IA domes **(B)** due to a higher content of type I collagen **(C)** and a lower content in type III collagen **(D)** in thin regions. No significant differences have been found for these parameters in R-IAs **(G–I)**. Elastin content is not influenced by the thickness of aneurysmal wall in UR-IA **(E)** and R-IA **(J)** domes. Results are shown as individual values and as median ± interquartile range **(A, C–F, H–J)** or in percentage **(B, G)**. *$p < 0.05$, **$p < 0.01$, ***$p < 0.001$, nonparametric Mann-Whitney *U* test for comparison of median and Fisher exact test for comparison of distributions.

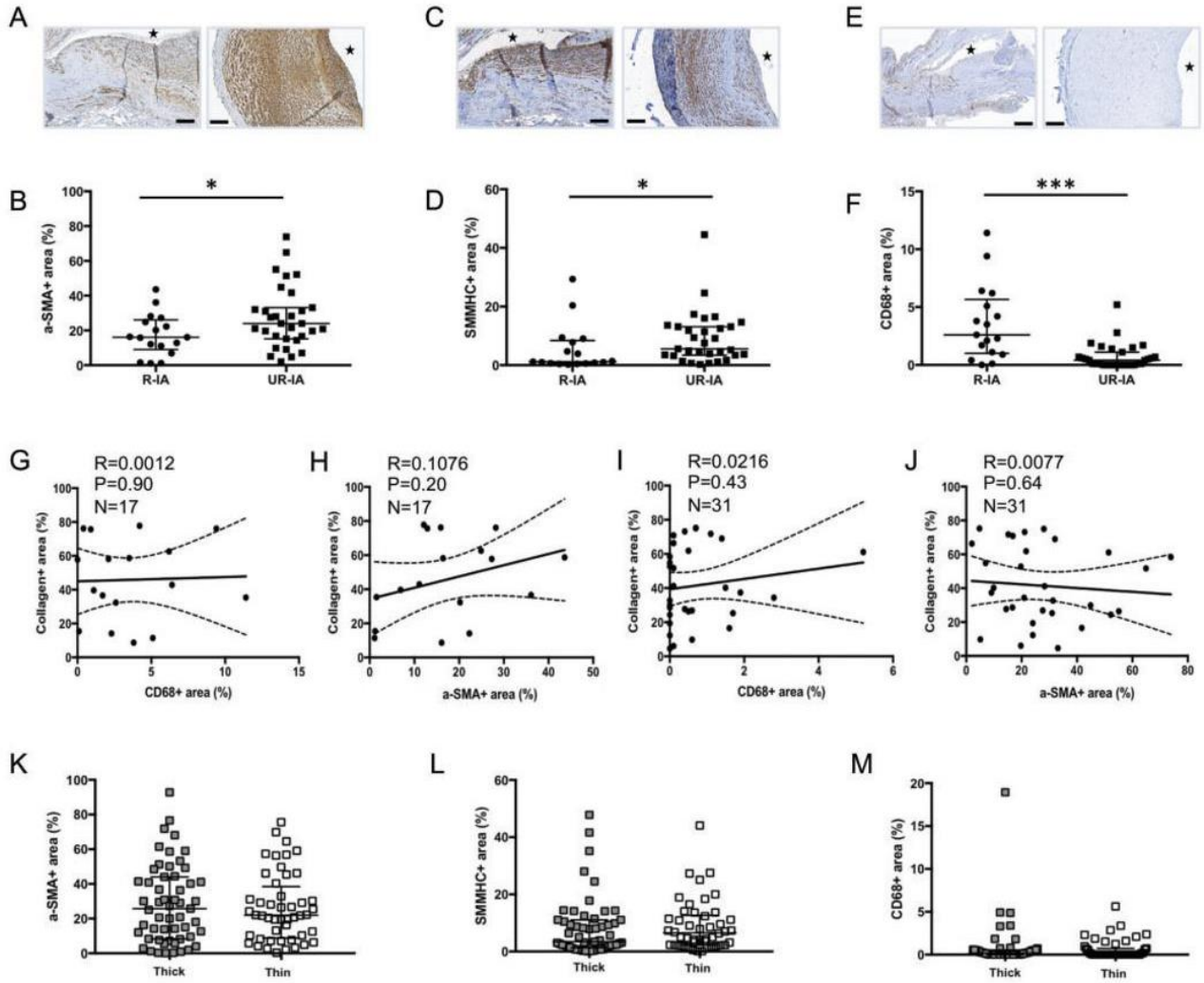

FIGURE 4. Cellular content of ruptured and unruptured intracranial aneurysms (IAs). Representative examples and quantification of α-SMA (SMCs in brown, **A, B**), SMMHCs (differentiated SMCs in brown, **C, D)** and CD68 (macrophages in brown, **E, F**) in ruptured and unruptured IA domes. Total collagen content is not correlated with CD68 **(G, I)** or α-SMA **(H, J)** contents in R-IAs (**G**, **H**) and UR-IAs **(I, J)**. Total SMC **(K)**, differentiated SMC **(L)** and macrophage **(M)** contents are not affected by the thickness of the aneurysmal wall in UR-IAs. The lumen of the vessel is indicated by a star. Results are shown as individual values and as median ± interquartile range. *$p \leq 0.05$, ***$p < 0.001$, nonparametric Mann-Whitney *U* test. Scale bars: **A**, **C**, **E** = 100 μm.

between age, sex or blood pressure and any of the histological IA wall characteristics.

DISCUSSION

The pathogenesis of IA formation and growth is complex and the precise biomechanical processes leading to aneurysmal wall rupture are not yet understood. The goal of our study was to characterize the aneurysmal wall histologically and to correlate histological characteristics with clinical and radiological factors used to estimate the risk of IA rupture. By establishing a new biobank of IA domes from patients surgically treated at the Geneva University Hospitals, we have unequivocally demonstrated that IA walls prone to rupture present a lower content in SMCs and collagen, a higher content in macrophages but no difference in elastin content (Figs. 2, 4). These results are in agreement with previously published studies performed in Japanese (11) or Finnish (12) cohorts. In addition, we showed that collagen content is different depending of the thickness of the IA wall in unruptured IAs, whereas no such difference was found in ruptured aneurysms (Fig. 3). Aneurysm dome classification, based on the histological score defined by Frösen et al (12), revealed a significant increased percentage of degenerative histological phenotypes (grades c and d) of ruptured IA walls compared with walls of unruptured IAs (Fig. 5). Finally, novel associations between histological characteristics of the IA wall and 3 clinical risk factors have been found. First, large size IAs have higher total collagen, type III collagen and macrophage contents; second, high content of type III collagen is associated

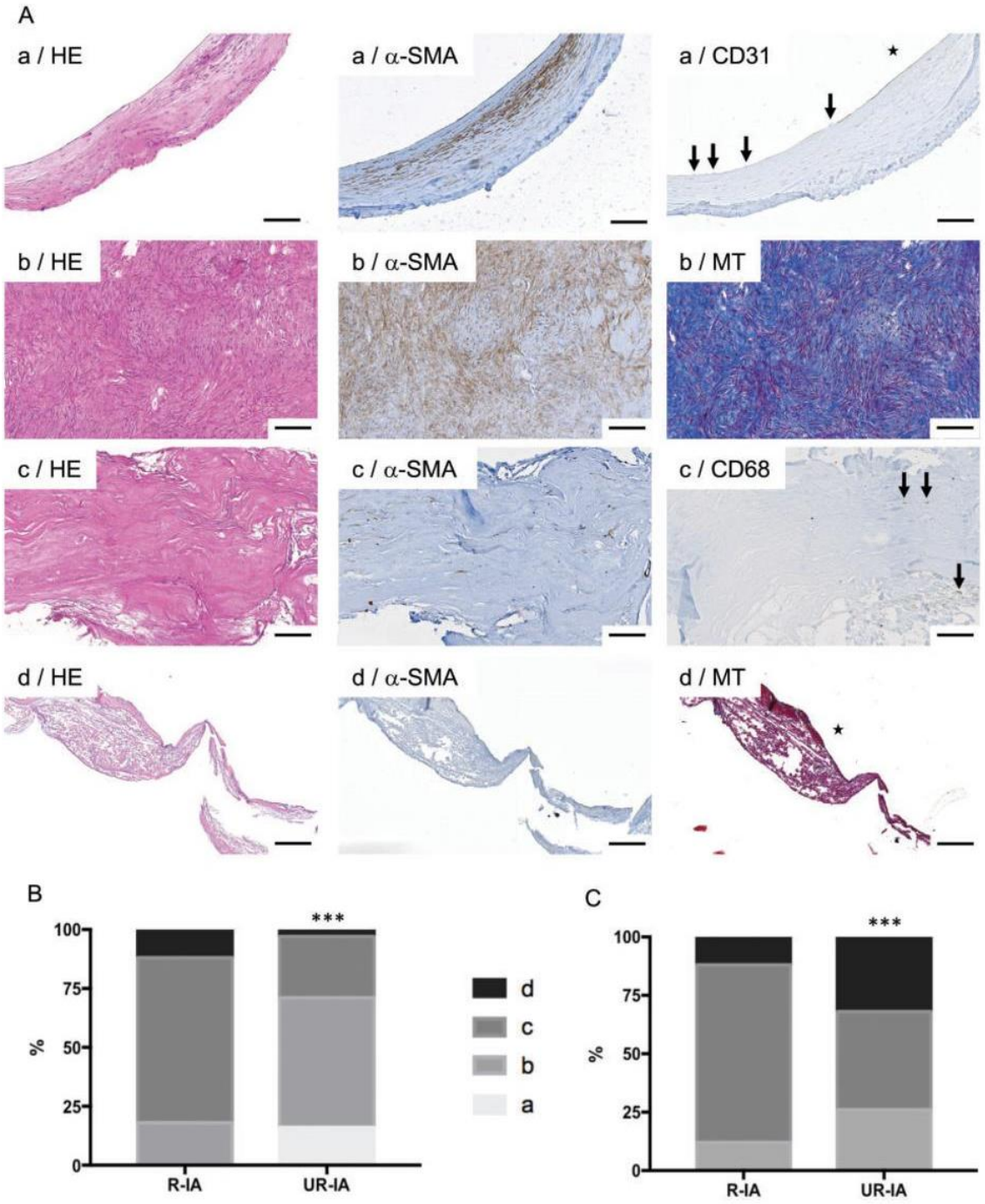

FIGURE 5. Classification of ruptured and unruptured intracranial aneurysms (IAs) based on histological characteristics. **(A)** Representative examples of stainings allowing IA histological classification following the definitions: **(a)** Endothelialized wall with linearly organized SMCs (first row); **(b)** Thickened wall with disorganized SMC (second row); **(c)** Hypocellular wall with either intimal hyperplasia or organizing luminal thrombosis (third row), and **(d)** An extremely thin thrombosis-lined hypocellular wall (fourth row). Scale bars: 100 μm. HE: hematoxylin and eosin staining; α-SMA: α-smooth muscle actin immunostaining (SMCs in brown); CD31: endothelial cell staining (in brown, endothelium indicated by arrows); MT: Masson-trichrome staining (collagen in blue); CD68: macrophage staining (in brown, some macrophages are indicated by arrows). The lumen of the vessel is indicated by a star. **(B, C)** Classification of ruptured and unruptured IAs following the (**a,** very light gray), (**b,** light gray), (**c,** dark grey) and (**d,** black) classification based on the dominant wall type **(B)** or on the most pathological region **(C)** observed in the resected sample. ***$p < 0.001$, Chi-square test.

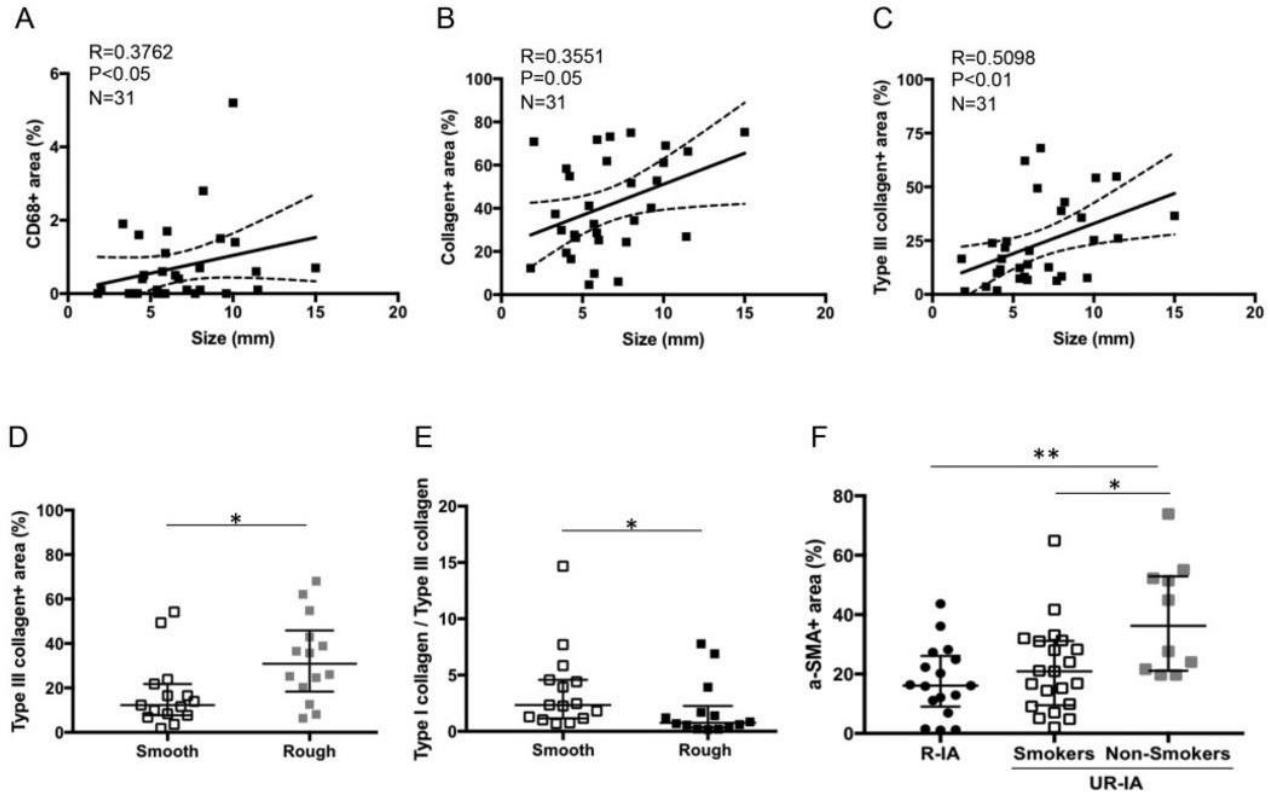

FIGURE 6. Risk factors and aneurysmal wall composition. Spearman correlation between intracranial aneurysm (IA) size and CD68 **(A)**, total collagen **(B)**, and type III collagen **(C)** contents in UR-IAs. UR-IAs with a rough appearance have a higher content of type III collagen **(D)** and a lower type I collagen-type III collagen ratio **(E)** than UR-IA with a smooth appearance ($n = 15$ and 14, respectively, $^*p < 0.05$, nonparametric Mann-Whitney *U* test). SMC content is lower in the unruptured aneurysmal wall of smokers (current and former) in comparison to nonsmokers (**F**, $n = 17$ for R-IA, $n = 21$ for UR-IA/smokers, and $n = 10$ for UR-IA/nonsmokers, $^*p < 0.05$, $^{***}p < 0.001$, nonparametric Mann-Whitney *U* test).

with increased aneurysm dome roughness; and third, SMC content is lower in unruptured IA walls of smokers (Fig. 6).

ECM components are constantly being synthesized and degraded in the arterial wall. ECM produced by SMCs and fibroblasts contributes to the maintenance of the structural integrity of the IA wall, whereas proteases and other matrix degrading enzymes secreted by inflammatory cells demolish ECM and destabilize the IA wall. In both ruptured and unruptured IAs we did not observe any correlation between α-SMA-positive cells and the total collagen content or the type I or type III collagen content (Fig. 4). An earlier study comparing the IA wall with the normal vessel wall of intracranial arteries demonstrated that medial SMCs in IAs switch to a synthetic phenotype characterized by a decreased expression of α-SMA and SMMHCs, the disappearance of smoothelin and an increased expression of S100A4 (22). S100A4 is a protein known to favor degradation and remodeling of the ECM by modulation of proteolytic activity (23, 24), and it has been proposed that S100A4 could, in part, play a role in the remodeling process observed in IAs (22). Immunostainings for α-SMA and SMMHCs performed on our samples to distinguish subpopulations of SMCs showed that SMCs were less abundant and less differentiated in ruptured IAs (Fig. 4) but no difference in the proportion of dedifferentiated SMCs between ruptured and unruptured IAs were observed. As elective IA treatment requires a critical size or growth of the aneurysm, our patient population is likely biased towards more advanced disease stages and the switch to the synthetic SMC phenotype might have already occurred during the initiation phase or early stages of the disease. However, we observed a lower collagen content in the wall of ruptured IAs compared with unruptured aneurysms. ECM degradation is induced by secretion of various metalloproteinases (MMPs) by inflammatory cells but also by resident vascular cells (25). Infiltrated tissular macrophages secrete, among others, MMP-2 and MMP-9 known to digest type I and III collagen fibers (26). Type I and III collagen fibers are important structural components of cerebral arteries. Whereas type I collagen plays a key role in the support of high tensile strength, type III collagen is an important regulatory element in type I collagen fibrillogenesis (27). Indeed, premature vascular aneurysms and fragility of cerebral arteries are associated with genetic mutations in type I and III collagen (28, 29). Furthermore, an increased activity and/or expression of MMP-2 and MMP-9 has been previously shown in ruptured IAs (compared with unruptured IAs) (26). In agreement with this observation, our study revealed lower

contents of both type I and type III collagen fibers in R-IAs. However, we did not find a direct correlation between CD68-positive cells and collagen contents (total, type I or III), thus the decrease of collagen content in ruptured IAs cannot be attributed to a specific type of cells but rather seems to be the consequence of the concomitant reduction in SMCs and the increase in macrophages in R-IAs. Of note, >60% of the IA domes have been resected <2 days after the first clinical symptoms of IA rupture, suggesting that a large part of the CD68-positive cells present in the aneurysmal wall were already infiltrated before the rupture, as already described by others (30).

Type III collagen is important for type I collagen fibrillogenesis (27) and deficiency or mutation of type III collagen have been described to favor IAs (28, 29). In our study, we confirmed that R-IAs have a lower content of type I and III collagen fibers; however, the overall ratio type III/type I is not different between the 2 groups (Fig. 2). Histologically, thin regions in UR-IAs appeared to be associated with a different relative contribution of type III and type I collagen in comparison to thicker wall regions of such IAs. In addition, we show that a clinical rough appearance of IAs associates with a higher content in type III collagen fibers in histology. As previous studies have pointed to the importance of collagen expression and organization in aneurysm wall strength (31) or regional wall shear stress (32), our observation provides a histological validation for the use of the rough appearance of the IA and urges towards further studies providing mechanistic insight in the critical relation between collagen subtype, the presence of submillimetric irregularities, blebs/lobules and risk of IA rupture.

Following the classification established by Frösen et al (12) for dominant wall type, we observed that ruptured IAs are in vast majority (82%) histologically characterized by hypocellular and/or very thin vascular walls and luminal thrombosis (grades c and d). In contrast, 71% of unruptured IA samples contain endothelial cells and/or a thickened media with SMCs. Furthermore, an important clinical risk factor for IA rupture, that is, smoking, was histologically associated with reduced SMC content in UR-IAs. In fact, the SMC content in UR-IAs of smokers was similar to the one found in R-IAs, suggesting that smoking enhances the process of IA degeneration thereby enhancing the risk of rupture. In support with this hypothesis, Starke et al showed recently in cultured cerebral vascular SMCs that cigarette smoke exposure increased NOX1 expression followed by an upregulation of pro-inflammatory/matrix remodeling genes and downregulation of contractile genes such as α-SMA and SMMHCs (33). For clinical practice, it will be difficult to develop specific radiological markers recognizing a hypocellular thin wall for the identification of IAs at high risk of rupture. In contrast, it might be a more fruitful approach to aim for the development of a SMC-related marker to identify the IAs at low risk to better stratify patients for (no) intervention.

An important limitation of our study is the relatively small number of patients. By comparing characteristics of patients and aneurysm in different outcomes groups of large cohorts, clinicians identified risk factors and estimate the rupture probability using scores integrating multiple variables (ISUIA [6], UCAS [5], PHASES [4], UIATS [3]). Histological studies open an avenue to better understand the mechanisms and progression of the disease and could reveal bio-markers to improve the estimation of risk. To rapidly progress in the field, it is of paramount importance to agree on standard operating procedures and reporting globally to better allow meta-analysis and pooling of individual studies or data. The associations found in our study between presently available clinical/radiological data such as IA size, rough appearance, smoking and specific histological characteristics underline once more the importance of combining clinical and histological data. Recent developments in augmented reality assisted surgery allow the precise mapping of aneurysm dome characteristics (34). Aneurysm wall aspects as observed during surgical interventions can be associated to particular lumen shape features or imaging characteristics observed as clinical markers and bridged to immuno-histological characteristics giving insights on the vessel wall constitution and remodeling. These developments will further strengthen the possible use of histology-based clinical markers in aneurysm wall risk assessment in the near future.

ACKNOWLEDGMENTS

We thank Juhana Frösen (Associate Professor, Kuopio University Hospital, Kuopio, Finland) and Riikka Tulamo, MD, PhD (Helsinki University Hospital, Helsinki, Finland) for their valuable advice on the histological IA classification. We thank the Bioimaging Core Facility, Faculty of Medicine, University of Geneva for technical help. This work has been performed with the contribution of the Clinical Trial Unit, Faculty of Medicine, Geneva University Hospitals.

REFERENCES

1. Vlak MH, Algra A, Brandenburg R, et al. Prevalence of unruptured intracranial aneurysms, with emphasis on sex, age, comorbidity, country, and time period: A systematic review and meta-analysis. Lancet Neurol 2011;10:626–36
2. Schatlo B, Fung C, Fathi AR, et al. Introducing a nationwide registry: The Swiss study on aneurysmal subarachnoid haemorrhage (Swiss SOS). Acta Neurochir (Wien) 2012;154:2173–8
3. Etminan N, Brown RD, Jr., Beseoglu K, et al. The unruptured intracranial aneurysm treatment score: A multidisciplinary consensus. Neurology 2015;85:881–9
4. Greving JP, Wermer MJ, Brown RD, Jr., et al. Development of the PHASES score for prediction of risk of rupture of intracranial aneurysms: A pooled analysis of six prospective cohort studies. Lancet Neurol 2014;13:59–66.
5. Investigators UJ, Morita A, Kirino T, et al. The natural course of unruptured cerebral aneurysms in a Japanese cohort. N Engl J Med 2012;366:2474–82
6. Wiebers DO, Whisnant JP, Huston J, 3rd, et al. Unruptured intracranial aneurysms: Natural history, clinical outcome, and risks of surgical and endovascular treatment. Lancet 2003;362:103–10
7. Etminan N, Beseoglu K, Barrow DL, et al. Multidisciplinary consensus on assessment of unruptured intracranial aneurysms: Proposal of an international research group. Stroke 2014;45:1523–30
8. Kotowski M, Naggara O, Darsaut TE, et al. Safety and occlusion rates of surgical treatment of unruptured intracranial aneurysms: A systematic review and meta-analysis of the literature from 1990 to 2011. J Neurol Neurosurg Psychiatry 2013;84:42–8
9. Naggara ON, Lecler A, Oppenheim C, et al. Endovascular treatment of intracranial unruptured aneurysms: A systematic review of the literature on safety with emphasis on subgroup analyses. Radiology 2012;263:828–35

10. Darsaut TE, Findlay JM, Magro E, et al. Surgical clipping or endovascular coiling for unruptured intracranial aneurysms: A pragmatic randomised trial. J Neurol Neurosurg Psychiatry 2017;88:663–8
11. Kataoka K, Taneda M, Asai T, et al. Structural fragility and inflammatory response of ruptured cerebral aneurysms. A comparative study between ruptured and unruptured cerebral aneurysms. Stroke 1999;30: 1396–401
12. Frosen J, Piippo A, Paetau A, et al. Remodeling of saccular cerebral artery aneurysm wall is associated with rupture: Histological analysis of 24 unruptured and 42 ruptured cases. Stroke 2004;35:2287–93
13. Tulamo R, Frosen J, Junnikkala S, et al. Complement activation associates with saccular cerebral artery aneurysm wall degeneration and rupture. Neurosurgery 2006;59:1069–76
14. Frosen J, Tulamo R, Heikura T, et al. Lipid accumulation, lipid oxidation, and low plasma levels of acquired antibodies against oxidized lipids associate with degeneration and rupture of the intracranial aneurysm wall. Acta Neuropathol Commun 2013;1:71
15. Ollikainen E, Tulamo R, Frosen J, et al. Mast cells, neovascularization, and microhemorrhages are associated with saccular intracranial artery aneurysm wall remodeling. J Neuropathol Exp Neurol 2014; 73:855–64
16. Korkmaz E, Kleinloog R, Verweij BH, et al. Comparative ultrastructural and stereological analyses of unruptured and ruptured saccular intracranial aneurysms. J Neuropathol Exp Neurol 2017;76:908–16
17. Hirsch S, Bijlenga P. Shape? Shape. Shape! Pan Eur Netw: Sci Technol 2016;18:178–81
18. Dunlop R, Arbona A, Rajasekaran H, et al. @neurIST – chronic disease management through integration of heterogeneous data and computer-interpretable guideline services. Stud Health Technol Inform 2008;138: 173–7
19. Gondar R, Gautschi OP, Cuony J, et al. Unruptured intracranial aneurysm follow-up and treatment after morphological change is safe: Observational study and systematic review. J Neurol Neurosurg Psychiatry 2016; 87:1277–82
20. Bijlenga P, Ebeling C, Jaegersberg M, et al. Risk of rupture of small anterior communicating artery aneurysms is similar to posterior circulation aneurysms. Stroke 2013;44:3018–26
21. Skalli O, Ropraz P, Trzeciak A, et al. A monoclonal antibody against alpha-smooth muscle actin: A new probe for smooth muscle differentiation. J Cell Biol 1986;103:2787–96
22. Coen M, Burkhardt K, Bijlenga P, et al. Smooth muscle cells of human intracranial aneurysms assume phenotypic features similar to those of the atherosclerotic plaque. Cardiovasc Pathol 2013;22:339–44
23. Bresnick AR, Weber DJ, Zimmer DB. S100 proteins in cancer. Nat Rev Cancer 2015;15:96–109
24. Donato R, Cannon BR, Sorci G, et al. Functions of S100 proteins. Curr Mol Med 2013;13:24–57
25. Newby AC. Metalloproteinase expression in monocytes and macrophages and its relationship to atherosclerotic plaque instability. Arterioscler Thromb Vasc Biol 2008;28:2108–14
26. Kilic T, Sohrabifar M, Kurtkaya O, et al. Expression of structural proteins and angiogenic factors in normal arterial and unruptured and ruptured aneurysm walls. Neurosurgery 2005;57:997–1007
27. Liu X, Wu H, Byrne M, et al. Type III collagen is crucial for collagen I fibrillogenesis and for normal cardiovascular development. Proc Natl Acad Sci U S A1997;94:1852–6
28. Pope FM, Kendall BE, Slapak GI, et al. Type III collagen mutations cause fragile cerebral arteries. Br J Neurosurg 1991;5:551–74
29. Mohan D, Munteanu V, Coman T, et al. Genetic factors involves in intracranial aneurysms – actualities. J Med Life 2015;8:336–41
30. Frosen J, Tulamo R, Paetau A, et al. Saccular intracranial aneurysm: Pathology and mechanisms. Acta Neuropathol 2012;123:773–86
31. Robertson AM, Duan X, Aziz KM, et al. Diversity in the strength and structure of unruptured cerebral aneurysms. Ann Biomed Eng 2015;43: 1502–15
32. Cebral JR, Duan X, Gade PS, et al. Regional mapping of flow and wall characteristics of intracranial aneurysms. Ann Biomed Eng 2016;44: 3553–67
33. Starke RM, Thompson JW, Ali MS, et al. Cigarette smoke initiates oxidative stress-induced cellular phenotypic modulation leading to cerebral aneurysm pathogenesis. Arterioscler Thromb Vasc Biol 2018;38:610–21
34. Cabrilo I, Bijlenga P, Schaller K. Augmented reality in the surgery of cerebral aneurysms: A technical report. Neurosurgery 2014;10(Suppl. 2): 252–60

Chapter 3: Primary cilia control endothelial permeability by regulating expression and location of junction proteins.

 # Original manuscript 2

Physiological high WSS is an important regulator of vascular function and it is now clear that disturbed flow conditions could lead to significant damage. The blood flow pattern within wide neck saccular IAs induces a low WSS (2-5 dynes/cm^2) to the ECs within the aneurysm and may be an important yet underestimated factor in IA growth and rupture. Primary cilia are increasingly recognized as important biological sensors of low WSS. Defective primary cilia might impair the EC response to low WSS, which might exacerbate the disease outcome as seen in PKD patients. In this third chapter, I investigate how primary cilia influence EC behavior under physiological or aneurysmal flow. The transcriptome profile of ECs with and without primary cilia has been determined and I performed further functional investigations according to these results.

Personal contribution: For this project, I performed all the experiments except for the human IA data analysis described in Figure 4. I analyzed and interpreted the results, and wrote the manuscript under the supervision of Prof. Brenda KWAK.

Manuscript Status: The manuscript is under preparation for submission

Primary cilia control endothelial permeability by regulating expression and location of junction proteins.

Mannekomba R Diagbouga[1], Sandrine Morel[1,2], Sylvain Lemeille[1], Beerend Hierck[3], Philippe Bijlenga[2], Brenda R Kwak[1]

[1]Department of Pathology and Immunology, Faculty of Medicine, University of Geneva, Switzerland
[2]Department of Clinical Neurosciences, Neurosurgery Division, Faculty of Medicine, University of Geneva, Switzerland
[3]Department of Anatomy and Embryology, Leiden University Medical Center, the Netherlands

Word count: 6094 manuscript body words and abstract: 249 words

* Address correspondence to:
Brenda R Kwak, PhD
Dept. of Pathology and Immunology
University of Geneva
CMU - lab F06.2764.a
Rue Michel-Servet 1
CH-1211 Geneva 4
Switzerland
Phone: +41 22 379 57 37
E-mail: Brenda.KwakChanson@unige.ch

Abstract

Background and purpose: Wall shear stress (WSS) plays an important role in the pathogenesis of intracranial aneurysms (IAs). There is a high incidence and risk of rupture for IAs of polycystic kidney disease (PKD) patients. The dysfunction/absence of primary cilia in PKD endothelial cells may impair mechano-transduction of WSS and favor vascular disorders. The molecular links between primary cilia dysfunction and IAs are however unknown.

Methods: Endothelial cells from wild-type and primary cilia-deficient *Tg737*$^{orpk/orpk}$ mice were submitted to physiological WSS (30 dynes/cm^2) or aneurysmal low WSS (2 dynes/cm^2) and gene expression was studied using an unbiased transcriptomics. Moreover, clinical and histological characteristics of IA domes from control and PKD patients were analyzed.

Results: *Tg737*$^{orpk/orpk}$ endothelial cells displayed a 5-fold increase in the number of WSS-responsive genes compared to wild-type cells. We observed a lower trans-endothelial resistance and a higher permeability to 4 kDa FITC-dextran that correlated with disorganized intercellular junctions in *Tg737*$^{orpk/orpk}$ cells. We identified ZO-1 as a central regulator of shear stress-dependent endothelial integrity. IA domes of PKD patients appeared thinner with less collagen and reduced endothelial ZO-1 as compared to domes from non-PKD patients.

Conclusions: Primary cilia dampen the endothelial response to aneurysmal low WSS. In absence of primary cilia, ZO-1 expression levels are reduced, which disorganizes intercellular junctions resulting in increased endothelial permeability. This altered endothelial function may not only contribute to the severity of IA disease observed in PKD patients, but may also serve as a potential diagnostic tool to determine the vulnerability of IAs.

Introduction

Intracranial aneurysms (IAs) are local dilatations in cerebral arteries that predominantly develop at bifurcations in the circle of Willis, regions exposed to disturbed blood flow [1]. Rupture of an IA causes subarachnoid hemorrhage and is a life-threatening event. The treatment options to prevent IAs from rupturing are either surgical or endovascular and are both associated with clinical risks as well [2]. IAs are characterized by a disrupted internal elastic lamina (IEL), dysfunction or loss of endothelial cells (ECs), inflammatory cell infiltration, extracellular matrix degradation and loss of smooth muscle cells [3, 4]. The formation and growth of IAs is multifactorial and wall shear stress (WSS) is a determinant factor. A healthy endothelium is essential to maintain vascular integrity as it regulates vascular tone, thrombosis and inflammatory events [5]. EC dysfunction is considered as the primary event of IA disease [6-8]. Available evidence suggests that an excessive high WSS at bifurcations in the circle of Willis can trigger pro-inflammatory signaling in ECs that would stimulate leukocyte infiltration [9, 10]. Recruited leukocytes secrete proteases, which enhance IEL disruption promoting the out-bulging of the arterial wall. The processes inducing growth of the IA are not yet fully understood. Interestingly, blood flow conditions in the IA lumen have been associated with progression of inflammation and degenerative changes of the aneurysm wall [11]. WSS controls vascular wall remodeling through mechano-sensors present at ECs surface, including primary cilia [2]. Within the normal range of arterial flow, ECs release biochemical signals, which maintain the physiological function of these blood vessels [2]. Abnormal WSS or impaired mechano-transduction would trigger degenerative remodeling leading to an instable arterial wall prone to disease [2]. Indeed, patients with polycystic kidney disease (PKD) carrying a mutation in polycystin-1 (PC1) or polycystin-2 (PC2) genes that affects the expression or function of primary cilia are prone to vascular complications such as hypertension,

atherosclerosis and IAs [12]. The prevalence of IAs in PKD patients ranges from 5% to 40%, five times higher than in the general population [13].

Primary cilia are microtubule-based organelles found in most mammalian cell types that transmit extracellular microenvironment clues into intracellular signals for molecular and cellular responses [2]. Correct assembly and maintenance of primary cilia relies on a wide range of proteins including intra-flagellar transport (IFT) proteins [14]. In the vasculature, endothelial primary cilia are essential for proper vascular development and maintenance of structural integrity through calcium (Ca^{2+}) and nitric oxide (NO) signaling [15, 16]. In adult mice, primary cilia are particularly abundant in ECs of arterial regions experiencing low WSS [17], a condition that is typically observed in wide-neck IAs [18]. In agreement, EC-specific deletion of PC1, PC2 or IFT88 promotes IA development in mice [19]. We hypothesize that absence or dysfunction of primary cilia might impair the adaptive EC response to low WSS [16, 20, 21], which might further compromise the integrity of the endothelial barrier and exacerbate the outcome of IA disease as seen in PKD patients. In the present study, we sought to investigate the molecular role of primary cilia in EC integrity using *in vitro* approaches. Finally, the results were compared with human IAs of the AneuX biobank.

Material and methods

In vitro model

Embryonic aortic ECs from wild-type (WT) and *Tg737*$^{orpk/orpk}$ (ORPK) mice [20] were grown in dishes coated with 0.1% gelatin (Sigma-Aldrich) at 37°C in a humidified atmosphere containing 5% CO_2. Cells were cultured in advanced-DMEM (Gibco 12491-015) supplemented with 2% fetal bovine serum (Sigma), 10.000 U/mL penicillin-streptomycin (Gibco 15140-122), 1% glutamax (Gibco 35050-038), 1% insulin-transferrin-selenium (Gibco 41400-045).

Human saccular IA samples

Human saccular IA samples were retrieved from the Swiss AneuX biobank [3]. Briefly, IA domes after clipping were fixed in formol, embedded in paraffin and 5μm sections were used for histology analysis. IA domes were stained for hematoxylin and eosin, Masson-trichrome (total collagen), Victoria blue (elastin) and picrosirius red (type I and III collagen, Sigma-Aldrich, Buchs, Switzerland).

Immunohistochemistry was performed on IA dome sections using antibodies recognizing α-smooth muscle actin (SMA) (mouse IgG2a antibody, clone 1A4 [22, 23], 1/100; a general marker of smooth muscle cells), CD68 (mouse IgG1 antibody, clone KP1, Dako, Glostrup, Denmark, 1/200; marker of macrophages), CD31 (rabbit polyclonal antibody, clone pAK, Dianova, Hamburg, Germany, 1/25; a marker of endothelial cells) and Zonula occludens (ZO)-1 (rabbit polyclonal, ThermoFisher Scientific 33-9100, 1/100). Before using the first antibody, immunoreactivity was retrieved by microwave treatment (600W, 5min) in citrate buffer (10mmol/L, pH 6.0) for α-SMA and CD68, and by pressure cooker treatment (3min) in citrate buffer for CD31 and ZO-1. Goat antimouse- or antirabbit-biotinylated IgGs (Dako) were used as secondary antibodies and the streptavidin-biotin peroxidase complex and 3, 3′-diamino-benzidine chromophore were used for visualization (EnVision system; Dako). Hemalun

(Merck, Darmstadt, Germany) was used as counterstaining. All stainings were performed on consecutive sections.

Tjp1 Knockdown

Wild-type ECs were transfected 24-hours after seeding with ON-TARGETplus Mouse Tjp1 siRNA SMARTpool (Dharmacon) comprising individual siRNAs targeting the sequences CGAUAGUUAUGACGAAGAA, GAUGAAGGUUAGCGAGCAU, GCAGAGAGGAAGAGCGAAU and UGGAAAUGAUGUCGGAAUA. Non-targeting (NT) control siRNA was used as a control (Dharmacon). The transfections were performed in serum-free conditions using 25nmol/L siRNA and 4µL DharmaFECT 4 transfection reagent. Tjp1/ZO-1 expression level was determined by quantitative RT-PCR (qPCR), immunofluorescence and Western blotting at 48-hours post-transfection.

Alternatively, stable Tjp1 knockdown cells were obtained using the CRISPR-Cas9 system (Genecopoeia, Rockville, Maryland, USA). First, wild-type ECs were infected in medium containing 8mg/ml of polybrene (0.2µL) and lentiviral particles for Cas9 nuclease (LPP-CP-LYC9NU-10-100-CS) at MOI 10. At 6-hours post-infection, the medium was changed and cells were selected with hygromycin (150µg/mL) and FACS sorting. Secondly, selected cells were infected following the same protocol with Tjp1 (LPPMCP274411L03-1-50) or scrambled (LPPCCPCTR01203-100-CS) sgRNA lentiviral particles at MOI 10 and cells were selected with puromycin (2µg/mL) and FACS sorting. ZO-1 expression level was determined by immunofluorescence and Western blotting.

Flow experiments

Wild-type and *Tg737*$^{orpk/orpk}$ ECs were seeded at 30.000 cells per channel in Ibidi µ-Slide VI$^{0.4}$ slides coated with 0.1% gelatin and grown till confluence. Cells were serum starved for 24-

hours prior exposure to flow. Laminar shear stress of 30 or 2 dynes/cm^2 was applied for 48-hours. For each set of flow experiments, control cells were kept under static condition.

Trans-endothelial electrical resistance and permeability assays

Polyester Membrane Transwell inserts (6.5mm diameter, 0.4µm pore size, Costar 3470) were coated with 0.1% gelatin. Cells were grown on the apical side of the Transwell insert until confluency.

Trans-endothelial electrical resistance (TEER) of cell monolayers was assessed using a pair of electrodes (Epithelial Voltohmmeter EVOM, World precision instrument). One electrode was placed in the upper compartment of the Transwell and the second in the lower compartment. Control conditions included an empty gelatin-coated filter. TEER ($\Omega \bullet cm^2$) was calculated using the formula $TEER = R \times area_{filter}$.

Trans-endothelial permeability was assessed by the measurement of paracellular flux (or passage) of FITC-dextran (4kDa) across the monolayer. FITC-dextran was added to the apical side of the Transwell and the medium of the baso-lateral side was collected after 1-, 4- and 6-hours for analysis of the fluorescence intensity (excitation 485 nm, emission 525 nm, SpectraMax Paradigm, Molecular DEVICES).

Reverse transcription and quantitative PCR

Total RNA was isolated from cells using the nucleospin RNA II kit (Machery-Nagel) according to the manufacturers' instructions. The concentration of RNA was determined using a Nanodrop 2000c (ThermoFisher Scientific). Equal amounts of RNA were converted to cDNA using QuantiTect Reverse Transcription Kit (Qiagen) and the qPCR were performed using ABI StepOne Plus detection system. We used Taqman gene expression assays (Applied Biosystems). The following

primers were used: Tjp1 (Mm00493699_m1) and Gapdh (Mm99999915_g1) from ThermoFisher Scientific.

Protein quantification and Western blot

Cell cultures were rinsed with PBS (pH=7.4) and lysed in RIPA buffer (50mmol/L Tris–HCl, pH=8, 30mmol/L NaCl, 1% NP40, 10mmol/L NaF, 2mmol/L Na_3VO_4, 1mmol/L phenylmethylsulfonyl fluoride, complete protease inhibitor cocktail (Roche Applied Science), 1mmol/L EDTA, pH=7.4, 0.05% sodium dodecyl sulfate, 5mmol/L sodium-deoxycholate). Cell lysates were gently mixed at 4°C for 20min, and then spun at 13.500rpm for 20min to collect the supernatant. The concentration of the isolated proteins was determined using BCA Protein Assay Reagent (ThermoFisher Scientific). Ten μg of protein was separated by SDS-PAGE and electrophoretically transferred to PVDF membranes (Immobilon, Millipore). After 2-hours blocking with 5% milk and 1% Tween in PBS, the membranes were incubated with primary antibodies recognizing ZO-1 (rabbit polyclonal, ThermoFisher Scientific 33-9100, 1/250) or GAPDH (Mouse monoclonal IgG, EMD Millipore MAB374, 1/30.000). Thereafter, the appropriate secondary horseradish peroxidase-conjugated antibodies (Jackson ImmunoResearch; 1/5.000) were used, followed by ECL detection (Millipore) using ImageQuant LAS 4000 software. Band intensities were thereafter quantified using the NIH Image software (NIH AutoExtractor 1.51; National Institutes of Health).

Immunofluorescence and immunohistochemistry

Cultured cells were fixed in ice-cold 100% methanol for 5 min, permeabilized with 0.2% Triton X-100 for 1-hour, charges were neutralized with 0.5mol/L NH_4Cl in PBS for 15min and cells were blocked for 30min with 2% bovine serum albumin (AppliChem). Primary antibodies recognizing acetylated α-tubulin (Mouse IgG2b, Sigma T7451, 1/2000), ZO-1 (rabbit

polyclonal, ThermoFisher Scientific 33-9100, 1/50), ZO-2 (rabbit polyclonal, Cell signaling 2847, 1/50), Catenin α-1 (rabbit polyclonal, Cell signaling 3236, 1/200), Catenin β-1 (rabbit polyclonal, Cell signaling 8480, 1/100), Claudin-3 (rabbit polyclonal, Abcam 15102) and Connexin43 (Cx43, rabbit polyclonal, Alpha diagnostic, 1/50) were diluted in blocking buffer and incubated with the samples overnight at 4°C. Finally, Alexa Fluor (488, 568)-conjugated goat anti-rabbit or goat anti-mouse antibodies (ThermoFisher Scientific, 1/2000) were used for signal detection. Nuclei and cytoplasm were counterstained with 4',6-diamidino-2-phenylindol (DAPI) and 0.003% Evans Blue, respectively. Samples were mounted with Vectashield (Vector Laboratories). Images were obtained with an epifluorescent Zeiss Axiocam fluorescent microscope (Zeiss Axio Imager Z1) equipped with an AxioCam 506 mono camera (Carl Zeiss AG) or with a LSM800 Airyscan confocal microscope. Images were analyzed using the software ZEN2.3 (Zeiss). Thereafter, quantifications were done using the NIH Image software (NIH AutoExtractor 1.51; National Institutes of Health).

For quantification of all junction proteins, the area of positive staining at the cell membrane and the total area was measured using ImageJ software. Results are given as the ratio of positive area/total area. In addition, intercellular junctions were classified into sharp (thin and continuous), wide (thick, diffuse/scattered) or discontinuous (zigzag-like, with gaps) junctions (adapted from [24]). Cells of 15 images from 3 different experiments were quantified.

RNA extraction, library preparation, sequencing, read mapping to the reference genome and gene coverage reporting

RNA was isolated from ECs after exposure to flow. Three experiments for each condition were performed. Total RNA was extracted using the NucleoSpin RNA II kit (Macherey-Nagel) according to the manufacturers' instructions. The quality of all samples was verified using the Agilent 2100 Bioanalyzer with the Agilent RNA 6000 Nano Kit (Agilent Technologies). cDNA

libraries were constructed by the Genomic platform of the University of Geneva using the Illumina TruSeq RNA sample preparation kit according to the manufacturers' protocol. Libraries were sequenced using single-end (50 nt-long) on Illumina HiSeq2000. FastQ reads were mapped to the ENSEMBL reference genome (GRCm38.80) using STAR version 2.4.0j [25] with standard settings, except that any reads mapping to more than one location of the genome (ambiguous reads) were discarded (m=1). Sequence data have been submitted to GEO database under accession number GSE139580. A unique gene model was used to quantify reads per gene. In short, the model considers all annotated exons of all annotated protein coding isoforms of a gene to create a unique gene where the genomic region of all exons was considered as coming from the same RNA molecule and merged together.

RNA-seq data analysis

All reads overlapping the exons of each unique gene model were reported using featureCounts version 1.4.6-p1 [26]. Gene expression was reported as raw counts and in parallel normalized in RPKM in order to filter out genes with low expression value (1 RPKM) before calling for differentially expressed genes. Library size normalizations and differential gene expression calculations have been performed using the package edgeR [27] designed for the R software [28]. Only genes having a significant fold change ≥3 and the Benjamini-Hochberg corrected p-value <0.001 were considered for the differentially expressed genes analysis. Variation between samples was measured using a multi-dimensional scaling plot. Differentially expressed genes were annotated based on the PANTHER tool gene ontology: protein class. Genes coding for proteins involved in cell-cell junctions were selected and categorized per junction type using the cut-off value of 15 RPKM, and a fold change ≥1.5. Heatmaps were generated in GraphPad prism 8.0.1.

Statistical analysis

All analyses were done with GraphPad Prism 8.0.1 software. Results are shown in mean±SD, in median (interquartile range, IQR) or in percentage. Comparisons of means have been performed using *t*-test. Comparisons of medians have been performed using non-parametric Mann-Whitney U test. Comparisons of distributions and percentages have been performed using Chi-square test. Data were considered statistically significant at $p \leq 0.05$.

Results

Tg737$^{orpk/orpk}$ ECs exhibit a larger number of WSS-responsive genes compared to wild-type ECs

The transgenic mouse model *Tg737*$^{orpk/orpk}$ with a mutation in Tg737/IFT88 has been largely used to decrypt the role of primary cilia [16, 20]. Wild-type and *Tg737*$^{orpk/orpk}$ ECs were stained for primary cilia using antibodies against acetylated α-tubulin. As expected, wild-type ECs exhibit primary cilia and no such structures were detected in *Tg737*$^{orpk/orpk}$ ECs **(Figure 1A**). First, we assessed whether the incidence of primary cilia in wild-type ECs was affected by WSS. Thus, ECs were cultured into a flow chamber and exposed during 48-hours to a physiological WSS (30 dynes/cm^2) or to an aneurysmal-type of low WSS (2 dynes/cm^2). A static condition was used as a reference. The percentage of cells containing primary cilia under each condition was not affected by the level of WSS **(Figure 1A)**, indicating that our EC culture model with wild-type and *Tg737*$^{orpk/orpk}$ cells could allow us to decipher the role of primary cilia in the response of ECs to flow. Next, we performed unbiased transcriptomics (RNA-seq) and compared gene expression level at 30 and 2 dynes/cm^2 in wild-type and *Tg737*$^{orpk/orpk}$ ECs. Visualizing the data on a multidimensional scaling plot **(Figure 1B)** illustrates the divergence in response to WSS between wild-type and *Tg737*$^{orpk/orpk}$ ECs. Indeed, wild-type ECs under different levels of shear stress show a high degree of similarity, whereas *Tg737*$^{orpk/orpk}$ ECs represent much more variation of gene expression in response to shear stress. Actually, *Tg737*$^{orpk/orpk}$ ECs show approximately a 5-fold increase in the number of WSS-responsive genes compared to wild-type ECs **(Figure 1C, Supplementary tables 1-2)**. The comparison of physiological flow to pathological flow identified 28 and 24 up- and down-regulated genes **(**fold change ≥3; p≤0.001, **Supplementary table 1)** in wild-type ECs. The same comparison in *Tg737*$^{orpk/orpk}$ ECs yielded 171 and 125 up- and down-regulated genes **(Supplementary table 2)**. As shown in the Venn diagram of **Figure 1D**, 17 differentially express genes in wild-type

ECs in response to aneurysmal low flow, overlapped with differentially express genes in *Tg737*$^{orpk/orpk}$ ECs indicating that they are regulated independently of the presence of the cilia. Moreover, 35 genes were uniquely affected by pathological flow in presence of cilia and 279 genes were uniquely affected by this flow in absence of cilia.

To further understand the biological functions of these uniquely differentially expressed genes, we performed a protein class functional annotation using PANTHER software. Predictably, the *Tg737*$^{orpk/orpk}$ genes were spread into more groups than wild-type genes with varying distributions of protein classes amongst the two cell types. For example, it may be pointed out that 10%, 3.3%, 6.7% and 3.3% of genes in wild-type cells were involved in cell junctions, extracellular matrix, cytoskeletal regulation and defense/immunity, respectively, as compared to 0.6%, 6.5%, 1.8% and 1.2% in *Tg737*$^{orpk/orpk}$ cells. Altogether, our results show that lack of primary cilia increases the sensitivity of ECs to low WSS, and that genes involved in vascular wall structure are affected.

Tg737$^{orpk/orpk}$ endothelium exhibit low barrier integrity and perturbed junctions

An intact endothelial barrier is important for the integrity of the vascular wall. Therefore, we investigated the barrier property of wild-type and *Tg737*^{orpk}/orpk EC monolayers by 2 different methods, *i.e.* TEER and trans-endothelial permeability. Monolayers of wild-type ECs exhibited a TEER of about 80Ω•cm^2. TEER was reduced in *Tg737*$^{orpk/orpk}$ ECs to 50Ω•cm^2, a value that was close to the resistance of the empty filters (*i.e.* 40 Ω•cm^2) (**Figure 2A**). As expected, trans-endothelial permeability of 4kDa FITC-dextran in wild-type EC monolayers displayed a linear increase between 1-, 4- and 6-hours. The permeability of the fluorescent tracer was 3-fold increased in *Tg737*$^{orpk/orpk}$ EC monolayers (**Figure 2B**). Together, these results show decreased endothelial barrier properties in ECs without primary cilia.

The integrity of the endothelial barrier is critically regulated by different protein families at the interface between ECs, forming tight junctions (TJs), adherens junctions (AJs) and gap junctions (GJs) at cell-cell contacts [29]. Altered expression or organization of these junctional proteins would result in endothelial barrier disruption and increased trans-endothelial permeability. Thus, we next compared the RNA expression levels of junctional proteins between wild-type and *Tg737*$^{orpk/orpk}$ ECs using a cut-off of 15 RPKM and a fold change ≥1.5. The transcripts of the TJ genes *Claudin* (*Cldn*)*-3, -9, -12*, *Tight junction protein* (*Tjp1, Tjp2)* and *Junction adhesion molecule* (*Jam*)*-1* were reduced in *Tg737*$^{orpk/orpk}$ ECs, whereas *Jam3* transcripts were increased in *Tg737*$^{orpk/orpk}$ ECs in comparison to wild-type ECs (**Figure 2C; left panel**). The transcripts of the AJ genes *Cadherin (Cdh)3, 6, 16*, *Catenin α-1* (*Ctnna1*), *Catenin α like-1 (Ctnnal1)*, *Catenin β like-1 (Ctnnbl1)* and *Nectin2 (Pvrl2)* were decreased, whereas the expression of *Cdh11*, *Catenin β-1 (Ctnnb1)*, *Catenin δ-1 (Ctnnd1)* mRNA was larger in *Tg737*$^{orpk/orpk}$ ECs (**Figure 2C; middle panel**). The endothelial GJ transcripts *Gja1* and *Gjc1* showed an inverse expression pattern in wild-type and *Tg737*$^{orpk/orpk}$ ECs with the expression of *Gja1* being highest in *Tg737*$^{orpk/orpk}$ ECs (**Figure 2C; right panel)**. mRNA of other junction associated genes such as *Desmoplakin* (*Dsp*), *Junction Plakoglobin* (*Jup*), *Plakophilin* (*Pkp)2, 4*, *Pinin* (*Pnn*) and *Periplakin* (*Ppl*) were all less expressed in *Tg737*$^{orpk/orpk}$ in comparison to wild-type ECs (**Figure 2C; right panel**). Based on these transcripts, the potential differential expression of a number of junctional proteins between wild-type and *Tg737*$^{orpk/orpk}$ ECs was investigated by immunofluorescent stainings (**Figure 2D**). We observed that *Tg737*$^{orpk/orpk}$ ECs expressed less ZO-1, ZO-2, Catenin α-1, Catenin β-1, Claudin-3 and more Cx43 in comparison to wild-type ECs (**Figure 2D**). In addition to these differences in expression level, junctional proteins in *Tg737*$^{orpk/orpk}$ ECs displayed a scattered organization at cell-cell contacts. Altogether these experiments show that the *Tg737*$^{orpk/orpk}$ endothelium exhibits a reduced barrier integrity and perturbed intercellular junctions**.**

Silencing ZO-1 modifies the arrangement of other junction proteins

TJ, AJ and GJ complexes consist of specific junction molecules at the membrane and intracellular interactors that mediate their distinctive functions (**Figure 3A**) [29]. However, the 3 types of junctions are interconnected through the cytoskeleton and also share common components. As ZO-1 binds to important protein components of the TJ (e.g. Claudins), AJ (e.g. Catenin α and β) and GJ (e.g. Cx43), we have first focused our attention on the role of this shared protein for membrane organization and permeability. Thus, we transfected wild-type ECs with siRNA directed against *Tjp1* or with a non-targeting siRNA. SiTjp1 reduced *Tjp1* mRNA (**Figure 3B, left panel**) and ZO-1 protein expression (**Figure 3B, middle and right panels**) as compared to siNT. Importantly, knock-down of ZO-1 expression in ECs induced important alterations in the expression and subcellular location of other junction proteins. Similar to the *Tg737*$^{orpk/orpk}$ ECs, we observed a lower expression of ZO-2 and Claudin-3 and a trend towards increased expression of Cx43 and Catenin β-1 (**Figure 3C, top and middle panels**). To examine the consequences of reduced expression of ZO-1 for junctional protein arrangement at the cell-cell contacts, we classified each cell positively stained for ZO-2, Catenin α-1, Catenin β-1, Claudin-3 or Cx43 as having a sharp, wide or discontinuous junctional signal (**Supplementary figure 1A**). Reduced expression of ZO-1 lead to significant differences in the junctional arrangement of ZO-2, Catenin α-1, Catenin β-1 Claudin-3 and Cx43 into a wider and more discontinuous direction (**Figure 3C, bottom panel**).

Since loss of ZO-1 is associated with impaired junctional organization, we next investigated the barrier function in ZO-1 stable knock-down cells (**Supplementary figure 1B**). Thus, TEER was lower in ECs with stable knock-down of *Tjp1* as compared to control ECs transduced with a scrambled sequence (**Figure 3D, left panel**). Trans-endothelial permeability of 4kDa FITC-dextran in control EC monolayers displayed a linear increase between 1-, 4- and 6-hours. The permeability of the fluorescent tracer was 2-fold increased in *Tjp1* knock-down EC monolayers

at 4 and 6-hours (**Figure 3D, right panel**). Together, these results indicate that ZO-1 plays a key role in regulation of the integrity of the endothelium.

IA domes from PKD and non-PKD patient

To test whether impaired function or absence of primary cilia would affect endothelial ZO-1 expression and IA wall organization, we analyzed IA domes from PKD patients and compared their composition to control (non-PKD) patients. Human IA domes located on the middle cerebral artery were extracted from the Swiss AneuX biobank [3]. Patient and IA characteristics are shown in **Table 1**. As expected, PKD patients reported more frequently a positive familial history of IAs and hypertension than non-PKD patients. Previous aneurysmal subarachnoid hemorrhage incidence was null in PKD patients and their IAs appeared to have a lower diameter, with less rough appearance and a lower incidence of blebs compared to non-PKD IAs; these differences are probably due to the fact that in PKD patients IAs are promptly treated. Importantly, IAs of PKD patients were taken from the same location and IA neck size were comparable to the ones of non-PKD patients, suggesting that they might have been submitted to similar WSS. First, we measured IA vessel wall surface area and showed that in PKD patients IAs were thinner compared to non-PKD IAs (**Figure 4A**). Then, we performed histological characterization of the IA domes by immunostaining. No differences were found between PKD and non-PKD IAs in smooth muscle cell, macrophage and elastin contents (data not shown). However, PKD IAs contained less total collagen than non-PKD IAs (**Figure 4B, upper panel**) and the relative contribution of type I and III collagen was different with more type I collagen and less type III collagen in PKD IAs (**Figure 4B, lower panel**). Then, we classified the IA domes in four grades based on previously defined histological characteristics [3, 30]; *i.e.* endothelialized wall with linearly organized smooth muscle cells (grade A), thickened wall with disorganized smooth muscle cells (grade B), hypocellular wall with either intimal hyperplasia

or organizing luminal thrombus (grade C) or extremely thin thrombosis-lined hypocellular wall (grade D). Each dome was classified based on the most severe grade observed in the sample. Fifty percent of IAs from PKD patients were classified with the most severe phenotype (grade D), the other half was classified as grade B (**Figure 4C**). Non-PKD IA domes showed in general less damaged phenotype with 20% grade B, 50% grade C and only 30% grade D (**Figure 4C**). Finally, we assessed ZO-1 expression in ECs of IA domes. A superficial temporal artery with well-preserved ECs was used to support the validity of the immunostaining (**Figure 4D, top panels**). As expected, the majority of IAs displayed a loss of ECs. However, ZO-1 staining seemed less strong in ECs of PKD than non-PKD IA domes (**Figure 4D, bottom panels**). Taken together, our results show that even if PKD IA domes were of smaller size, they displayed a severe IA wall degradation and the remaining ECs in the aneurysm dome exhibit a lower ZO-1 content.

Discussion

Primary cilia absence or dysfunction in PKD patients has been associated with increased IA formation and progression [19, 31]. The molecular mechanism by which primary cilia promotes IA disease is however not yet understood. In the present study, we investigated the role of mechano-sensitive primary cilia on EC function in the context of IA disease. Using *in vitro* flow experiments and an unbiased transcriptomic approach, we showed that the loss of primary cilia in *Tg737*$^{orpk/orpk}$ ECs was associated with a 5-fold increase in the number of WSS-responsive genes (**Figure 1**), indicating that primary cilia in ECs may have a dampening effect on the pathological response to aneurysmal low WSS. In addition, we showed that primary cilia-deficient ECs had a reduced TEER and a higher trans-endothelial permeability in comparison to wild-type ciliated ECs (**Figure 2**). We further showed that the loss of barrier integrity was concomitant with disrupted junction proteins such as ZO-1, ZO-2, Catenin α-1, Catenin β-1, Cx43 and Claudin-3 (**Figure 2**). Reducing ZO-1 in wild-type ECs altered the junctional organization of afore-mentioned TJ, AJ and GJ proteins, generated a drop in TEER and an increase in trans-endothelial permeability, pointing to a central role of ZO-1 for a proper endothelial barrier function (**Figure 3**). The histological analysis of IA domes from PKD in comparison to non-PKD patients revealed that they have thinner walls with a lower collagen content, as well as a shift in collagen type towards more type I collagen and less type III collagen, and that they displayed a more degraded vascular wall phenotype. Histological changes in PKD aneurysms were similar to those described for ruptured IAs when compared to non-ruptured IAs [3]. Finally, ECs in IA domes from PKD patients appeared to have lower ZO-1 levels compared to ECs of aneurysm domes of non-PKD patients (**Figure 4**).

WSS is considered as an important driver of IA disease. Substantial evidence supports that aneurysmal remodeling starts when high WSS in combination with high positive WSS gradients go beyond a certain threshold [7, 32] causing injury to the endothelium, disruption of the

internal elastic lamina and loss of smooth muscle cells. Furthermore, it appeared that both low and high WSS can drive the growth of IAs [18]. In fact, low WSS in combination with high oscillatory shear index have been associated with inflammatory cell-mediated destructive remodeling, while high and positive WSS gradient cause mural cell-mediated remodeling [18]. Nevertheless, only few IAs rupture during a lifetime. It is therefore essential to understand how the WSS experienced by the vascular wall relates to tissue changes leading to IA growth and rupture. The response of ECs to flow is mediated by mechano-sensors such as primary cilia. Genetic diseases characterized by dysfunction or absence of primary cilia, such as PKD, have been associated with an increased risk of developing vascular disorders. In this study we show that loss of primary cilia in ECs impaired junctional gene and protein expression as well as altered junction organization. The latter effect may involve microtubule disassembly since they participate in trafficking of TJ proteins [33]. Indeed, loss of IFT88 has been associated with the hyper-acetylation of microtubules altering microtubule stability [34]. An alternative mechanism may involve endothelial-to-mesenchymal transition (EndMT). It is known that the lack of primary cilia promotes EndMT through the control of the transcription factor SLUG [20, 35]. Interestingly, SLUG has been associated with reduced expression of TJ proteins [36]. We hypothesized that primary cilia-induced junction remodeling would be mediated by ZO-1 as a central regulator. Targeting ZO-1 in wild-type ciliated ECs induced a shift towards a wider and discontinuous distribution of some junction proteins (**Figure 3**). Interestingly, it has been demonstrated that irregular and diffuse junctions between ECs are associated to lower TEER [37], hence supporting our findings.

Observations in different studies support a role of ZO-1 as key regulator of intercellular junctions. The absence of ZO-1 induced defects in vascular development and impaired formation of vascular trees, thus demonstrating the absolute requirement of ZO-1 in cellular junction establishment and maintenance [38, 39]. In addition, ZO-1 can regulate gene

expression through its interaction with ZONAB (ZO-1 associated nucleic acid protein) [40]. It is also known that ZO-1 has the ability to translocate itself into the nucleus even though its function at this location has not yet been described [40, 41]. At an early stage of junction formation, ZO-1 is found at AJs and concentrates later at TJs [42]. ZO-1 recruitment and distribution along the cell border permits the recruitment and insertion of claudins and occludins into the cell membrane [43]. It has also been demonstrated that ZO-1 can regulate the rate of Cx43 accumulation at GJs [44, 45]. The interaction of ZO-1 with its associated junctional proteins is mediated through its PDZ domain [40, 46]. A reduction of ZO-1 content would thus generate a competition for its PDZ domain and would result in reduced or a less sharp intercellular localization of junctional proteins with the lowest affinity.

IA incidence [47] and the frequency of their rupture [48] is higher in PKD patients than in the general population, raising the question of a tailored screen for IA stability in this patient population. We have shown that the decrease of ZO-1 observed in ECs lacking primary cilia leads to an increased permeability for a large (4 kDa) fluorescent tracer. In analogy, one might expect that contrast agents used for radiological imaging may display more diffuse distribution patterns due to leakiness of the endothelium in IAs of PKD patients. Interestingly, vessel wall contrast enhancement on magnetic resonance imaging visualizing the local accumulation of a colloid contrast agent is considered as a promising tool for clinical staging of IA disease [49]. Indeed, vessel wall enhancement presents in different but distinctive patterns. Although the association with wall instability has been demonstrated [50], the biological and radiological mechanisms resulting in vessel wall enhancement and the diagnostic interpretation of the different patterns are presently unclear. Although a limitation of our study is that we have investigated the differential gene expression and function of ECs in an *in vitro* model, this reductionist approach helped to understand some of the mechano-transduction events occurring in the endothelium devoid of primary cilia. Future work using mutant animal models will shed

some light on the role of primary cilia and ZO-1 in the pathogenesis of IAs. Such work will also allow for linking vessel wall imaging directly to vessel wall function and histology. Moreover, further research should also provide insight whether the signaling pathways identified with the help of this PKD cell model may be generalized to the endothelium of instable IAs, thus allowing for the development of biomarkers or radiological tracers for vulnerable IAs.

Acknowledgements

This work was supported by grants from the Swiss SystemsX.ch initiative, evaluated by the Swiss National Science Foundation, the Foundation Carlos et Elsie De Reuter, the Swiss Heart Foundation, the Novartis Foundation for medical-biological Research and the Gottfried und Julia Bangerter-Rhyner-Stiftung. We thank Esther Sutter, Bernard Foglia and Graziano Pelli for their technical help.

References

1. Brisman, J.L., J.K. Song, and D.W. Newell, *Cerebral aneurysms.* N Engl J Med, 2006. **355**(9): p. 928-39.
2. Diagbouga, M.R., et al., *Role of hemodynamics in initiation/growth of intracranial aneurysms.* Eur J Clin Invest, 2018. **48**(9): p. e12992.
3. Morel, S., et al., *Correlating Clinical Risk Factors and Histological Features in Ruptured and Unruptured Human Intracranial Aneurysms: The Swiss AneuX Study.* J Neuropathol Exp Neurol, 2018. **77**(7): p. 555-566.
4. Frosen, J., et al., *Flow-induced, inflammation-mediated arterial wall remodeling in the formation and progression of intracranial aneurysms.* Neurosurg Focus, 2019. **47**(1): p. E21.
5. Galley, H.F. and N.R. Webster, *Physiology of the endothelium.* Br J Anaesth, 2004. **93**(1): p. 105-13.
6. Kolega, J., et al., *Cellular and molecular responses of the basilar terminus to hemodynamics during intracranial aneurysm initiation in a rabbit model.* J Vasc Res, 2011. **48**(5): p. 429-42.
7. Meng, H., et al., *Complex hemodynamics at the apex of an arterial bifurcation induces vascular remodeling resembling cerebral aneurysm initiation.* Stroke, 2007. **38**(6): p. 1924-31.
8. Wang, Z., et al., *Molecular alterations associated with aneurysmal remodeling are localized in the high hemodynamic stress region of a created carotid bifurcation.* Neurosurgery, 2009. **65**(1): p. 169-77; discussion 177-8.
9. Aoki, T., et al., *Macrophage-derived matrix metalloproteinase-2 and -9 promote the progression of cerebral aneurysms in rats.* Stroke, 2007. **38**(1): p. 162-9.
10. Aoki, T., et al., *NF-kappaB is a key mediator of cerebral aneurysm formation.* Circulation, 2007. **116**(24): p. 2830-40.
11. Cebral, J., et al., *Flow Conditions in the Intracranial Aneurysm Lumen Are Associated with Inflammation and Degenerative Changes of the Aneurysm Wall.* AJNR Am J Neuroradiol, 2017. **38**(1): p. 119-126.
12. Krishnappa, V., et al., *Autosomal dominant polycystic kidney disease and the heart and brain.* Cleve Clin J Med, 2017. **84**(6): p. 471-481.
13. Zhou, S., P.A. Dion, and G.A. Rouleau, *Genetics of Intracranial Aneurysms.* Stroke, 2018. **49**(3): p. 780-787.
14. Brown, J.M. and G.B. Witman, *Cilia and Diseases.* Bioscience, 2014. **64**(12): p. 1126-1137.
15. AbouAlaiwi, W.A., et al., *Ciliary polycystin-2 is a mechanosensitive calcium channel involved in nitric oxide signaling cascades.* Circ Res, 2009. **104**(7): p. 860-9.
16. Nauli, S.M., et al., *Endothelial cilia are fluid shear sensors that regulate calcium signaling and nitric oxide production through polycystin-1.* Circulation, 2008. **117**(9): p. 1161-71.
17. Van der Heiden, K., et al., *Endothelial primary cilia in areas of disturbed flow are at the base of atherosclerosis.* Atherosclerosis, 2008. **196**(2): p. 542-50.
18. Meng, H., et al., *High WSS or low WSS? Complex interactions of hemodynamics with intracranial aneurysm initiation, growth, and rupture: toward a unifying hypothesis.* AJNR Am J Neuroradiol, 2014. **35**(7): p. 1254-62.
19. Liu, M., et al., *Primary Cilia Deficiency Induces Intracranial Aneurysm.* Shock, 2018. **49**(5): p. 604-611.
20. Egorova, A.D., et al., *Lack of primary cilia primes shear-induced endothelial-to-mesenchymal transition.* Circ Res, 2011. **108**(9): p. 1093-101.

21. Jones, T.J., et al., *Primary cilia regulates the directional migration and barrier integrity of endothelial cells through the modulation of hsp27 dependent actin cytoskeletal organization.* J Cell Physiol, 2012. **227**(1): p. 70-6.
22. Coen, M., et al., *Smooth muscle cells of human intracranial aneurysms assume phenotypic features similar to those of the atherosclerotic plaque.* Cardiovasc Pathol, 2013. **22**(5): p. 339-44.
23. Skalli, O., et al., *A monoclonal antibody against alpha-smooth muscle actin: a new probe for smooth muscle differentiation.* J Cell Biol, 1986. **103**(6 Pt 2): p. 2787-96.
24. Sabine, A., et al., *FOXC2 and fluid shear stress stabilize postnatal lymphatic vasculature.* J Clin Invest, 2015. **125**(10): p. 3861-77.
25. Dobin, A., et al., *STAR: ultrafast universal RNA-seq aligner.* Bioinformatics, 2013. **29**(1): p. 15-21.
26. Quinlan, A.R. and I.M. Hall, *BEDTools: a flexible suite of utilities for comparing genomic features.* Bioinformatics, 2010. **26**(6): p. 841-2.
27. Robinson, M.D., D.J. McCarthy, and G.K. Smyth, *edgeR: a Bioconductor package for differential expression analysis of digital gene expression data.* Bioinformatics, 2010. **26**(1): p. 139-40.
28. RDC, T., *R: a language and environment for statistical computing*, in *R Foundation for Statistical Computing*. 2011: Vienna, Austria.
29. Bazzoni, G. and E. Dejana, *Endothelial cell-to-cell junctions: molecular organization and role in vascular homeostasis.* Physiol Rev, 2004. **84**(3): p. 869-901.
30. Frosen, J., et al., *Remodeling of saccular cerebral artery aneurysm wall is associated with rupture: histological analysis of 24 unruptured and 42 ruptured cases.* Stroke, 2004. **35**(10): p. 2287-93.
31. Aboualaiwi, W.A., et al., *Survivin-induced abnormal ploidy contributes to cystic kidney and aneurysm formation.* Circulation, 2014. **129**(6): p. 660-72.
32. Metaxa, E., et al., *Characterization of critical hemodynamics contributing to aneurysmal remodeling at the basilar terminus in a rabbit model.* Stroke, 2010. **41**(8): p. 1774-82.
33. Glotfelty, L.G., et al., *Microtubules are required for efficient epithelial tight junction homeostasis and restoration.* Am J Physiol Cell Physiol, 2014. **307**(3): p. C245-54.
34. Berbari, N.F., et al., *Microtubule modifications and stability are altered by cilia perturbation and in cystic kidney disease.* Cytoskeleton (Hoboken), 2013. **70**(1): p. 24-31.
35. Sanchez-Duffhues, G., et al., *SLUG is expressed in endothelial cells lacking primary cilia to promote cellular calcification.* Arterioscler Thromb Vasc Biol, 2015. **35**(3): p. 616-27.
36. Wang, Z., et al., *Raf 1 represses expression of the tight junction protein occludin via activation of the zinc-finger transcription factor slug.* Oncogene, 2007. **26**(8): p. 1222-30.
37. Hilfenhaus, G., et al., *Vav3-induced cytoskeletal dynamics contribute to heterotypic properties of endothelial barriers.* J Cell Biol, 2018. **217**(8): p. 2813-2830.
38. Dejana, E., *Endothelial cell-cell junctions: happy together.* Nat Rev Mol Cell Biol, 2004. **5**(4): p. 261-70.
39. Alfano, J.M., et al., *Intracranial aneurysms occur more frequently at bifurcation sites that typically experience higher hemodynamic stresses.* Neurosurgery, 2013. **73**(3): p. 497-505.
40. Gonzalez-Mariscal, L., et al., *Tight junctions and the regulation of gene expression.* Semin Cell Dev Biol, 2014. **36**: p. 213-23.

41. Gottardi, C.J., et al., *The junction-associated protein, zonula occludens-1, localizes to the nucleus before the maturation and during the remodeling of cell-cell contacts.* Proc Natl Acad Sci U S A, 1996. **93**(20): p. 10779-84.
42. Itoh, M., et al., *The 220-kD protein colocalizing with cadherins in non-epithelial cells is identical to ZO-1, a tight junction-associated protein in epithelial cells: cDNA cloning and immunoelectron microscopy.* J Cell Biol, 1993. **121**(3): p. 491-502.
43. Fanning, A.S. and J.M. Anderson, *Zonula occludens-1 and -2 are cytosolic scaffolds that regulate the assembly of cellular junctions.* Ann N Y Acad Sci, 2009. **1165**: p. 113-20.
44. Hunter, A.W., et al., *Zonula occludens-1 alters connexin43 gap junction size and organization by influencing channel accretion.* Mol Biol Cell, 2005. **16**(12): p. 5686-98.
45. Laing, J.G., B.C. Chou, and T.H. Steinberg, *ZO-1 alters the plasma membrane localization and function of Cx43 in osteoblastic cells.* J Cell Sci, 2005. **118**(Pt 10): p. 2167-76.
46. Nomme, J., et al., *Structural Basis of a Key Factor Regulating the Affinity between the Zonula Occludens First PDZ Domain and Claudins.* J Biol Chem, 2015. **290**(27): p. 16595-606.
47. Kuo, I.Y. and A. Chapman, *Intracranial Aneurysms in ADPKD How Far Have We Come?* Clinical Journal of American Society of Nephrology, 2019. **14**: p. 1119–1121.
48. Sanchis, I.M., et al., *Presymptomatic Screening for Intracranial Aneurysms in Patients with Autosomal Dominant Polycystic Kidney Disease.* Clin J Am Soc Nephrol, 2019. **14**(8): p. 1151-1160.
49. Backes, D., et al., *Determinants of Gadolinium-Enhancement of the Aneurysm Wall in Unruptured Intracranial Aneurysms.* Neurosurgery, 2018. **83**(4): p. 719-725.
50. Matouk, C.C., et al., *Vessel wall magnetic resonance imaging identifies the site of rupture in patients with multiple intracranial aneurysms: proof of principle.* Neurosurgery, 2013. **72**(3): p. 492-6; discussion 496.

Legends

Figure 1: Primary cilia regulate gene expression in response to aneurysmal low flow.

(A) Acetylated α-tubulin staining for primary cilia (in green) in wild-type (WT) and *Tg737*$^{orpk/orpk}$ ECs (ORPK). Nuclei were stained with DAPI (blue). Evans blue counterstaining is in red. Scale bar represents 10μm. Quantification of primary cilia in WT ECs after 48-hours exposure to WSS of 30 dynes/cm^2 (black) or 2 dynes/cm^2 (gray). The number of cilia under flow was normalized to the number of cilia in parallel cultures kept under static conditions. Results are shown as individual values and as mean±SD; N=5. (B) Multidimensional scaling plot representing similarities in gene expression between WT and ORPK ECs. Violet (30 dynes/cm^2) and blue (2 dynes/cm^2) dots represent WT ECs; green (30 dynes/cm^2) and red (2 dynes/cm^2) dots represent ORPK ECs; N=3. (C) Volcano plot displaying differential expressed genes under aneurysmal low flow (2 dynes/cm^2) compared to physiological flow (30 dynes/cm^2) in WT ECs (left panel) and ORPK ECs (right panel). The y-axis corresponds to the mean expression value of $\log_{10}$ (p-value), and the x-axis displays the $\log_2$ fold change value. The red and blue dots represent the up- and down-regulated genes, respectively, under 2 dynes/cm^2 compared to 30 dynes/cm^2 (fold change ≥ 3; p≤0.001). (D) Venn diagrams of the number of genes that are differentially regulated by flow conditions in ORPK ECs compared to WT ECs. Colors represent differentially expressed genes in presence of primary cilia (blue) and in absence (red) of primary cilia. The purple color represents differentially expressed genes that are independent of the presence of primary cilia (left panel). Pie charts of differentially expressed genes in WT (middle panel) and ORPK (right panel) ECs based on Gene Ontology protein class. 1: Calcium-binding proteins (PC00060); 2: Cell junction proteins (PC00070); 3: Cytoskeletal proteins (PC00085); 4: Defense/immunity proteins (PC00090); 5: Enzyme modulators (PC00095); 6: Extracellular matrix proteins (PC00102); 7: Hydrolases (PC00121); 8: Nucleic acid binding proteins (PC00171); 9: Oxidoreductases (PC00176); 10: Receptors

(PC00197); 11: Signaling molecules (PC00207); 12: Transcription factors (PC00218); 13: Transfer/carrier proteins (PC00219); 14: Transferases (PC00220); 15: Cell adhesion molecules (PC00069); 16: Chaperones (PC00072); 17: Isomerases (PC00135); 18: Ligases (PC00142); 19: Lyases (PC00144); 20: Membrane traffic proteins (PC00150); 21: Storage proteins (PC00210); 22 : Structural proteins (PC00211); 23: Transporters (PC00227).

Figure 2: Primary cilia regulate EC barrier integrity and gene expression.

(A) Trans-endothelial resistance in *Tg737*$^{orpk/orpk}$ (ORPK) ECs compared to wild-type (WT) ECs. Results are shown as individual values and as mean±SD; N=3. *t*-test, **p≤0.01; ****p ≤0.0001. (B) Comparison of WT and ORPK ECs barrier properties using FITC-dextran permeability assay at 1-, 4- and 6-hours. Results are shown as individual values and as mean±SD; N=3. (C) Heatmaps representation of tight junction genes (left), adherens junction genes (middle), gap junction- and associated desmosomal-family genes (right) expression levels comparing WT and ORPK ECs. Gene expression levels are represented in RPKM. Represented genes are ≥ 15 RPKM in at least 1 condition, with a fold change ≥1.5 between WT and ORPK ECs. (D) Immunofluorescent staining (in red) of Zonula occludens 1 (ZO-1), Zonula occludens 2 (ZO-2), Catenin α-1, Catenin β-1, Claudin-3 (cldn3) and Connexin43 (Cx43) on confluent cultures of WT and ORPK ECs. Nuclei were stained with DAPI (blue). Scale bar represents 10μm.

Figure 3: Reduction of *Tjp1* affects expression and organization of junction proteins

(A) Schematic representation of the key role of ZO-1 in tight-, adherens-, and gap junctions. (B) *Tjp1* expression level in wild-type ECs treated with *Tjp1* siRNA (siTjp1) or non-targeting siRNA (NT) assessed by qPCR (left panel), immunofluorescence (middle panel; ZO-1 in green) and Western blot (right panel). Results are shown as individual values and as mean±SD; N=3.

t-test, ***p≤0.001 (C) Representative images (top panels) and quantification (middle panel) of immunostainings (in red) for ZO-2, Catenin α-1, Catenin β-1, cldn3 and Cx43 on confluent cultures of siTjp1 and siNT transfected ECs. The organization of junction proteins (bottom panel) was classified following the definitions: sharp (light gray), wide (dark gray), discontinuous (Discont., black). Scale bar represents 10μm. N=3. Chi-square test, *p≤0.05; **p≤0.01; ***p≤0.001. (D) Trans-endothelial resistance (left panel) and FITC-dextran permeability (right panel) at 1-, 4- and 6-hours in *Tjp1* knock-down ECs compared to control (scramble) ECs. Results are shown as individual values and as mean±SD; N=3. *t*-test, *p≤0.05; ***p≤0.001.

Figure 4: Characterization of IA domes of non-PKD and PKD patients

(A) Mean surface area, measured in 3 to 4 regions of interest (ROI) covering almost the entire surface of the sample, was lower in PKD patients in comparison to non-PKD patients. Results are shown as individual values and in median±interquartile range. Non-parametric Mann-Whitney U test, *p≤0.05. (B) Total collagen content (upper panel) was lower in PKD patients than in non-PKD patients. Results are shown as individual values and in median±interquartile range. Non-parametric Mann-Whitney U test, *p≤0.05. Moreover, the relative distribution of collagen type I and III (lower panel) was different between non-PKD and PKD patients. Results are shown as percentage. *p≤0.05. (C) Classification of IA domes following the definitions: B: Thickened wall with disorganized smooth muscle cells (light gray); C: Hypocellular wall with either intimal hyperplasia or organizing luminal thrombosis (dark grey); and D: An extremely thin thrombosis-lined hypocellular wall (black). IA domes from PKD patients had more severe phenotype (grade D) than domes of non-PKD patients. Chi-square test, ****p≤0.0001. (D) Representative examples of ZO-1 immunostaining (in brown, some positive ECs are indicated in red) performed on a human superficial temporal artery (upper left panel) and on IA domes

from non-PKD (lower left panel) and PKD (lower right panel) patients. Not stained ECs are indicated in green in the negative control performed on the superficial temporal artery (upper right panel). Scale bar represents 20μm.

Figure S1: (A) Representative pictures showing junctional organization categories. (B) *Tjp1* expression level in scrambled or *Tjp1* knock-down ECs assessed by immunofluorescence (left panel; ZO-1 in red) and Western blot (right panel). Scale bars represent 10μm.

	Non-PKD patients	**PKD patients**	**p-value**
Patients	***N=20***	***N=3***	
Age, years: median (IQR)	55 (48-64)	49 (44-73)	0.98
Sex, female: N (%)	15 (75)	2 (67)	0.21
Eurasian ethnicity: N (%)	20 (100)	3 (100)	1
Multiple aneurysms: N (%)	11 (55)	2 (67)	0.08
Previous aSAH: N (%)	4 (20)	0 (0)	0.0001
Positive familial history for IA: N (%)	3 (15)	1 (50)	0.00001
Smoker (former and current): N (%)	14 (70)	1 (33)	0.00001
Hypertension: N (%)	8 (40)	3 (100)	0.0001
Intracranial aneurysms	***N=20***	***N=4***	
Rough appearance: N (%)	11 (58)	1 (25)	0.0001
Presence of blebs or lobules: N (%)	11 (55)	1 (25)	0.0001
Neck size, mm: median (IQR)	4.0 (3.0-5.8)	3.5 (3.0-4.0)	0.24
Maximal diameter, mm: median (IQR)	6.5 (5.0-10.0)	4.0 (2.5-6.3)	0.04

Table 1: Patient and IA characteristics before surgery

Comparisons of medians and percentages have been performed using non-parametric Mann-Whitney U test or Fisher's exact test, respectively. Positive familial history for IA is defined as one or more 1st degree relative(s) with IA. A current smoker is a patient currently smoking more than 300 cigarettes and a former smoker is a patient who smoked more than 300 cigarettes

and who stopped at least 6 months ago. Arterial hypertension is defined as blood pressure greater than 140/90 mmHg independently of the existence or not of a treatment against hypertension. Rough appearance is defined as the presence of sub-millimetric irregularities. aSAH = aneurysmal sub-arachnoid haemorrhage; IQR= interquartile range.

Figure 1

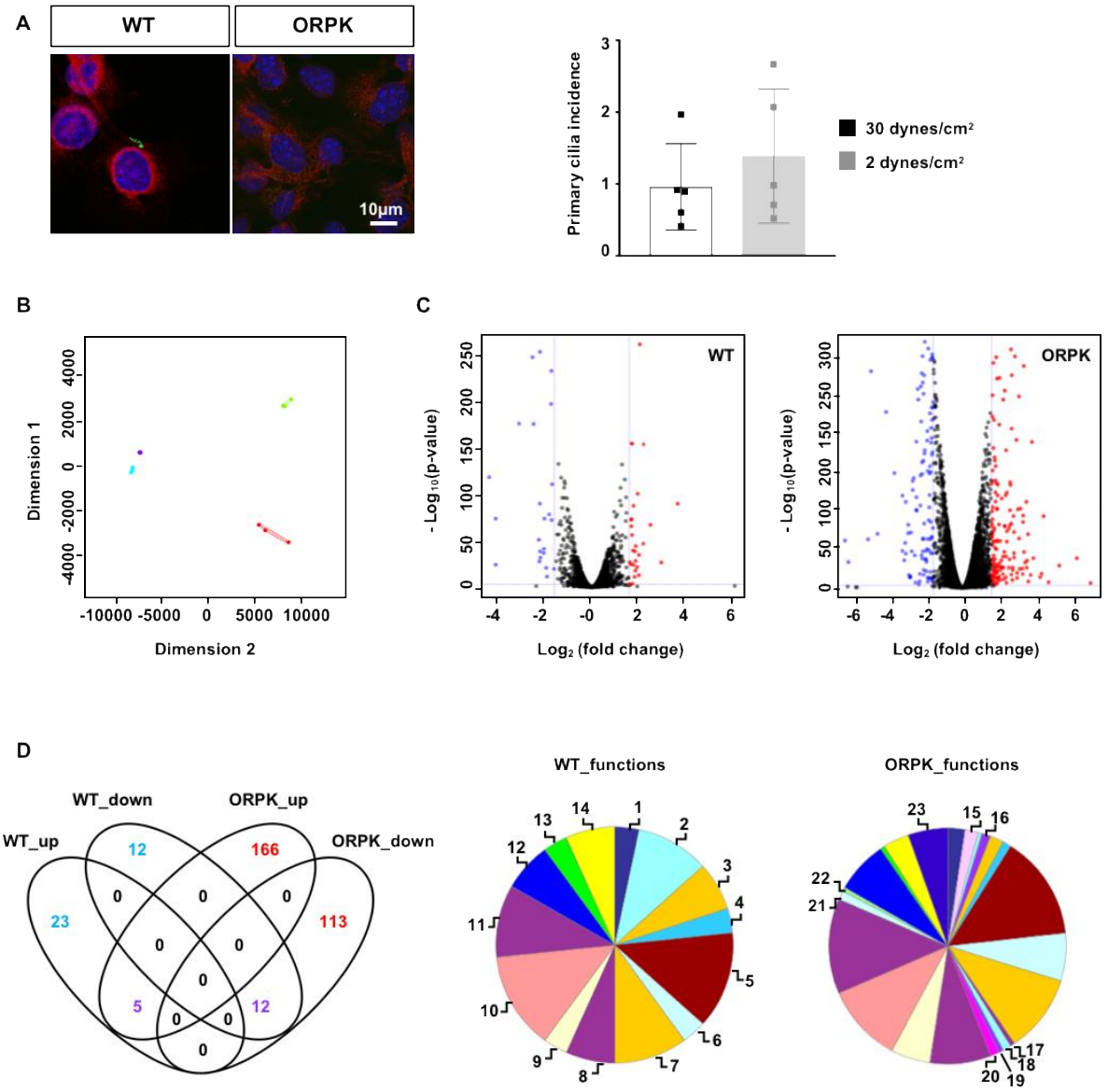
A
WT
ORPK
10μm
Primary cilia incidence
30 dynes/cm²
2 dynes/cm²
B
Dimension 1
Dimension 2
C
WT
ORPK
- Log10(p-value)
Log2 (fold change)
D
WT_up
WT_down
ORPK_up
ORPK_down
WT_functions
ORPK_functions

Figure 2

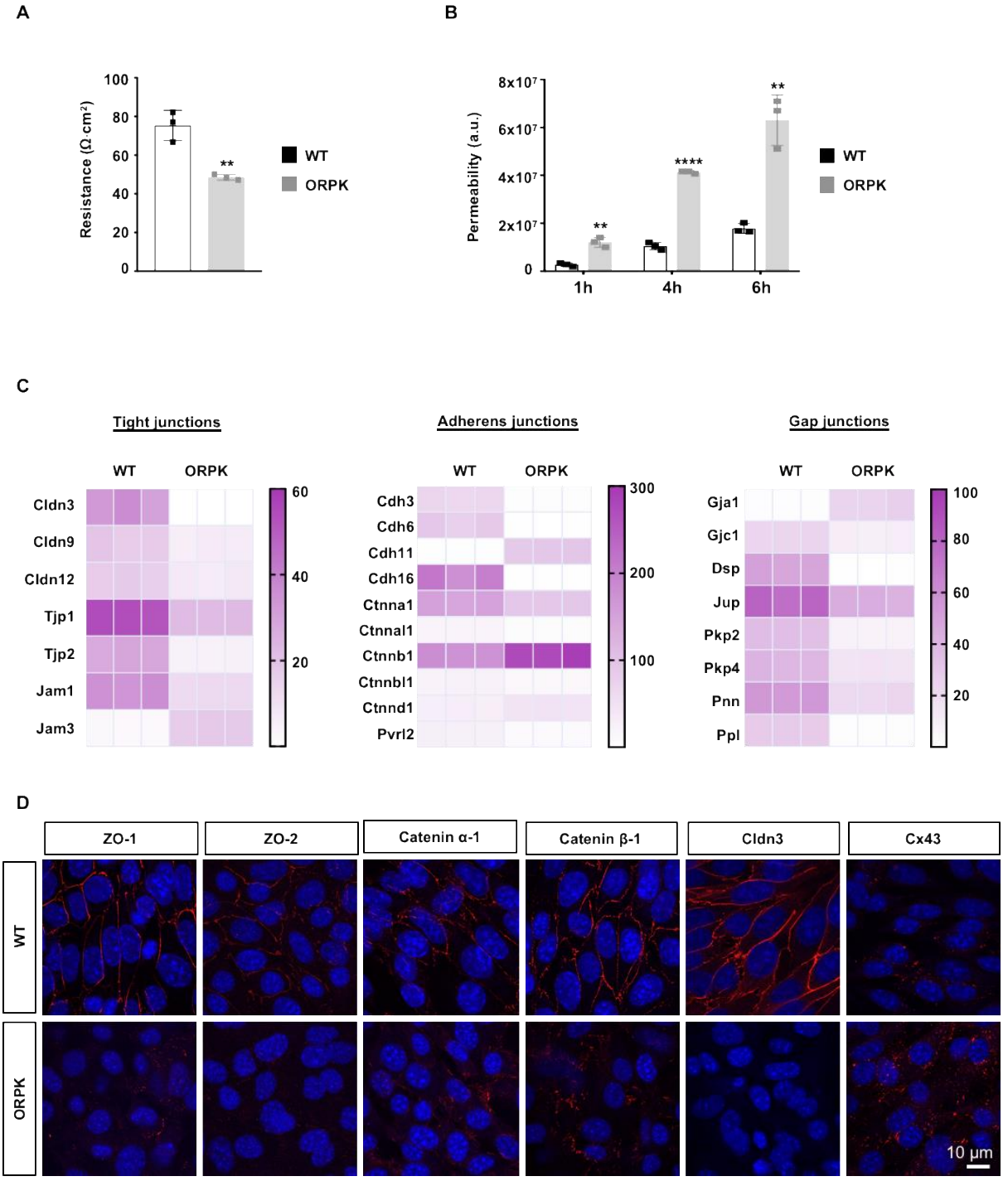
A
Resistance (Ω.cm²)
100
80
60
40
20
0
**
WT
ORPK
B
Permeability (a.u.)
8x10⁷
6x10⁷
4x10⁷
2x10⁷
0
**
****
**
1h
4h
6h
WT
ORPK
C
Tight junctions
Adherens junctions
Gap junctions
WT
ORPK
Cldn3
Cldn9
Cldn12
Tjp1
Tjp2
Jam1
Jam3
60
40
20
Cdh3
Cdh6
Cdh11
Cdh16
Ctnna1
Ctnnal1
Ctnnb1
Ctnnbl1
Ctnnd1
Pvrl2
300
200
100
Gja1
Gjc1
Dsp
Jup
Pkp2
Pkp4
Pnn
Ppl
100
80
60
40
20
D
ZO-1
ZO-2
Catenin α-1
Catenin β-1
Cldn3
Cx43
WT
ORPK
10 µm

Figure 3

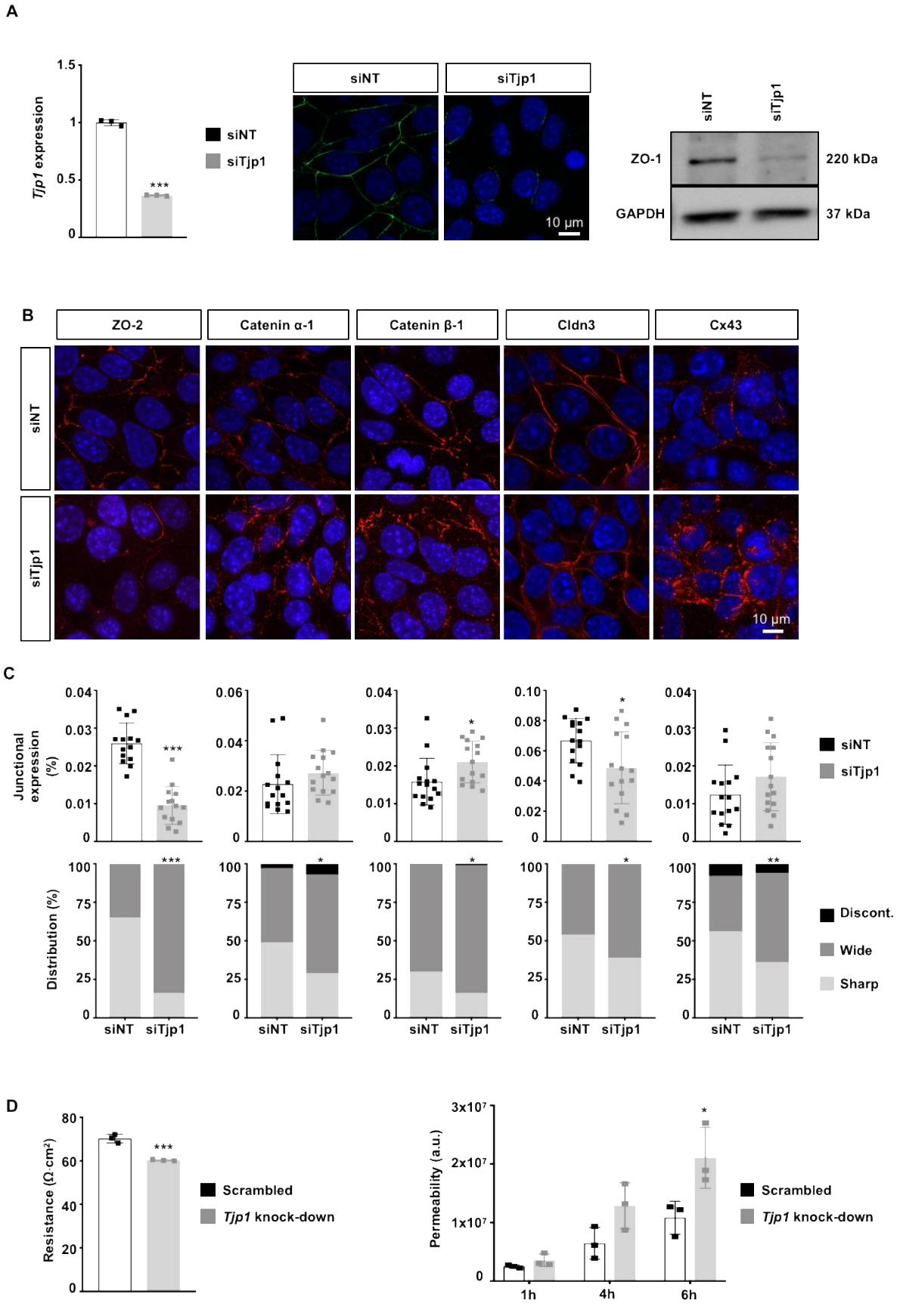
A
Tjp1 expression
siNT
siTjp1
10 µm
ZO-1
GAPDH
220 kDa
37 kDa
B
ZO-2
Catenin α-1
Catenin β-1
Cldn3
Cx43
C
Junctional expression (%)
Distribution (%)
Discont.
Wide
Sharp
D
Resistance (Ω·cm²)
Scrambled
Tjp1 knock-down
Permeability (a.u.)
1h
4h
6h

Figure 4

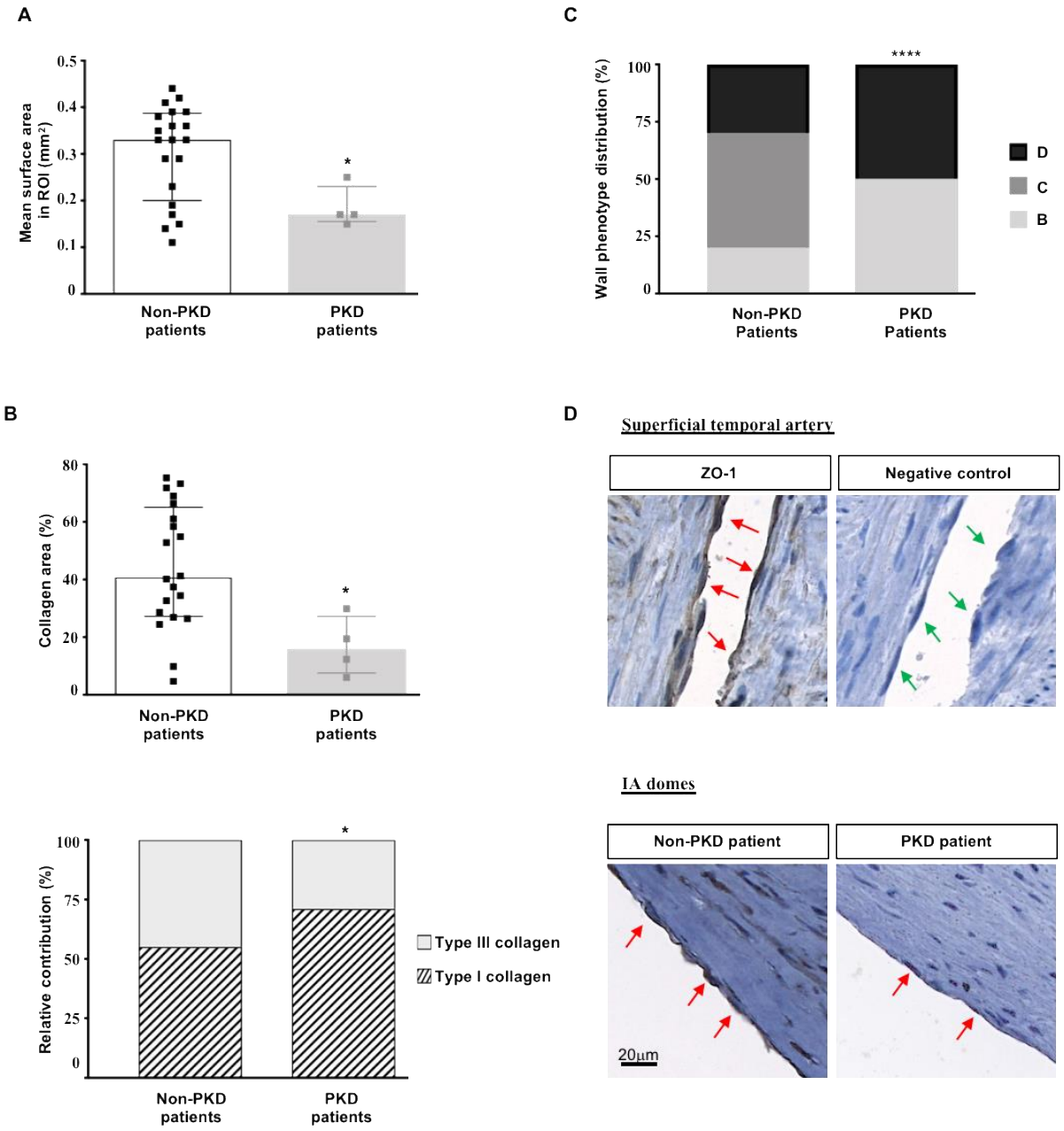
A
Mean surface area in ROI (mm²)
0.5
0.4
0.3
0.2
0.1
0
*
Non-PKD patients
PKD patients
C
Wall phenotype distribution (%)
100
75
50
25
0
****
Non-PKD Patients
PKD Patients
D
C
B
B
Collagen area (%)
80
60
40
20
0
*
Non-PKD patients
PKD patients
Relative contribution (%)
100
75
50
25
0
*
Non-PKD patients
PKD patients
Type III collagen
Type I collagen
D
Superficial temporal artery
ZO-1
Negative control
IA domes
Non-PKD patient
PKD patient
20µm

Figure S1

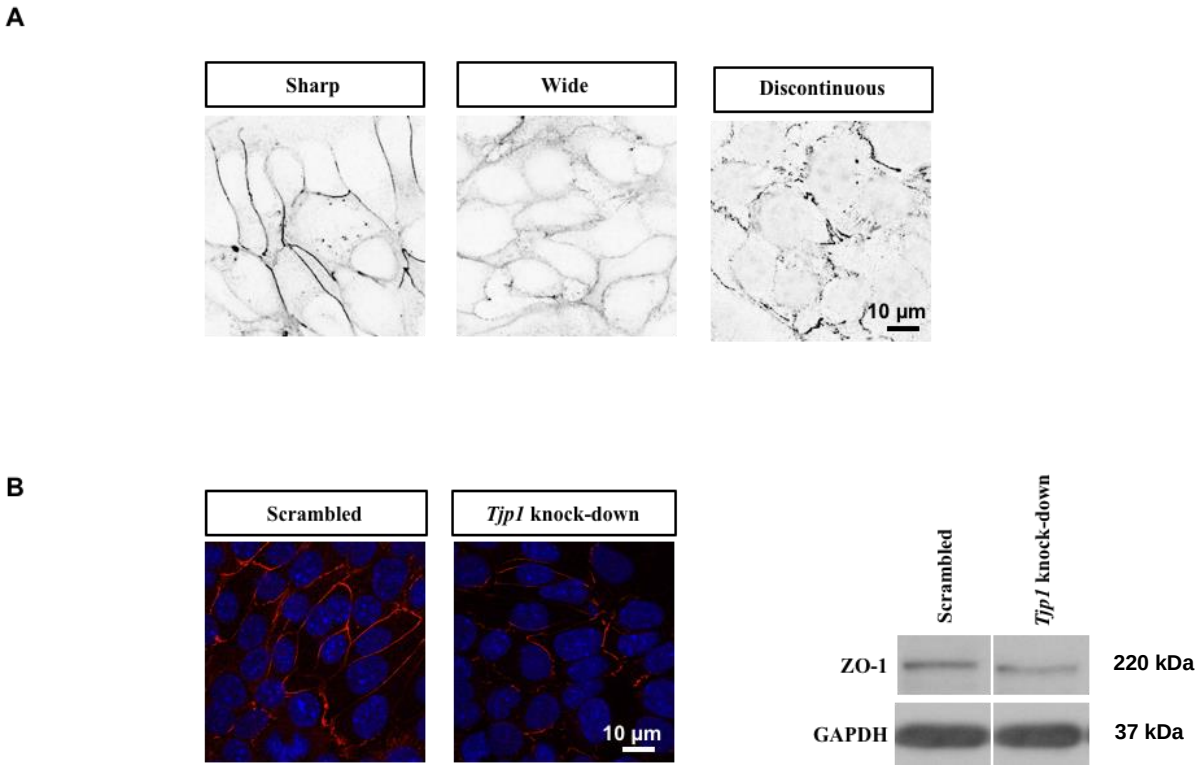
A
Sharp
Wide
Discontinuous
10 μm
B
Scrambled
Tjp1 knock-down
10 μm
Scrambled
Tjp1 knock-down
ZO-1
220 kDa
GAPDH
37 kDa

Table S1: Differentially expressed genes in wild-type ECs: 2 *vs.* 30dynes/cm^2

Genes in **bold** are cilia-independent regulated genes, also changed in Tg737$^{orpk/orpk}$ ECs

Gene_id	Gene_name	Log_2 fold change	p-value
ENSMUSG00000074896	***Ifit3***	**3.64**	**9.437E-91**
ENSMUSG00000062488	*I830012O16Rik*	2.95	2.296E-27
ENSMUSG00000023122	*Sult1c2*	2.49	6.648E-68
ENSMUSG00000024621	*Csf1r*	2.20	3.114E-155
ENSMUSG00000016942	*Tmprss6*	2.18	1.207E-47
ENSMUSG00000022206	***Npr3***	**2.03**	**1.268E-263**
ENSMUSG00000027831	*Veph1*	2.00	1.683E-35
ENSMUSG00000029372	*Ppbp*	1.99	1.066E-13
ENSMUSG00000047230	*Cldn2*	1.94	1.727E-101
ENSMUSG00000023914	*Mep1a*	1.91	2.243E-22
ENSMUSG00000035451	*Foxa1*	1.86	5.023E-45
ENSMUSG00000057265	*Ccdc176*	1.85	4.890E-29
ENSMUSG00000017002	*Slpi*	1.84	1.197E-18
ENSMUSG00000020990	*Cdkl1*	1.82	1.752E-39
ENSMUSG00000018126	*Baiap2l2*	1.81	7.513E-12
ENSMUSG00000023959	*Clic5*	1.77	1.385E-88
ENSMUSG00000017868	*Sgk2*	1.76	6.567E-25
ENSMUSG00000031980	***Agt***	**1.74**	**2.851E-40**
ENSMUSG00000079017	*Ifi27l2a*	1.72	1.955E-04
ENSMUSG00000049907	*Rasl11b*	1.70	8.453E-156
ENSMUSG00000034459	***Ifit1***	**1.70**	**5.828E-57**
ENSMUSG00000037010	***Apln***	**1.69**	**4.517E-156**
ENSMUSG00000020486	*Sept4*	1.68	4.606E-74
ENSMUSG00000021223	*Papln*	1.68	1.747E-66
ENSMUSG00000005232	*G6pc2*	1.67	1.532E-73
ENSMUSG00000071551	*Akr1c19*	1.64	2.008E-25
ENSMUSG00000028357	*Kif12*	1.61	1.148E-27
ENSMUSG00000074183	*Gsta1*	1.59	4.871E-04
ENSMUSG00000024910	***Ctsw***	**-4.34**	**1.499E-119**
ENSMUSG00000036381	*P2ry14*	-4.07	1.134E-74
ENSMUSG00000046318	***Ccbe1***	**-4.07**	**5.731E-25**
ENSMUSG00000026414	***Tnnt2***	**-3.07**	**1.175E-177**
ENSMUSG00000007888	*Crlf1*	-2.50	1.250E-249
ENSMUSG00000031075	***Ano1***	**-2.45**	**2.651E-177**
ENSMUSG00000079465	***Col4a3***	**-2.23**	**6.600E-52**
ENSMUSG00000038400	***Pmepa1***	**-2.23**	**0.000E+00**
ENSMUSG00000027750	***Postn***	**-2.21**	**2.023E-28**

Gene_id	Gene_name	Log_2 fold change	p-value
ENSMUSG00000019564	*Arid3a*	-2.19	7.423E-91
ENSMUSG00000037411	*Serpine1*	-2.18	1.451E-255
ENSMUSG00000026069	*Il1rl1*	-2.18	2.381E-39
ENSMUSG00000047501	*Cldn4*	-2.17	1.604E-32
ENSMUSG00000042436	*Mfap4*	-2.03	1.369E-37
ENSMUSG00000020325	*Fstl3*	-2.02	4.927E-42
ENSMUSG00000067158	*Col4a4*	-2.00	1.089E-74
ENSMUSG00000049699	*Ucn2*	-1.92	1.798E-21
ENSMUSG00000003283	*Hck*	-1.89	5.014E-12
ENSMUSG00000033722	*BC034090*	-1.80	2.775E-79
ENSMUSG00000019997	*Ctgf*	-1.71	3.342E-199
ENSMUSG00000025650	*Col7a1*	-1.70	5.813E-235
ENSMUSG00000030827	*Fgf21*	-1.69	3.520E-73
ENSMUSG00000032332	*Col12a1*	-1.67	7.540E-112
ENSMUSG00000009687	*Fxyd5*	-1.59	2.288E-20

Table S2: Differentially expressed genes in Tg737$^{orpk/orpk}$ ECs: 2 *vs.* 30dynes/cm^2

Genes in **bold** are cilia-independent regulated genes, also changed in wild-type ECs

Gene_id	Gene_name	Log_2 fold change	p-value
ENSMUSG00000052143	*Gm9869*	6.94	9.107E-07
ENSMUSG00000096001	*2610528A11Rik*	6.66	0.000E+00
ENSMUSG00000068122	*Agtr2*	6.20	1.627E-39
ENSMUSG00000020297	*Nsg2*	5.25	7.285E-30
ENSMUSG00000025488	*Cox8b*	4.67	7.148E-08
ENSMUSG00000027875	*Hmgcs2*	4.40	4.338E-94
ENSMUSG00000103344	*Gbp11*	4.30	2.596E-19
ENSMUSG00000038393	*Txnip*	4.22	0.000E+00
ENSMUSG00000026023	*Cdk15*	4.22	1.453E-14
ENSMUSG00000037010	***Apln***	**3.90**	**0.000E+00**
ENSMUSG00000105096	*Gbp10*	3.85	1.827E-39
ENSMUSG00000036295	*Lrrn3*	3.77	1.474E-190
ENSMUSG00000068874	*Selenbp1*	3.70	1.780E-17
ENSMUSG00000026894	*Morn5*	3.58	7.221E-09
ENSMUSG00000035258	*Abi3bp*	3.56	1.295E-70
ENSMUSG00000024810	*Il33*	3.51	2.514E-36
ENSMUSG00000019359	*Gdpd2*	3.49	3.574E-27
ENSMUSG00000079363	*Gbp4*	3.47	1.163E-112
ENSMUSG00000027996	*Sfrp2*	3.41	6.732E-34
ENSMUSG00000029298	*Gbp9*	3.39	0.000E+00
ENSMUSG00000060224	*Pyroxd2*	3.34	1.653E-47
ENSMUSG00000053199	*Arhgap20*	3.33	3.854E-289
ENSMUSG00000025784	*Clec3b*	3.30	9.026E-95
ENSMUSG00000074207	*Adh1*	3.29	2.488E-86
ENSMUSG00000004035	*Gstm7*	3.27	9.476E-19
ENSMUSG00000104713	*Gbp6*	3.25	6.290E-26
ENSMUSG00000039155	*Cdh26*	3.15	6.864E-104
ENSMUSG00000043073	*Usp17le*	3.11	1.305E-25
ENSMUSG00000052957	*Gas1*	3.09	0.000E+00
ENSMUSG00000041797	*Abca9*	3.07	3.773E-65
ENSMUSG00000039518	*Cdsn*	3.07	1.184E-249
ENSMUSG00000067780	*Pi15*	3.01	5.218E-103
ENSMUSG00000030406	*Gipr*	2.97	1.951E-13
ENSMUSG00000028713	*Cyp4b1*	2.97	3.667E-20
ENSMUSG00000034438	*Gbp8*	2.93	3.238E-193
ENSMUSG00000078566	*Bnip3*	2.92	0.000E+00
ENSMUSG00000019880	*Rspo3*	2.85	1.047E-301

Gene_id	Gene_name	Log_2 fold change	p-value
ENSMUSG00000035042	*Ccl5*	2.80	2.275E-40
ENSMUSG00000022512	*Cldn1*	2.80	2.223E-73
ENSMUSG00000040253	*Gbp7*	2.80	3.810E-46
ENSMUSG00000034459	***Ifit1***	**2.78**	**3.792E-94**
ENSMUSG00000021872	*Rnase10*	2.73	4.961E-24
ENSMUSG00000038233	*Fam198a*	2.72	2.639E-27
ENSMUSG00000061082	*Plac1*	2.71	9.470E-11
ENSMUSG00000037206	*Islr*	2.68	2.705E-277
ENSMUSG00000041112	*Elmo1*	2.68	0.000E+00
ENSMUSG00000028270	*Gbp2*	2.67	6.640E-208
ENSMUSG00000037161	*Mgarp*	2.65	6.541E-18
ENSMUSG00000034810	*Scn7a*	2.65	2.158E-84
ENSMUSG00000059921	*Unc5c*	2.64	9.397E-311
ENSMUSG00000029167	*Ppargc1a*	2.61	1.413E-134
ENSMUSG00000036446	*Lum*	2.59	4.639E-138
ENSMUSG00000017446	*C1qtnf1*	2.58	9.769E-102
ENSMUSG00000029838	*Ptn*	2.58	0.000E+00
ENSMUSG00000073530	*Pappa2*	2.58	5.852E-82
ENSMUSG00000009246	*Trpm5*	2.56	5.212E-38
ENSMUSG00000037379	*Spon2*	2.52	5.362E-78
ENSMUSG00000037621	*Atoh8*	2.51	4.116E-27
ENSMUSG00000020644	*Id2*	2.42	1.534E-74
ENSMUSG00000049409	*Prokr1*	2.41	5.751E-61
ENSMUSG00000074794	*Arrdc3*	2.41	1.298E-124
ENSMUSG00000079580	*Tmem217*	2.39	3.164E-07
ENSMUSG00000028289	*Epha7*	2.37	9.740E-180
ENSMUSG00000030222	*Rerg*	2.37	9.340E-42
ENSMUSG00000024084	*Qpct*	2.36	2.581E-14
ENSMUSG00000046546	*Fam43a*	2.35	3.974E-121
ENSMUSG00000071047	*Ces1a*	2.31	5.534E-81
ENSMUSG00000006494	*Pdk1*	2.30	2.870E-257
ENSMUSG00000027408	*Cpxm1*	2.29	2.756E-81
ENSMUSG00000067276	*Capn6*	2.28	0.000E+00
ENSMUSG00000022883	*Robo1*	2.27	1.022E-47
ENSMUSG00000021806	*Nid2*	2.26	0.000E+00
ENSMUSG00000074604	*Mgst2*	2.24	6.825E-12
ENSMUSG00000037362	*Nov*	2.22	1.709E-245
ENSMUSG00000096727	*Psmb9*	2.21	1.153E-41
ENSMUSG00000001663	*Gstt1*	2.20	1.895E-27
ENSMUSG00000057346	*Apol9a*	2.20	1.005E-18

Gene_id	Gene_name	Log_2 fold change	p-value
ENSMUSG00000029371	*Cxcl5*	2.20	1.458E-27
ENSMUSG00000039031	*Arhgap18*	2.13	3.245E-117
ENSMUSG00000022758	*P2rx6*	2.13	4.055E-27
ENSMUSG00000015090	*Ptgds*	2.12	1.017E-36
ENSMUSG00000050359	*Sprr1a*	2.06	1.962E-10
ENSMUSG00000022148	*Fyb*	2.06	4.640E-24
ENSMUSG00000005950	*P2rx5*	2.05	1.600E-28
ENSMUSG00000019768	*Esr1*	2.05	8.149E-62
ENSMUSG00000024066	*Xdh*	2.03	0.000E+00
ENSMUSG00000014782	*Plekhg4*	2.02	1.198E-273
ENSMUSG00000064373	*Sepp1*	2.00	4.159E-213
ENSMUSG00000025911	*Adhfe1*	2.00	7.057E-33
ENSMUSG00000032246	*Calml4*	1.99	2.684E-83
ENSMUSG00000039217	*Il18*	1.99	2.003E-15
ENSMUSG00000074896	***Ifit3***	**1.96**	**2.422E-13**
ENSMUSG00000032625	*Thsd7a*	1.93	0.000E+00
ENSMUSG00000033355	*Rtp4*	1.93	1.192E-13
ENSMUSG00000005360	*Slc1a3*	1.92	3.957E-135
ENSMUSG00000052160	*Pld4*	1.91	3.101E-09
ENSMUSG00000038527	*C1rl*	1.91	5.506E-121
ENSMUSG00000029380	*Cxcl1*	1.90	1.213E-28
ENSMUSG00000057596	*Trim30d*	1.90	3.625E-61
ENSMUSG00000057897	*Camk2b*	1.89	2.424E-23
ENSMUSG00000015243	*Abca1*	1.89	0.000E+00
ENSMUSG00000029563	*Foxp2*	1.89	1.720E-62
ENSMUSG00000037005	*Xpnpep2*	1.89	3.230E-103
ENSMUSG00000029231	*Pdgfra*	1.88	7.336E-273
ENSMUSG00000003949	*Hlf*	1.88	6.467E-29
ENSMUSG00000022836	*Mylk*	1.88	7.587E-104
ENSMUSG00000045031	*Cetn4*	1.87	8.703E-06
ENSMUSG00000052921	*Arhgef15*	1.86	1.769E-20
ENSMUSG00000004558	*Ndrg2*	1.85	9.398E-137
ENSMUSG00000028565	*Nfia*	1.85	4.073E-51
ENSMUSG00000029561	*Oasl2*	1.84	7.685E-21
ENSMUSG00000022707	*Gbe1*	1.84	1.378E-300
ENSMUSG00000028268	*Gbp3*	1.83	6.178E-14
ENSMUSG00000022537	*Tmem44*	1.82	2.679E-31
ENSMUSG00000030257	*Srgap3*	1.81	5.628E-159
ENSMUSG00000025931	*Paqr8*	1.80	5.568E-113
ENSMUSG00000025321	*Itgb8*	1.80	2.220E-140

Gene_id	Gene_name	Log_2 fold change	p-value
ENSMUSG00000022419	*Deptor*	1.80	5.475E-125
ENSMUSG00000054640	*Slc8a1*	1.78	8.617E-53
ENSMUSG00000020623	*Map2k6*	1.78	8.107E-28
ENSMUSG00000023064	*Sncg*	1.77	7.504E-05
ENSMUSG00000028359	*Orm3*	1.77	2.418E-08
ENSMUSG00000027832	*Ptx3*	1.77	2.854E-166
ENSMUSG00000049985	*Ankrd55*	1.77	2.822E-22
ENSMUSG00000026896	*Ifih1*	1.76	2.240E-38
ENSMUSG00000017417	*Plxdc1*	1.76	1.973E-170
ENSMUSG00000041688	*Amot*	1.75	0.000E+00
ENSMUSG00000024610	*Cd74*	1.75	4.024E-25
ENSMUSG00000024109	*Nrxn1*	1.74	2.547E-16
ENSMUSG00000053475	*Tnfaip6*	1.74	4.753E-22
ENSMUSG00000040254	*Sema3d*	1.74	1.593E-78
ENSMUSG00000022206	***Npr3***	**1.73**	**1.327E-61**
ENSMUSG00000029096	*Htra3*	1.72	4.157E-28
ENSMUSG00000038146	*Notch3*	1.72	4.020E-219
ENSMUSG00000034855	*Cxcl10*	1.71	1.427E-12
ENSMUSG00000022032	*Scara5*	1.71	1.809E-75
ENSMUSG00000019899	*Lama2*	1.71	6.069E-43
ENSMUSG00000040428	*Plekha4*	1.71	3.420E-33
ENSMUSG00000041272	*Tox*	1.70	1.550E-60
ENSMUSG00000039814	*Xkr5*	1.70	6.364E-23
ENSMUSG00000022330	*Osr2*	1.69	1.658E-06
ENSMUSG00000035493	*Tgfbi*	1.69	1.044E-182
ENSMUSG00000003955	*Fam162a*	1.68	3.095E-293
ENSMUSG00000055782	*Abcd2*	1.68	2.387E-36
ENSMUSG00000021123	*Rdh12*	1.68	6.463E-18
ENSMUSG00000020911	*Krt19*	1.65	1.145E-105
ENSMUSG00000060063	*Alox5ap*	1.65	1.477E-06
ENSMUSG00000056870	*Gulp1*	1.65	1.933E-139
ENSMUSG00000052581	*Lrrtm4*	1.65	5.187E-90
ENSMUSG00000031380	*Figf*	1.64	2.599E-251
ENSMUSG00000036334	*Igsf10*	1.64	2.990E-153
ENSMUSG00000021591	*Glrx*	1.64	2.458E-56
ENSMUSG00000036109	*Mbnl3*	1.64	1.918E-16
ENSMUSG00000059013	*Sh2d3c*	1.64	1.714E-30
ENSMUSG00000039883	*Lrrc17*	1.63	2.480E-223
ENSMUSG00000006586	*Runx1t1*	1.63	1.364E-100
ENSMUSG00000025422	*Agap2*	1.63	3.098E-71

Gene_id	Gene_name	Log_2 fold change	p-value
ENSMUSG00000035692	*Isg15*	1.62	2.185E-38
ENSMUSG00000068762	*Gstm6*	1.62	1.843E-07
ENSMUSG00000031980	***Agt***	**1.62**	**2.535E-13**
ENSMUSG00000027217	*Tspan18*	1.61	2.463E-14
ENSMUSG00000019817	*Plagl1*	1.61	4.611E-71
ENSMUSG00000038319	*Kcnh2*	1.61	2.711E-84
ENSMUSG00000024338	*Psmb8*	1.61	2.971E-68
ENSMUSG00000031099	*Smarca1*	1.61	8.532E-67
ENSMUSG00000028555	*Ttc39a*	1.60	2.476E-16
ENSMUSG00000022548	*Apod*	1.59	1.623E-17
ENSMUSG00000039063	*Echdc3*	1.59	3.778E-17
ENSMUSG00000031618	*Nr3c2*	1.59	9.667E-81
ENSMUSG00000039519	*Cyp7b1*	1.59	2.961E-17
ENSMUSG00000022231	*Sema5a*	1.59	5.065E-136
ENSMUSG00000046275	*Tusc5*	-6.38	2.232E-62
ENSMUSG00000083282	*Ctsf*	-6.19	1.738E-34
ENSMUSG00000045545	*Krt14*	-5.12	5.084E-64
ENSMUSG00000024910	***Ctsw***	**-4.96**	**2.615E-282**
ENSMUSG00000031780	*Ccl17*	-4.61	4.735E-71
ENSMUSG00000021950	*Anxa8*	-4.22	0.000E+00
ENSMUSG00000024011	*Pi16*	-4.14	1.553E-229
ENSMUSG00000022596	*Slurp1*	-3.70	6.207E-150
ENSMUSG00000037411	***Serpine1***	**-3.45**	**0.000E+00**
ENSMUSG00000056498	*Tmem154*	-3.26	6.790E-49
ENSMUSG00000000489	*Pdgfb*	-3.26	1.045E-120
ENSMUSG00000038840	*Birc7*	-3.15	9.355E-37
ENSMUSG00000022096	*Hr*	-3.10	2.425E-59
ENSMUSG00000006014	*Prg4*	-3.07	1.700E-112
ENSMUSG00000030109	*Slc6a12*	-3.07	2.306E-45
ENSMUSG00000058914	*C1qtnf3*	-3.04	0.000E+00
ENSMUSG00000002020	*Ltbp2*	-3.02	0.000E+00
ENSMUSG00000019997	***Ctgf***	**-3.01**	**0.000E+00**
ENSMUSG00000026639	*Lamb3*	-2.94	5.987E-72
ENSMUSG00000032172	*Olfm2*	-2.93	8.143E-83
ENSMUSG00000048521	*Cxcr6*	-2.90	1.484E-17
ENSMUSG00000032487	*Ptgs2*	-2.86	0.000E+00
ENSMUSG00000004371	*Il11*	-2.84	1.997E-14
ENSMUSG00000073433	*Arhgdig*	-2.84	3.358E-14
ENSMUSG00000022018	*Rgcc*	-2.82	1.362E-15
ENSMUSG00000045777	*Ifitm10*	-2.79	9.615E-73

Gene_id	Gene_name	Log_2 fold change	p-value
ENSMUSG00000052316	*Lrrc15*	-2.75	2.225E-48
ENSMUSG00000026414	***Tnnt2***	**-2.69**	**1.071E-139**
ENSMUSG00000079465	***Col4a3***	**-2.69**	**4.576E-128**
ENSMUSG00000038400	***Pmepa1***	**-2.68**	**0.000E+00**
ENSMUSG00000044006	*Cilp2*	-2.64	1.437E-143
ENSMUSG00000027470	*Mylk2*	-2.58	3.450E-43
ENSMUSG00000031530	*Dusp4*	-2.55	0.000E+00
ENSMUSG00000021208	*Ifi27l2b*	-2.54	1.551E-07
ENSMUSG00000023915	*Tnfrsf21*	-2.50	2.506E-102
ENSMUSG00000037225	*Fgf2*	-2.50	7.787E-191
ENSMUSG00000036256	*Igfbp7*	-2.50	0.000E+00
ENSMUSG00000028179	*Cth*	-2.50	1.129E-118
ENSMUSG00000031972	*Acta1*	-2.49	3.141E-101
ENSMUSG00000027737	*Slc7a11*	-2.48	0.000E+00
ENSMUSG00000054555	*Adam12*	-2.42	2.243E-259
ENSMUSG00000029765	*Plxna4*	-2.39	1.366E-245
ENSMUSG00000042124	*Lce1f*	-2.36	4.131E-05
ENSMUSG00000029019	*Nppb*	-2.32	4.195E-09
ENSMUSG00000020099	*Unc5b*	-2.32	0.000E+00
ENSMUSG00000030827	***Fgf21***	**-2.31**	**9.827E-19**
ENSMUSG00000000126	*Wnt9a*	-2.28	6.808E-108
ENSMUSG00000079014	*Serpina3i*	-2.28	5.402E-147
ENSMUSG00000022661	*Cd200*	-2.25	8.623E-263
ENSMUSG00000031841	*Cdh13*	-2.24	3.468E-217
ENSMUSG00000046318	***Ccbe1***	**-2.22**	**3.541E-43**
ENSMUSG00000024486	*Hbegf*	-2.21	8.345E-280
ENSMUSG00000020023	*Tmcc3*	-2.18	6.203E-164
ENSMUSG00000022240	*Ctnnd2*	-2.18	7.366E-149
ENSMUSG00000076441	*Ass1*	-2.17	6.351E-39
ENSMUSG00000037419	*Endod1*	-2.16	4.816E-302
ENSMUSG00000029223	*Uchl1*	-2.15	1.037E-267
ENSMUSG00000067001	*Serpinb7*	-2.15	2.334E-48
ENSMUSG00000063727	*Tnfrsf11b*	-2.14	3.515E-65
ENSMUSG00000054136	*Adm2*	-2.13	6.251E-64
ENSMUSG00000031075	***Ano1***	**-2.11**	**4.962E-166**
ENSMUSG00000044258	*Ctla2a*	-2.11	0.000E+00
ENSMUSG00000032715	*Trib3*	-2.11	4.199E-253
ENSMUSG00000000782	*Tcf7*	-2.10	9.162E-18
ENSMUSG00000037428	*Vgf*	-2.10	3.227E-24
ENSMUSG00000009687	***Fxyd5***	**-2.08**	**3.069E-277**

Gene_id	Gene_name	Log_2 fold change	p-value
ENSMUSG00000006221	*Hspb7*	-2.08	1.577E-84
ENSMUSG00000053062	*Jam2*	-2.06	2.009E-175
ENSMUSG00000020689	*Itgb3*	-2.04	1.447E-320
ENSMUSG00000039813	*Tbc1d2*	-2.04	1.011E-179
ENSMUSG00000020788	*Atp2a3*	-2.00	1.590E-38
ENSMUSG00000075012	*Fjx1*	-1.98	7.453E-49
ENSMUSG00000032415	*Ube2cbp*	-1.98	1.278E-37
ENSMUSG00000038264	*Sema7a*	-1.97	1.491E-22
ENSMUSG00000020846	*Fam101b*	-1.96	0.000E+00
ENSMUSG00000036687	*Tmem184a*	-1.96	8.522E-35
ENSMUSG00000028542	*Slc6a9*	-1.95	0.000E+00
ENSMUSG00000044254	*Pcsk9*	-1.91	1.939E-51
ENSMUSG00000022952	*Runx1*	-1.91	1.501E-192
ENSMUSG00000025068	*Gsto1*	-1.91	0.000E+00
ENSMUSG00000074676	*Foxs1*	-1.90	1.635E-64
ENSMUSG00000005124	*Wisp1*	-1.90	1.157E-204
ENSMUSG00000027456	*Sdcbp2*	-1.88	1.566E-08
ENSMUSG00000020614	*Fam20a*	-1.88	1.297E-152
ENSMUSG00000029161	*Cgref1*	-1.87	1.219E-13
ENSMUSG00000072494	*Ppp1r3e*	-1.86	8.370E-14
ENSMUSG00000016918	*Sulf1*	-1.85	8.448E-312
ENSMUSG00000026494	*Kif26b*	-1.83	7.015E-89
ENSMUSG00000036181	*Hist1h1c*	-1.81	1.322E-49
ENSMUSG00000051669	*AU021092*	-1.80	1.838E-105
ENSMUSG00000027313	*Chac1*	-1.79	1.836E-149
ENSMUSG00000053846	*Lipg*	-1.78	1.740E-121
ENSMUSG00000051048	*P4ha3*	-1.76	8.983E-159
ENSMUSG00000027750	***Postn***	**-1.76**	**1.130E-227**
ENSMUSG00000032281	*Acsbg1*	-1.76	7.088E-64
ENSMUSG00000027397	*Slc20a1*	-1.75	0.000E+00
ENSMUSG00000022367	*Has2*	-1.74	3.372E-297
ENSMUSG00000036040	*Adamtsl2*	-1.74	1.279E-21
ENSMUSG00000026475	*Rgs16*	-1.73	3.475E-12
ENSMUSG00000032060	*Cryab*	-1.73	0.000E+00
ENSMUSG00000038244	*Mical2*	-1.72	0.000E+00
ENSMUSG00000024544	*Ldlrad4*	-1.72	2.176E-151
ENSMUSG00000026069	***Il1rl1***	**-1.72**	**1.841E-86**
ENSMUSG00000037370	*Enpp1*	-1.72	7.727E-46
ENSMUSG00000002847	*Pla1a*	-1.71	1.086E-13
ENSMUSG00000025140	*Pycr1*	-1.70	9.875E-190

Gene_id	Gene_name	Log_2 fold change	p-value
ENSMUSG00000001918	*Slc1a5*	-1.70	8.816E-209
ENSMUSG00000036390	*Gadd45a*	-1.67	9.520E-196
ENSMUSG00000030562	*Nox4*	-1.67	5.418E-66
ENSMUSG00000027656	*Wisp2*	-1.67	3.447E-235
ENSMUSG00000017724	*Etv4*	-1.67	2.920E-67
ENSMUSG00000026548	*Slamf9*	-1.66	9.054E-12
ENSMUSG00000029446	*Psph*	-1.66	6.715E-174
ENSMUSG00000022817	*Itgb5*	-1.65	0.000E+00
ENSMUSG00000014846	*Tppp3*	-1.65	2.236E-219
ENSMUSG00000032911	*Cspg4*	-1.64	1.281E-300
ENSMUSG00000068196	*Col8a1*	-1.64	3.165E-304
ENSMUSG00000006301	*Tmbim1*	-1.63	4.422E-299
ENSMUSG00000042622	*Maff*	-1.62	3.707E-177
ENSMUSG00000038508	*Gdf15*	-1.61	2.152E-08
ENSMUSG00000050222	*Il17d*	-1.60	1.157E-78
ENSMUSG00000074874	*Ctla2b*	-1.60	4.204E-46
ENSMUSG00000041120	*Nbl1*	-1.60	6.149E-236
ENSMUSG00000024529	*Lox*	-1.59	2.996E-242
ENSMUSG00000021260	*Hhipl1*	-1.59	2.947E-56

Chapter 4: Endothelial cells display a unique transcriptional profile due to lack of cyclic stretch as observed in saccular intracranial aneurysms

Cyclic circumferential stretch (CCS) induced by pulsatile blood pressure affects EC gene expression and regulates vascular mechanical properties. Although alterations in EC gene expression in response to increased CCS as observed in hypertensive patients is well known, the EC response to low or lack of CCS as observed in IA disease has been poorly investigated. In this fourth chapter, I explored how exposure of ECs to low CCS may contribute to IA disease. I describe gene expression profile obtained by RNA sequencing from human umbilical veins ECs (HUVECs) under physiological or aneurysmal cyclic stretch conditions, and discuss their relevance based on existing literature.

Personal contribution: For this project, I have established the new FlexCell device in the laboratory. I have performed all experiments, interpreted the RNA-seq analysis and designed further experimentation, under the supervision of Prof. Brenda KWAK.

Manuscript Status: The manuscript is under preparation.

Endothelial cells display a unique transcriptional profile due to lack of cyclic stretch as observed in saccular intracranial aneurysms

Mannekomba R Diagbouga, Sylvain Lemeille, Brenda R Kwak

Department of Pathology and Immunology, Faculty of Medicine, University of Geneva, Switzerland

* Address correspondence to:
Brenda R Kwak, PhD
Dept. of Pathology and Immunology
University of Geneva
CMU - lab F06.2764.a
Rue Michel-Servet 1
CH-1211 Geneva 4
Switzerland
Phone: +41 22 379 57 37
E-mail: Brenda.KwakChanson@unige.ch

Abstract

Background and purpose: Hemodynamic forces play a critical role in intracranial aneurysm (IA) disease. While the role of wall shear stress in IA is well established, the influence of cyclic circumferential stretch (CCS) still needs to be clarified. IAs are generally characterized by a lack of CCS. In this study, we sought to understand the effect of aneurysmal CCS on endothelial cell (EC) function and the potential significance in IA disease.

Material and methods: Human umbilical veins ECs (HUVECs) were exposed to physiological arterial (6%) or to aneurysmal (0%) CCS. Then, we performed RNA sequencing to profile EC gene expression under the two conditions. Selected genes expression was confirmed by qPCR and we performed enrichment pathway analysis.

Results: We observed based on a multidimensional scaling plot that stretched EC samples display a high similarity between each other while non-stretched EC samples were spread-out. The differential gene expression of ECs exposed to aneurysmal or physiological CCS revealed 51 upregulated genes and 49 downregulated genes in absence of CCS. The GSEA analysis indicated that under aneurysmal CCS upregulated pathways were involved in oxidative stress, angiogenic and inflammatory pathways and downregulated pathways involved in proliferation and ECM-receptor interaction. We also found that in addition to regulate gene expression, CCS may also govern protein function through post-translational modifications.

Conclusion: Our results showed that physiological CCS prevents large deviation in ECs, indicating that CCS is essential for maintaining vascular homeostasis and would therefore prevent EC dysfunction and vascular diseases. Further investigation will give more insight on the significance of CCS responsive genes to IA disease.

Introduction

Intracranial aneurysm (IA) rupture is a common cause of hemorrhagic stroke. The treatment of unruptured IAs is a challenging decision that requires a delicate risk stratification [1-4]. The rate of poor clinical outcomes after surgical intervention (aneurysm clipping) or endovascular coiling remains elevated (6.7% and 4.8%, respectively) and don't give an absolute guarantee to prevent IA growth and rupture [5, 6]. So far, there is no pharmaceutical treatment to cure IA. Improving current or developing new treatment for IA disease would require a better understanding on the cellular and molecular mechanisms occurring in the different stages of the disease. The pathogenesis of IA is highly controversial and complex. The contribution of wall shear stress (WSS) in IA disease has been demonstrated in several studies [7-10], whereas the role of cyclic circumferential stretch (CCS) remains poorly understood. Endothelial cell (EC) dysfunction related to hemodynamic stresses is known to promote IA initiation [11-14]. Indeed, disturbed hemodynamic forces affect EC morphology and gene expression [15]. In addition of being exposed to WSS, ECs are also affected by CCS, the level of which varies along the vascular tree. The elastic human aorta undergoes ≈10% increase in diameter under physiological conditions, whereas muscular peripheral arteries undergo only ≈5% cyclic stretch [16]. Physiological CCS participates in vascular maintenance by regulating processes such as cell proliferation [17, 18] and morphology [19-21], extracellular matrix formation (ECM) [22] and vascular tone [23-26]. The levels of cyclic stretch in saccular IAs are unknown, but are generally considered very low as neurosurgeons cannot visually detect it during intervention. Moreover, the analysis of clipped IA domes generally shows damaged vascular walls with important loss in ECs, medial smooth muscle cells and ECM, mainly collagen [14, 27, 28]. In addition to these changes, calcium deposits and atherosclerotic plaques are frequently observed in IA walls [29]. As the IA wall enlarges and becomes stiffer, vascular cells gradually lose the cyclic stimulation required for their normal functioning. To this date, most studies onto the

response of ECs to CCS have focused on ECs exposed to high level of cyclic stretch as observed in hypertensive patients. The goal of our study was to investigate the transcriptional response of ECs to aneurysmal CCS (absence of CCS) and the potential impact on the function of the endothelium.

Material and methods

Cell culture

Human umbilical vein endothelial cells (HUVECs; Lonza) from six different donors were grown in dishes coated with 1.5% gelatin (Sigma-Aldrich) at 37°C in a humidified atmosphere containing 5% CO_2. Cells were cultured in Endothelial Cell Growth Medium (EGM)-2 medium (C-22111, PromoCell) and were used at passages 5–6.

Cyclic stretch exposure

HUVECS were seeded at 300'000 cells/well on pre-coated Collagen I BioFlex culture plates® (Flexcell International, USA) and grown until confluence. Then, the cells were submitted to cyclic stretch of 6% or not (0%) for 48-hours using the Flexcell strain unit FX-5000T (Flexcell International, USA) according to the manufacturers' instructions. Thus, the cells were stretched over a 25mm loading station or maintain under static condition (0%) by placing a Flexstop beneath the well of the BioFlex culture plate (**Figure 1A-C**). The mechanical stretch was applied following the pulse heart waveform with a frequency of 1Hz (**Figure 1D**). After 48-hours, we collected the cells that received a uniform strain, *i.e.* those in the middle of the well. The area of uniform strain was determined using the following formula: Diameter = (Diameter of Loading Station)/(1 + (Max %Elongation/100)).

RNA extraction, library preparation, sequencing, read mapping to the reference genome and gene coverage reporting

RNA was isolated from ECs after exposure to cyclic stretch of 6% or not (0%). Total RNA was extracted using the NucleoSpin RNA II kit (Macherey-Nagel) according to the manufacturers' instructions. The quality of all samples was verified using the Agilent 2100 Bioanalyzer with the Agilent RNA 6000 Nano Kit (Agilent Technologies). cDNA libraries were constructed by

the genomic platform of the University of Geneva using the Illumina TruSeq RNA sample preparation kit according to the manufacturers' protocol. Libraries were sequenced using single- end (50 nt-long) on Illumina HiSeq2000. FastQ reads were mapped to the ENSEMBL reference genome (GRCh38.96) using STAR version 2.4.0j [30] with standard settings, except that any reads mapping to more than one location of the genome (ambiguous reads) were discarded (m=1). In short, the model considers all annotated exons of all annotated protein coding isoforms of a gene to create a unique gene where the genomic region of all exons was considered as coming from the same RNA molecule and merged together.

RNA-seq data analysis

All reads overlapping the exons of each unique gene model were reported using featureCounts version 1.4.6-p1 [31]. Gene expression levels were reported as raw counts and in parallel normalized in RPKM in order to filter out genes with low expression value (1 RPKM) before calling for differentially expressed genes. Library size normalizations and differential gene expression calculations have been performed using the package edgeR [32] designed for the R software [33]. Only genes having a significant fold change ≥2 and the Benjamini-Hochberg corrected p-value<0.05 were considered for the differentially expressed genes analysis. Variation between samples were measured using a Multi-Dimensional Scaling (MDS) plot.

Gene set enrichment analysis (GSEA)

All annotated pathways for Homo sapiens, Mus musculus, Rattus norvegicus, Danio rerio, Sus scrofa and Saccharomyces cerevisiae available on WikiPathways database (http://www.wikipathways.org/index.php/WikiPathways) were used to generate gene sets, as well as the KEGG metabolic pathways (KEGG http://www.genome.jp/kegg/) relative to GRCh38.96. Genes were ranked by their calculated fold changes (decreasing ranking). A gene

set analysis using the GSEA package Version 2.2 [34, 35] from the Broad Institute (MIT, Cambridge, MA) was used to analyze the pattern of differential gene expression between the two groups. Gene set permutations were performed 1000 times for each analysis. The Normalized Enrichment Score (NES) was calculated for each gene set. GSEA results with a nominal False Discovery Rate (FDR) <0.05 and absolute normalized enrichment score (abs(NES)) >1 were considered significant.

Reverse transcription and quantitative PCR

Total RNA concentration was determined using a NanoDrop 2000 (ThermoFisher Scientific). cDNA was synthesized from equal amounts of RNA using QuantiTect Reverse Transcription Kit (Qiagen) and quantitative PCR (qPCR) was performed using ABI StepOne Plus detection system. We used Taqman gene expression assays (Applied Biosystems). The primers for *PTGS2* (Hs00153133_m1), *GJA1* (Hs00748445_s1), *GJA4* (Hs0074917_s1), *GJA5* (Hs00270952_s1) and *18S* (Hs03003631_g1) from ThermoFisher Scientific were used. All reactions were normalized to 18S.

Protein quantification and Western blot

Cell cultures were rinsed with PBS (pH7.4) and lysed in RIPA buffer (50mmol/L Tris–HCl, pH=8, 30mmol/L NaCl, 1% NP40, 10mmol/L NaF, 2mmol/L Na_3VO_4, 1mmol/L phenylmethylsulfonyl fluoride, complete protease inhibitor cocktail (Roche Applied Science), 1mmol/L EDTA, pH=7.4, 0.05% sodium dodecyl sulfate, and 5mmol/L sodium-deoxycholate). Cell lysates were gently mixed at 4°C for 20min, and then spun at 13.500rpm for 20min to collect the supernatant. The concentration of the isolated proteins was determined using BCA Protein Assay Reagent (ThermoScientific). Ten µg of protein was separated by SDS-PAGE and electrophoretically transferred to PVDF membranes (Immobilon, Millipore). After 2-hours blocking with 5% milk and 1% Tween in PBS, the membranes were incubated

with primary antibodies recognizing phosphorylated endothelial nitric oxide (eNOS) at Serine 1177 (9571s, Cell Signaling, 1/1000), eNOS (610297, BD Transduction 1/2500), Connexin43 (Cx43) (3512s, Cell Signaling, 1/1000), Glyceraldehyde 3-phosphate dehydrogenase (GAPDH) (MAB374, Millipore, 1/30000), Beta-actin (A5316, Sigma, 1/10000). Thereafter, the appropriate secondary horseradish peroxidase-conjugated antibodies (Jackson ImmunoResearch; 1/5000) were used, followed by ECL detection (Millipore) using ImageQuant LAS 4000 software. Band intensities were thereafter quantified using the NIH Image software (NIH AutoExtractor 1.51; National Institutes of Health).

Statistical analysis

qPCR analyses were done with GraphPad Prism 8.0.1 software. Results are shown in mean±SD. Comparisons of means have been performed using t-test. Data were considered statistically significant at $p<0.05$.

Results and discussion

The levels of eNOS phosphorylation increases in HUVECs submitted to stretch

To improve our understanding onto the role of CCS in IA disease, we exposed HUVECs to physiological (6%) or aneurysmal (0%) CCS for 48-hours. As the FlexCell device was a new tool in our lab, we have first tested whether we could observe in our experiments a well-known response of ECs to cyclic stretch, *i.e.* decrease of endothelial nitric oxide synthase (eNOS) phosphorylation on Serine 1177 (Ser1177) under reduced cyclic stretch as compared to physiological levels of CSS [36]. We verified the level of phosphorylated eNOS in our samples. As shown in **Figure 2**, we observed indeed higher levels of phosphorylated eNOS in HUVECs from all 6 donors at physiological CCS as compared to aneurysmal CCS, thus validating our methodology.

CCS regulates ECs gene expression profile

Next, we performed unbiased RNA-seq to investigate the effects of absence of CCS on gene expression in human ECs. Before calling for differentially expressed genes, we first checked the variation between samples using a Multi-Dimensional Scaling plot (**Figure 3A**). This graphic representation revealed that the HUVECs under pathological conditions (0% CCS) have a wide-spread distribution, which tends to converge under physiological CCS (6% CCS). This emphasizes the potential role of CCS in regulating vascular function by maintaining a well-defined (limited) transcriptome profile.

We considered genes with higher Benjamini-Hochberg corrected p-value<0.05 with at least a 2 fold change as differentially expressed (**Figure 3B, Table 1**). We found that 51 genes were upregulated and 49 genes were downregulated in absence of CCS (**Figure 3, Table 1**). To further investigate the pathways regulated by CCS, we used the gene set enrichment analysis (GSEA), which is a computational method that determines whether an a priori defined set of

genes shows statistically significant and concordant differences between two conditions [34]. Enriched pathways were identified from all available genes and not from differentially expressed genes only. The pathways with an abs(NES) >1 and FDR <0.05 were considered as significantly enriched. We identified 70 upregulated **(Figure 3C, Table 2)** and 38 downregulated pathways in HUVECs exposed to aneurysmal CCS (**Figure 3C, Table 3**).

Aneurysmal CCS upregulates oxidative stress, angiogenic and inflammatory pathways

Some of the identified pathways may be relevant for the regulation of endothelial function. First, we found that numerous categories involved in oxidative stress were upregulated under aneurysmal CCS, including transcriptional activation by NRF2, oxidation by cytochrome P450 and oxidative phosphorylation pathways (**Table 2**). Under conditions of oxidative stress, reactive oxygen species (ROS) production is enhanced and results in pro-inflammatory activation in ECs [37]. Physiological CCS was found to be vasoprotective by reducing ROS production in ECs [38]. Interestingly, a pathological increased level of CCS (typically associated with hypertension) has been correlated with excessive ROS production as well [39]. Our results suggest that a pathological low CCS as found in IAs would results in a boost of ROS production in ECs. In addition, we observed an enrichment of angiogenic related pathway. For instance, hypoxia-inducible factor-1 (HIF-1), vascular endothelial growth factor (VEGF) and prostaglandin synthesis and regulation signaling pathway were upregulated (**Table 2**). Previous studies have reported that a cooperation between Cyclooxygenase-2 (COX-2, encoded by *PTGS2*) and HIF-1α could promote angiogenesis through VEGF upregulation [40]. Lastly, fluid shear stress and atherosclerosis as well as inflammatory related pathways are of particular interest (**Table 2**). Indeed, the role of inflammation in IA disease has been largely proven and is associated with increased risk of IA growth and rupture [10, 27, 41]. Further investigations will identify endothelial key functions linking reduction/absence of CCS to IA disease.

Aneurysmal CCS downregulates pathways involved in cell proliferation and ECM-receptor interaction

Under physiological conditions, ECs tend to maintain a quiescent state. Any process affecting the proliferation rate of ECs would disturb their normal functioning. We observed that aneurysmal cyclic stretch appears to downregulate DNA replication and cell cycle pathways suggesting that cell proliferation processes could be altered (**Table 3**). Similarly, the Hippo signaling pathway that regulates EC proliferation, migration and survival was downregulated. Moreover, the ECM-receptor interaction pathway was negatively regulated. Whether the alteration of gene expression would result in enhanced or reduced levels of EC proliferation remains to be investigated. The growth of IA dome is mediated by a continuous remodeling of the vascular wall. Our results suggest that the absence of CCS can also contribute to ECM remodeling thus promoting aneurysm growth and ultimately rupture.

Leading-edge analysis and quantitative PCR confirmation

Next, we performed a leading-edge analysis from GSEA results allowing for extraction of the core members of high scoring gene sets that have high number of occurrences in GSEA pathways. The leading-edge genes are the most detected in different pathways; therefore, a change in expression of those genes would affect cell function significantly. As expected from the above-described pathway analysis, we identified genes involved in oxidative stress processes (*cytochrome P450 family 1 subfamily B member 1* (*CYP1B1*), *heme oxygenase 1* (*HMOX1*) and *NAD(P)H quinone dehydrogenase 1* (*NQO1*)), in prostaglandin synthesis (*prostaglandin-endoperoxide synthase* (*PTGS2*), *phospholipase A2 group IVA* (*PLA2G4A*)), in inflammation (*IL1A, SERPINB2*) and ECM regulation (*matrix metallopeptidase (MMP1*) as genes with a high number of occurrences (**Figure 4A**) and a high fold change (**Figure 4B**).

To confirm the differential gene expression between physiological and aneurysmal CCS, we performed qPCR on relevant genes that were upregulated (*PTGS2*), downregulated (*GJA4*, *GJA5*) or not changed (*GJA1*) under aneurysmal stretch in our RNA-seq results. *PTGS2* encodes for COX-2, an enzyme that catalyzes the conversion of arachidonic acid into prostaglandins [42]. COX-2 is known to be induced in inflammatory conditions and the COX-2-mediated prostaglandin E_2 (PGE_2) production further amplifies inflammation by activating nuclear factor kappa B (NFkB) [42]. COX-2 enzyme activity can also result in the formation of free radicals and ROS [43-45]. Interestingly, COX-2 has been detected in the wall of human IAs and more abundantly in the ruptured ones [46]. We confirmed increased *PTGS2* expression in HUVECs under aneurysmal CCS by qPCR (**Figure 5A**). Interestingly, increased expression of COX-2 and COX-2-mediated inflammatory signaling in IA endothelium has been previously related to disturbed WSS [47]. Our results demonstrated that the expression of this gene is also regulated by another hemodynamic force, namely CCS. The absence of CCS in an IA often coincides with disturbed WSS and concomitant action of the two hemodynamic factors would exacerbate inflammation and endothelial dysfunction, thus promoting IA progression. Next, we looked in details into gap junction (GJ) gene regulation by CCS as we confirmed that the expression of the endothelial GJ genes *Gja4* (**Figure 5C**) and *Gja5* (**Figure 5D**) was reduced by aneurysmal CCS.

GJs are clusters of intercellular channels that allow direct cell-cell communication by connecting the cytoplasm of one cell to its neighboring cell. The core proteins of GJs are connexins (Cx), which form a family of 21 members in humans [48]. Cxs assemble into hexameric hemichannels called connexons, and the docking of two connexons from adjacent cells form a GJ channel [49]. Arterial ECs express mainly Cx37 (encoded by *GJA4*) and Cx40 (encoded by *GJA5*), which are crucial for endothelial homeostasis and vascular function [49-51]. Apart from their role in direct intercellular communication, Cxs fulfill non-canonical

functions in other processes such as endothelial cell cycle regulation [50, 51] and inflammation [48]. Previous studies have shown that loss of endothelial Cx40 and Cx37 and induction of Cx43 (*GJA1*) expression induces endothelial dysfunction and promotes arterial disease such as atherosclerosis [52]. However, the potential role of these endothelial Cxs in IA disease is unknown. Similar to COX-2, Cx40 and Cx37 are regulated by WSS. In fact, physiological high WSS induces the expression of these genes via the Krüppel-like family of transcription factors (KLF4 [50] and KLF2 [53], respectively). We hypothesize that aneurysmal CCS coincides with low WSS in downregulating endothelial Cx40 and Cx37 in IAs, which likely contributes to endothelial dysfunction and possibly even to the atherosclerotic changes sometimes observed in IA walls.

Finally, we confirmed by qPCR that Cx43 mRNA expression levels were comparable under physiological and aneurysmal CCS (**Figure 5D)**. Moreover, we did not observe changes in the amount of Cx43 protein under these conditions (**Figure 5E)**. However, the Western blot analysis showed that the electrophoretic mobility of Cx43 was consequently different between 6% and 0% CSS. The electrophoretic mobility of Cx43 in Western blots is known to depend on the (Serine) phosphorylation state of the protein, with the more phosphorylated isoforms migrating slower. It is thus likely that physiological phosphorylation of Cx43 is disrupted by absence of CSS (**Figure 5E**).

Post-translational modifications such as ubiquitination, nitrosylation or phosphorylation determine the specific function or fate of a protein and these events are important in Cxs regulation [54]. The life cycle of Cx43 is loaded with phosphorylation and de-phosphorylation events. Cx43 has several sites of phosphorylation, and depending on the targeted site, phosphorylation regulate Cx43 trafficking to the plasma membrane or promote its internalization in the cytoplasm for subsequent degradation. Moreover, under pathological conditions such as ischemia, the phosphorylation of Cx43 on residues S373, S279, S282 and

Y247 leads to an acute increase in the size of the junction, followed by a rapid internalization leading to altered GJ communication [55]. Furthermore, Cx43 phosphorylation can also alter the gating properties of Cx43 GJ channels [56]. To understand the significance and implication of Cx40, Cx37 and Cx43 in IA disease, it may be fundamental to investigate their cellular location and their channels' functionality.

In summary, our results show that CCS is essential for maintaining vascular homeostasis. Our findings are in line with previous studies that show CCS involvement in several cellular processes including proliferation, oxidative stress, inflammation and ECM regulation [17, 18, 22, 26, 57]. In addition, we provide a complete transcriptome data set, representative for the lack of cyclic stretch experienced by ECs in IAs. This data will be valuable for decrypting the role of CCS on EC function in the context of IA disease. As shown in this thesis chapter, CCS does not only regulate gene expression but may also govern protein function through post-translational modifications. Further investigations may help to understand the significance of the absence of CCS in IA disease progression.

Acknowledgements

This work was supported by grants from the Swiss SystemsX.ch initiative, evaluated by the Swiss National Science Foundation, the Foundation Carlos et Elsie De Reuter, the Swiss Heart Foundation, the Novartis Foundation for medical-biological Research and the Gottfried und Julia Bangerter-Rhyner-Stiftung.

References

1. Greving, J.P., et al., *Development of the PHASES score for prediction of risk of rupture of intracranial aneurysms: a pooled analysis of six prospective cohort studies.* Lancet Neurol, 2014. **13**(1): p. 59-66.
2. Backes, D., et al., *ELAPSS score for prediction of risk of growth of unruptured intracranial aneurysms.* Neurology, 2017. **88**(17): p. 1600-1606.
3. Backes, D., et al., *Patient- and Aneurysm-Specific Risk Factors for Intracranial Aneurysm Growth: A Systematic Review and Meta-Analysis.* Stroke, 2016. **47**(4): p. 951-7.
4. Etminan, N., et al., *The unruptured intracranial aneurysm treatment score: a multidisciplinary consensus.* Neurology, 2015. **85**(10): p. 881-9.
5. Kotowski, M., et al., *Safety and occlusion rates of surgical treatment of unruptured intracranial aneurysms: a systematic review and meta-analysis of the literature from 1990 to 2011.* J Neurol Neurosurg Psychiatry, 2013. **84**(1): p. 42-8.
6. Naggara, O.N., et al., *Endovascular treatment of intracranial unruptured aneurysms: systematic review and meta-analysis of the literature on safety and efficacy.* Radiology, 2010. **256**(3): p. 887-97.
7. Meng, H., et al., *Complex hemodynamics at the apex of an arterial bifurcation induces vascular remodeling resembling cerebral aneurysm initiation.* Stroke, 2007. **38**(6): p. 1924-31.
8. Metaxa, E., et al., *Characterization of critical hemodynamics contributing to aneurysmal remodeling at the basilar terminus in a rabbit model.* Stroke, 2010. **41**(8): p. 1774-82.
9. Castro, M.A., et al., *Hemodynamic patterns of anterior communicating artery aneurysms: a possible association with rupture.* AJNR Am J Neuroradiol, 2009. **30**(2): p. 297-302.
10. Cebral, J., et al., *Flow Conditions in the Intracranial Aneurysm Lumen Are Associated with Inflammation and Degenerative Changes of the Aneurysm Wall.* AJNR Am J Neuroradiol, 2017. **38**(1): p. 119-126.
11. Aoki, T., et al., *Impact of monocyte chemoattractant protein-1 deficiency on cerebral aneurysm formation.* Stroke, 2009. **40**(3): p. 942-51.
12. Aoki, T., et al., *NF-kappaB is a key mediator of cerebral aneurysm formation.* Circulation, 2007. **116**(24): p. 2830-40.
13. Dolan, J.M., et al., *Endothelial cells express a unique transcriptional profile under very high wall shear stress known to induce expansive arterial remodeling.* Am J Physiol Cell Physiol, 2012. **302**(8): p. C1109-18.
14. Sheinberg, D.L., et al., *Endothelial dysfunction in cerebral aneurysms.* Neurosurg Focus, 2019. **47**(1): p. E3.
15. Diagbouga, M.R., et al., *Role of hemodynamics in initiation/growth of intracranial aneurysms.* Eur J Clin Invest, 2018. **48**(9): p. e12992.
16. Anwar, M.A., et al., *The effect of pressure-induced mechanical stretch on vascular wall differential gene expression.* J Vasc Res, 2012. **49**(6): p. 463-78.
17. Nishimura, K., et al., *Role of AKT in cyclic strain-induced endothelial cell proliferation and survival.* Am J Physiol Cell Physiol, 2006. **290**(3): p. C812-21.
18. Li, W. and B.E. Sumpio, *Strain-induced vascular endothelial cell proliferation requires PI3K-dependent mTOR-4E-BP1 signal pathway.* Am J Physiol Heart Circ Physiol, 2005. **288**(4): p. H1591-7.

19. Huang, W., et al., *Role of paxillin in the early phase of orientation of the vascular endothelial cells exposed to cyclic stretching.* Biochem Biophys Res Commun, 2012. **418**(4): p. 708-13.
20. Naruse, K., T. Yamada, and M. Sokabe, *Involvement of SA channels in orienting response of cultured endothelial cells to cyclic stretch.* Am J Physiol, 1998. **274**(5): p. H1532-8.
21. Yoshigi, M., E.B. Clark, and H.J. Yost, *Quantification of stretch-induced cytoskeletal remodeling in vascular endothelial cells by image processing.* Cytometry A, 2003. **55**(2): p. 109-18.
22. Wang, B.W., et al., *Induction of matrix metalloproteinases-14 and -2 by cyclical mechanical stretch is mediated by tumor necrosis factor-alpha in cultured human umbilical vein endothelial cells.* Cardiovasc Res, 2003. **59**(2): p. 460-9.
23. Hu, Z., et al., *Acute mechanical stretch promotes eNOS activation in venous endothelial cells mainly via PKA and Akt pathways.* PLoS One, 2013. **8**(8): p. e71359.
24. Fisslthaler, B., et al., *Inhibition of endothelial nitric oxide synthase activity by proline-rich tyrosine kinase 2 in response to fluid shear stress and insulin.* Circ Res, 2008. **102**(12): p. 1520-8.
25. Fisslthaler, B., et al., *Cyclic stretch enhances the expression and activity of coronary endothelium-derived hyperpolarizing factor synthase.* Hypertension, 2001. **38**(6): p. 1427-32.
26. Cheng, T.H., et al., *Reactive oxygen species mediate cyclic strain-induced endothelin-1 gene expression via Ras/Raf/extracellular signal-regulated kinase pathway in endothelial cells.* J Mol Cell Cardiol, 2001. **33**(10): p. 1805-14.
27. Morel, S., et al., *Correlating Clinical Risk Factors and Histological Features in Ruptured and Unruptured Human Intracranial Aneurysms: The Swiss AneuX Study.* J Neuropathol Exp Neurol, 2018. **77**(7): p. 555-566.
28. Frosen, J., et al., *Remodeling of saccular cerebral artery aneurysm wall is associated with rupture: histological analysis of 24 unruptured and 42 ruptured cases.* Stroke, 2004. **35**(10): p. 2287-93.
29. Gade, P.S., et al., *Calcification in Human Intracranial Aneurysms Is Highly Prevalent and Displays Both Atherosclerotic and Nonatherosclerotic Types.* Arterioscler Thromb Vasc Biol, 2019. **39**(10): p. 2157-2167.
30. Dobin, A., et al., *STAR: ultrafast universal RNA-seq aligner.* Bioinformatics, 2013. **29**(1): p. 15-21.
31. Quinlan, A.R. and I.M. Hall, *BEDTools: a flexible suite of utilities for comparing genomic features.* Bioinformatics, 2010. **26**(6): p. 841-2.
32. Robinson, M.D., D.J. McCarthy, and G.K. Smyth, *edgeR: a Bioconductor package for differential expression analysis of digital gene expression data.* Bioinformatics, 2010. **26**(1): p. 139-40.
33. RDC, T., *R: a language and environment for statistical computing*, in *R Foundation for Statistical Computing*. 2011: Vienna, Austria.
34. Subramanian, A., et al., *Gene set enrichment analysis: a knowledge-based approach for interpreting genome-wide expression profiles.* Proc Natl Acad Sci U S A, 2005. **102**(43): p. 15545-50.
35. Mootha, V.K., et al., *PGC-1alpha-responsive genes involved in oxidative phosphorylation are coordinately downregulated in human diabetes.* Nat Genet, 2003. **34**(3): p. 267-73.
36. Thacher, T., et al., *Reduced cyclic stretch, endothelial dysfunction, and oxidative stress: an ex vivo model.* Cardiovasc Pathol, 2010. **19**(4): p. e91-8.

37. Ross, R., *Atherosclerosis--an inflammatory disease.* N Engl J Med, 1999. **340**(2): p. 115-26.
38. Goettsch, C., et al., *Long-term cyclic strain downregulates endothelial Nox4.* Antioxid Redox Signal, 2009. **11**(10): p. 2385-97.
39. Ali, M.H., et al., *Mitochondrial requirement for endothelial responses to cyclic strain: implications for mechanotransduction.* Am J Physiol Lung Cell Mol Physiol, 2004. **287**(3): p. L486-96.
40. Huang, S.P., et al., *Cyclooxygenase-2 increases hypoxia-inducible factor-1 and vascular endothelial growth factor to promote angiogenesis in gastric carcinoma.* J Biomed Sci, 2005. **12**(1): p. 229-41.
41. Frosen, J., et al., *Flow-induced, inflammation-mediated arterial wall remodeling in the formation and progression of intracranial aneurysms.* Neurosurg Focus, 2019. **47**(1): p. E21.
42. Feletou, M., Y. Huang, and P.M. Vanhoutte, *Endothelium-mediated control of vascular tone: COX-1 and COX-2 products.* Br J Pharmacol, 2011. **164**(3): p. 894-912.
43. Hernanz, R., et al., *New roles for old pathways? A circuitous relationship between reactive oxygen species and cyclo-oxygenase in hypertension.* Clin Sci (Lond), 2014. **126**(2): p. 111-21.
44. Starke, R.M., et al., *The role of oxidative stress in cerebral aneurysm formation and rupture.* Curr Neurovasc Res, 2013. **10**(3): p. 247-55.
45. Rouzer, C.A. and L.J. Marnett, *Cyclooxygenases: structural and functional insights.* J Lipid Res, 2009. **50 Suppl**: p. S29-34.
46. Hasan, D., et al., *Upregulation of cyclooxygenase-2 (COX-2) and microsomal prostaglandin E2 synthase-1 (mPGES-1) in wall of ruptured human cerebral aneurysms: preliminary results.* Stroke, 2012. **43**(7): p. 1964-7.
47. Aoki, T., et al., *PGE(2) -EP(2) signalling in endothelium is activated by haemodynamic stress and induces cerebral aneurysm through an amplifying loop via NF-kappaB.* Br J Pharmacol, 2011. **163**(6): p. 1237-49.
48. Leybaert, L., et al., *Connexins in Cardiovascular and Neurovascular Health and Disease: Pharmacological Implications.* Pharmacol Rev, 2017. **69**(4): p. 396-478.
49. Molica, F., et al., *Connexins and Pannexins in Vascular Function and Disease.* Int J Mol Sci, 2018. **19**(6).
50. Denis, J.F., et al., *KLF4-Induced Connexin40 Expression Contributes to Arterial Endothelial Quiescence.* Front Physiol, 2019. **10**: p. 80.
51. Morel, S., et al., *Unexpected role for the human Cx37 C1019T polymorphism in tumour cell proliferation.* Carcinogenesis, 2010. **31**(11): p. 1922-31.
52. Morel, S., *Multiple roles of connexins in atherosclerosis- and restenosis-induced vascular remodelling.* J Vasc Res, 2014. **51**(2): p. 149-61.
53. Pfenniger, A., et al., *Shear stress modulates the expression of the atheroprotective protein Cx37 in endothelial cells.* J Mol Cell Cardiol, 2012. **53**(2): p. 299-309.
54. Johnstone, S.R., et al., *Posttranslational modifications in connexins and pannexins.* J Membr Biol, 2012. **245**(5-6): p. 319-32.
55. Ribeiro-Rodrigues, T.M., et al., *Role of connexin 43 in different forms of intercellular communication - gap junctions, extracellular vesicles and tunnelling nanotubes.* J Cell Sci, 2017. **130**(21): p. 3619-3630.
56. Takens-Kwak, B.R. and H.J. Jongsma, *Cardiac gap junctions: three distinct single channel conductances and their modulation by phosphorylating treatments.* Pflugers Arch, 1992. **422**(2): p. 198-200.
57. Jufri, N.F., et al., *Mechanical stretch: physiological and pathological implications for human vascular endothelial cells.* Vasc Cell, 2015. **7**: p. 8.

Figure 1: **Images of Flexcell system set-up**.

(A) Picture of Bioflex culture plate. (B) Equibiaxial strain application to cells in a well of BioFlex® culture plate. (C) Flexcell tension system 5000. (D) Pulse heart waveform regimen applied to HUVECs.

Figure 2: Total and phosphorylated eNOS (Serine 1177) expression.

Phosphorylated eNOS (Serine 1177), total eNOS expression in HUVECs exposed to physiological (6%) or aneurysmal (0%) CCS was assessed by Western blotting. Beta-actin was used as a loading control.

Figure 3: RNA-seq results

(A) Multidimensional scaling plot representing similarities of gene expression between HUVECs exposed to aneurysmal (red dots) or physiological CCS (blue dots). N=6 for each condition. (B) Volcano plot displaying differential expressed genes between HUVECs exposed to aneurysmal or physiological CCS. The y-axis corresponds to the mean expression value of $\log_{10}$ (p-value), and the x-axis displays the $\log_2$ fold change value. The red and blue dots represent respectively the up- and down-regulated genes (fold change$\geq$2; p$\leq$0.05). (C) Volcano plot displaying GSEA enriched pathway HUVECs exposed to aneurysmal or physiological CCS. The y-axis corresponds to the False Discovery Rate (FDR), and the x-axis corresponds to the normalized enrichment score (NES). The red and blue dots represent respectively the up- and down-regulated pathways (NES $\geq$1; FDR$\leq$0.05).

Figure 4: **GSEA leading-edge analysis**

Heatmap representation of the leading-edge analysis of GSEA results: (A) The color intensity represents the number of occurrences or (B) the fold change of each gene. Adjusted p-values were all <0.001.

Figure 5: RNA-seq confirmation

qPCR results: mRNA expression level of (A) *PTGS2* (COX-2), (B) *GJA4* (Cx37), (C) *GJA5* (Cx40), (D) *GJA1* (Cx43) in HUVECs exposed to physiological (6%) or aneurysmal (0%) CCS. (E) Cx43 expression in HUVECs exposed to physiological (6%) or aneurysmal (0%) CCS was assessed by Western blot. *p<0.05, *t*-test.

Table 1: Differentially expressed genes in static (0%) *vs* 6% CCS

Gene_id	Gene_name	Log_2 fold change	p-value
ENSG00000138061	*CYP1B1*	7.635	5.28792E-16
ENSG00000171246	*NPTX1*	6.491	1.30473E-17
ENSG00000108932	*SLC16A6*	3.237	7.24246E-54
ENSG00000108602	*ALDH3A1*	3.030	2.06045E-45
ENSG00000114812	*VIPR1*	2.675	2.55768E-14
ENSG00000127533	*F2RL3*	2.516	3.0887E-21
ENSG00000100292	*HMOX1*	2.490	1.01137E-14
ENSG00000137809	*ITGA11*	2.382	4.55362E-16
ENSG00000140465	*CYP1A1*	2.312	1.12782E-18
ENSG00000138356	*AOX1*	2.296	1.79963E-10
ENSG00000178878	*APOLD1*	2.092	3.34283E-29
ENSG00000073756	*PTGS2*	2.042	6.68677E-15
ENSG00000276600	*RAB7B*	1.835	4.3291E-11
ENSG00000102385	*DRP2*	1.723	8.60273E-18
ENSG00000197632	*SERPINB2*	1.723	4.9368E-20
ENSG00000108551	*RASD1*	1.548	1.67863E-12
ENSG00000103489	*XYLT1*	1.486	2.00133E-18
ENSG00000163659	*TIPARP*	1.414	7.30185E-24
ENSG00000170891	*CYTL1*	1.413	4.04601E-37
ENSG00000121895	*TMEM156*	1.393	8.78627E-10
ENSG00000115008	*IL1A*	1.391	3.08954E-06
ENSG00000174939	*ASPHD1*	1.362	2.28022E-07
ENSG00000159167	*STC1*	1.359	4.15973E-15
ENSG00000119714	*GPR68*	1.356	1.5672E-11
ENSG00000196611	*MMP1*	1.313	4.45702E-15
ENSG00000108846	*ABCC3*	1.306	1.63989E-07
ENSG00000166670	*MMP10*	1.275	2.37534E-11
ENSG00000185022	*MAFF*	1.258	1.39557E-28
ENSG00000167996	*FTH1*	1.235	2.01898E-14
ENSG00000117525	*F3*	1.233	1.0987E-09
ENSG00000181019	*NQO1*	1.229	7.17043E-13
ENSG00000286169	*AHRR*	1.222	5.56123E-15
ENSG00000103241	*FOXF1*	1.218	2.42977E-08
ENSG00000131386	*GALNT15*	1.190	1.76515E-15
ENSG00000184227	*ACOT1*	1.172	8.74975E-05
ENSG00000136160	*EDNRB*	1.148	8.4315E-09
ENSG00000108448	*TRIM16L*	1.144	8.15417E-09
ENSG00000110031	*LPXN*	1.134	4.75734E-18
ENSG00000140961	*OSGIN1*	1.118	1.03825E-14

Gene_id	Gene_name	Log_2 fold change	p-value
ENSG00000178773	*CPNE7*	1.110	1.51209E-05
ENSG00000189134	*NKAPL*	1.104	1.34869E-06
ENSG00000160111	*CPAMD8*	1.104	7.57673E-13
ENSG00000198431	*TXNRD1*	1.066	8.44928E-15
ENSG00000116711	*PLA2G4A*	1.065	1.3189E-13
ENSG00000151715	*TMEM45B*	1.052	0.000862449
ENSG00000151012	*SLC7A11*	1.050	3.13634E-14
ENSG00000184254	*ALDH1A3*	1.044	3.13859E-22
ENSG00000105967	*TFEC*	1.039	1.94228E-13
ENSG00000223547	*ZNF844*	1.025	6.6067E-07
ENSG00000133110	*POSTN*	-3.736	2.35677E-14
ENSG00000187513	*GJA4*	-2.477	6.7186E-21
ENSG00000275152	*CCL16*	-2.340	3.63484E-15
ENSG00000240583	*AQP1*	-2.283	6.11337E-17
ENSG00000132561	*MATN2*	-2.215	1.64929E-22
ENSG00000184344	*GDF3*	-2.193	2.40292E-48
ENSG00000265107	*GJA5*	-2.032	4.51866E-10
ENSG00000137573	*SULF1*	-1.871	1.32021E-23
ENSG00000164692	*COL1A2*	-1.831	3.74708E-22
ENSG00000255690	*TRIL*	-1.713	8.76024E-21
ENSG00000137033	*IL33*	-1.713	6.80028E-21
ENSG00000162706	*CADM3*	-1.653	4.90468E-07
ENSG00000145681	*HAPLN1*	-1.587	4.65268E-05
ENSG00000109193	*SULT1E1*	-1.579	1.36898E-07
ENSG00000162496	*DHRS3*	-1.539	2.37127E-13
ENSG00000146374	*RSPO3*	-1.516	2.62071E-06
ENSG00000170323	*FABP4*	-1.504	6.92627E-44
ENSG00000149212	*SESN3*	-1.492	2.08454E-26
ENSG00000103044	*HAS3*	-1.465	1.5474E-13
ENSG00000140511	*HAPLN3*	-1.412	8.53811E-21
ENSG00000185432	*METTL7A*	-1.376	1.21362E-17
ENSG00000276409	*CCL14*	-1.372	3.51553E-27
ENSG00000110675	*ELMOD1*	-1.353	1.0937E-05
ENSG00000128606	*LRRC17*	-1.345	7.64981E-11
ENSG00000185860	*CCDC190*	-1.323	1.39322E-05
ENSG00000156298	*TSPAN7*	-1.311	3.45538E-15
ENSG00000124749	*COL21A1*	-1.293	6.66564E-16
ENSG00000169129	*AFAP1L2*	-1.262	1.49167E-14
ENSG00000010319	*SEMA3G*	-1.257	1.58998E-21
ENSG00000121858	*TNFSF10*	-1.236	1.06687E-28

Gene_id	Gene_name	Log_2 fold change	p-value
ENSG00000183287	*CCBE1*	-1.234	1.00583E-05
ENSG00000136960	*ENPP2*	-1.224	2.29871E-12
ENSG00000075275	*CELSR1*	-1.202	1.47085E-12
ENSG00000109046	*WSB1*	-1.166	9.03702E-43
ENSG00000164619	*BMPER*	-1.162	1.9291E-06
ENSG00000139187	*KLRG1*	-1.123	1.18213E-18
ENSG00000138185	*ENTPD1*	-1.119	1.38866E-22
ENSG00000111341	*MGP*	-1.112	2.33181E-15
ENSG00000164116	*GUCY1A1*	-1.092	5.27415E-08
ENSG00000197635	*DPP4*	-1.086	6.3818E-15
ENSG00000082497	*SERTAD4*	-1.070	4.87213E-14
ENSG00000271447	*MMP28*	-1.048	5.65488E-07
ENSG00000124406	*ATP8A1*	-1.044	1.97797E-13
ENSG00000134323	*MYCN*	-1.031	1.26424E-09
ENSG00000185737	*NRG3*	-1.029	1.91693E-10
ENSG00000139263	*LRIG3*	-1.025	7.02803E-29
ENSG00000154258	*ABCA9*	-1.018	9.81449E-16
ENSG00000005108	*THSD7A*	-1.007	1.19209E-22
ENSG00000099204	*ABLIM1*	-1.005	5.66702E-23
ENSG00000173597	*SULT1B1*	-1.005	1.38209E-10
ENSG00000005187	*ACSM3*	-1.003	9.98314E-10

Table 2: Upregulated GSEA pathways in static (0%) *vs* 6% CCS

NES= normalized enrichment score; FDR= false discovery rate.

Pathway_name	NES	FDR
NRF2 pathway (Ref=hsapiens)	2.623	0
Chemical carcinogenesis (Ref=hsapiens_KEGG)	2.491	0
Aryl Hydrocarbon Receptor Pathway (Ref=hsapiens)	2.488	0
Metabolism of xenobiotics by cytochrome P450 (Ref=hsapiens_KEGG)	2.418	0
Aryl Hydrocarbon Receptor (Ref=hsapiens)	2.311	0
Melatonin metabolism and effects (Ref=hsapiens)	2.283	0
Tryptophan metabolism (Ref=hsapiens_KEGG)	2.276	0
Oxidative Stress (Ref=hsapiens)	2.274	0
Ovarian steroidogenesis (Ref=hsapiens_KEGG)	2.222	0
Tryptophan metabolism (Ref=hsapiens)	2.203	0.0054645
Oxidation by Cytochrome P450 (Ref=hsapiens)	2.113	0
Drug metabolism (Ref=hsapiens_KEGG)	2.106	0.0025907
Transcriptional activation by NRF2 (Ref=hsapiens)	2.072	0
Photodynamic therapy-induced NFE2L2 (NRF2) survival signaling (Ref=hsapiens)	2.038	0.0102564
Tyrosine metabolism (Ref=hsapiens_KEGG)	2.019	0.0024876
Ferroptosis (Ref=hsapiens_KEGG)	2.011	0.0028409
Oxidative phosphorylation (Ref=hsapiens_KEGG)	1.998	0
Hepatitis C and Hepatocellular Carcinoma (Ref=hsapiens)	1.930	0.0111111
JAK-STAT signaling pathway (Ref=hsapiens_KEGG)	1.899	0
Mitophagy (Ref=hsapiens_KEGG)	1.890	0.0031546
Pentose phosphate pathway (Ref=hsapiens_KEGG)	1.890	0.0126582
Photodynamic therapy-induced NF-kB survival signaling (Ref=hsapiens)	1.886	0.002611
Glutathione metabolism (Ref=hsapiens)	1.885	0.0121065
Metapathway biotransformation (Ref=hsapiens)	1.884	0.0148368
Fluid shear stress and atherosclerosis (Ref=hsapiens_KEGG)	1.883	0
Porphyrin and chlorophyll metabolism (Ref=hsapiens_KEGG)	1.880	0.0103359
Bladder Cancer (Ref=hsapiens)	1.844	0.0050125
Overview of nanoparticle effects (Ref=hsapiens)	1.832	0.0075758
Glutathione metabolism (Ref=hsapiens_KEGG)	1.826	0.0110193
Selenium Micronutrient Network (Ref=hsapiens)	1.825	0.0055402

Pathway_name	NES	FDR
Steroid hormone biosynthesis (Ref=hsapiens_KEGG)	1.823	0.0123153
beta-Alanine metabolism (Ref=hsapiens_KEGG)	1.806	0.0048544
Cori Cycle (Ref=hsapiens)	1.794	0.0119617
Nicotinate and nicotinamide metabolism (Ref=hsapiens_KEGG)	1.774	0.0193705
GPCRs, Class A Rhodopsin-like (Ref=hsapiens)	1.743	0.0186667
Collecting duct acid secretion (Ref=hsapiens_KEGG)	1.740	0.0078947
Oxidative phosphorylation (Ref=hsapiens)	1.732	0.0298103
Photodynamic therapy-induced HIF-1 survival signaling (Ref=hsapiens)	1.730	0.0216216
Prostaglandin Synthesis and Regulation (Ref=hsapiens)	1.730	0.0153061
Histidine metabolism (Ref=hsapiens_KEGG)	1.727	0.0271605
Preimplantation Embryo (Ref=hsapiens)	1.714	0.0248139
Senescence and Autophagy in Cancer (Ref=hsapiens)	1.711	0.0028653
VEGF signaling pathway (Ref=hsapiens_KEGG)	1.707	0.0115942
IL-3 Signaling Pathway (Ref=hsapiens)	1.707	0.0186667
MicroRNAs in cancer (Ref=hsapiens_KEGG)	1.703	0.0035088
Urea cycle and metabolism of amino groups (Ref=hsapiens)	1.687	0.0195652
Bladder cancer (Ref=hsapiens_KEGG)	1.678	0.0189189
Sudden Infant Death Syndrome (SIDS) Susceptibility Pathways (Ref=hsapiens)	1.678	0.022508
Arachidonic acid metabolism (Ref=hsapiens_KEGG)	1.677	0.0333333
Lung fibrosis (Ref=hsapiens)	1.661	0.0206186
Cytoplasmic Ribosomal Proteins (Ref=hsapiens)	1.655	0.017192
Prion diseases (Ref=hsapiens_KEGG)	1.644	0.044335
Synaptic vesicle cycle (Ref=hsapiens_KEGG)	1.640	0.0194986
Selenium Metabolism and Selenoproteins (Ref=hsapiens)	1.638	0.0318302
Mineral absorption (Ref=hsapiens_KEGG)	1.633	0.0255754
Oncostatin M Signaling Pathway (Ref=hsapiens)	1.631	0.0276243
Ribosome (Ref=hsapiens_KEGG)	1.602	0.014652
Zinc homeostasis (Ref=hsapiens)	1.596	0.041769
Cytoplasmic Ribosomal Proteins (Ref=scerevisiae)	1.594	0.0325203
Vibrio cholerae infection (Ref=hsapiens_KEGG)	1.570	0.0334262
HIF-1 signaling pathway (Ref=hsapiens_KEGG)	1.556	0.0188679
Proteasome (Ref=hsapiens_KEGG)	1.541	0.045584
Neuroactive ligand-receptor interaction (Ref=hsapiens_KEGG)	1.526	0.0289017
Parkinson disease (Ref=hsapiens_KEGG)	1.489	0.0307167

Pathway_name	NES	FDR
Translation Factors (Ref=hsapiens)	1.489	0.0426136
Oxytocin signaling pathway (Ref=hsapiens_KEGG)	1.469	0.04811
Non-alcoholic fatty liver disease (NAFLD) (Ref=hsapiens_KEGG)	1.431	0.0371747
Alzheimer disease (Ref=hsapiens_KEGG)	1.407	0.0335821
Pathways in cancer (Ref=hsapiens_KEGG)	1.253	0.043956

Table 3: Downregulated GSEA pathways in static (0%) *vs* 6% CCS

NES= normalized enrichment score; FDR= false discovery rate

Pathway_name	NES	FDR
Retinoblastoma (RB) in Cancer (Ref=hsapiens)	-2.213	0
DNA Replication (Ref=hsapiens)	-2.179	0
DNA replication (Ref=hsapiens_KEGG)	-2.061	0
DNA Replication (Ref=scerevisiae)	-2.005	0
Cell Cycle and Cell Division (Ref=scerevisiae)	-1.958	0
Fanconi anemia pathway (Ref=hsapiens_KEGG)	-1.921	0
mRNA Processing (Ref=hsapiens)	-1.894	0
Cell Cycle (Ref=hsapiens)	-1.883	0
Homologous recombination (Ref=hsapiens_KEGG)	-1.855	0
Cell cycle (Ref=hsapiens_KEGG)	-1.831	0
Gastric Cancer Network 2 (Ref=hsapiens)	-1.743	0.00649351
Statin Pathway (Ref=hsapiens)	-1.711	0.00664452
Axon guidance (Ref=hsapiens_KEGG)	-1.710	0
Oocyte meiosis (Ref=hsapiens_KEGG)	-1.707	0
Gastric Cancer Network 1 (Ref=hsapiens)	-1.693	0.00321543
Pathways Affected in Adenoid Cystic Carcinoma (Ref=hsapiens)	-1.687	0.00304414
G1 to S cell cycle control (Ref=hsapiens)	-1.674	0.00301659
NOTCH1 regulation of human endothelial cell calcification (Ref=hsapiens)	-1.666	0.00673401
DNA IR-Doble Strand Breaks (DSBs) and cellular response via ATM (Ref=hsapiens)	-1.652	0.00154083
Cytokine-cytokine receptor interaction (Ref=hsapiens_KEGG)	-1.635	0.0056101
Protein digestion and absorption (Ref=hsapiens_KEGG)	-1.633	0.01809955
Hippo signaling pathway (Ref=hsapiens_KEGG)	-1.627	0.01132686
Hypothesized Pathways in Pathogenesis of Cardiovascular Disease (Ref=hsapiens)	-1.618	0.01628665
ECM-receptor interaction (Ref=hsapiens_KEGG)	-1.617	0.01848999
Endochondral Ossification (Ref=hsapiens)	-1.611	0.01910828
Mismatch repair (Ref=hsapiens_KEGG)	-1.605	0.01451613
Development and heterogeneity of the ILC family (Ref=hsapiens)	-1.584	0.02763385
Spliceosome (Ref=hsapiens_KEGG)	-1.579	0.00546448
Renin secretion (Ref=hsapiens_KEGG)	-1.551	0.0288
Globo Sphingolipid Metabolism (Ref=hsapiens)	-1.526	0.04964539

Pathway_name	NES	FDR
Histone Modifications (Ref=hsapiens)	-1.505	0.02689873
MECP2 and Associated Rett Syndrome (Ref=hsapiens)	-1.496	0.03230769
Mesodermal Commitment Pathway (Ref=hsapiens)	-1.477	0.01820728
Progesterone-mediated oocyte maturation (Ref=hsapiens_KEGG)	-1.477	0.03129657
Base excision repair (Ref=hsapiens_KEGG)	-1.474	0.03886398
Endoderm Differentiation (Ref=hsapiens)	-1.420	0.01445087
Lysine degradation (Ref=hsapiens_KEGG)	-1.385	0.04682779

Figure 1

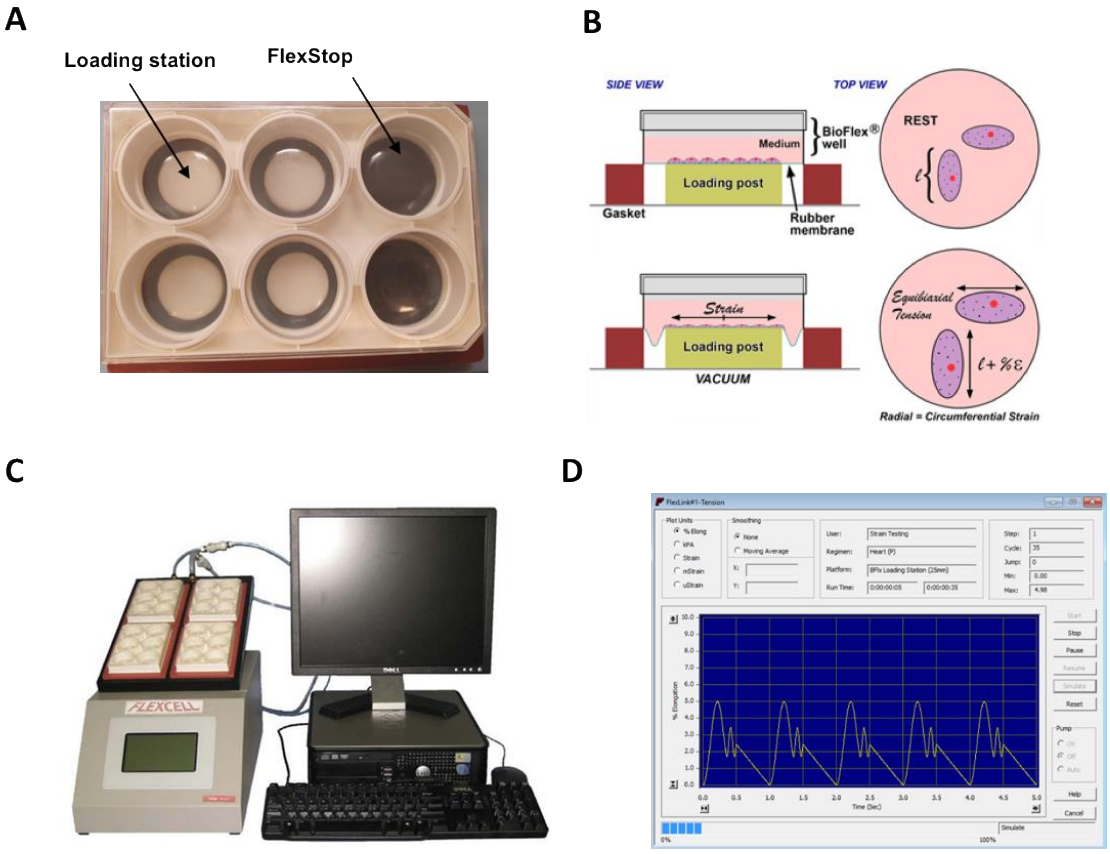
A
Loading station
FlexStop
B
SIDE VIEW
TOP VIEW
Medium
BioFlex®
well
REST
Loading post
Gasket
Rubber
membrane
Strain
Loading post
VACUUM
Equibiaxial
Tension
ℓ+ %ε
Radial = Circumferential Strain
C
FLEXCELL
D

Figure 2

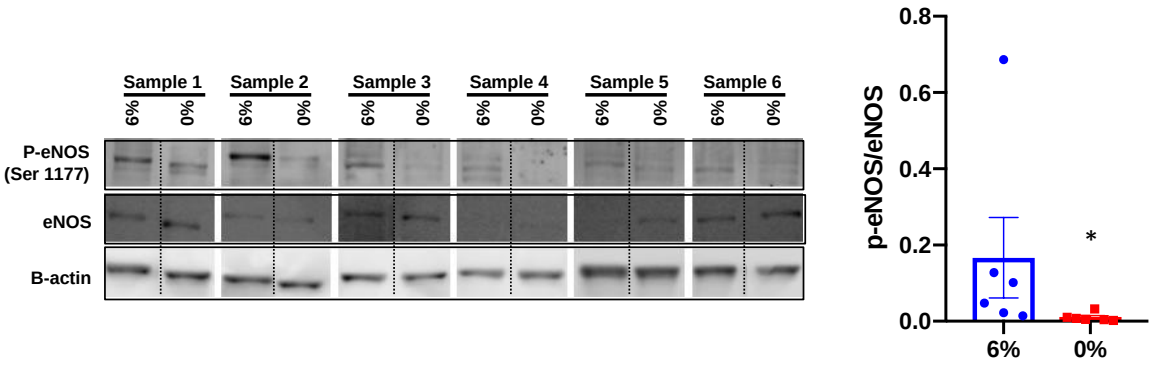
Sample 1
Sample 2
Sample 3
Sample 4
Sample 5
Sample 6
6%
0%
P-eNOS
(Ser 1177)
eNOS
B-actin
p-eNOS/eNOS
0.8
0.6
0.4
0.2
0.0
*
6%
0%

Figure 3

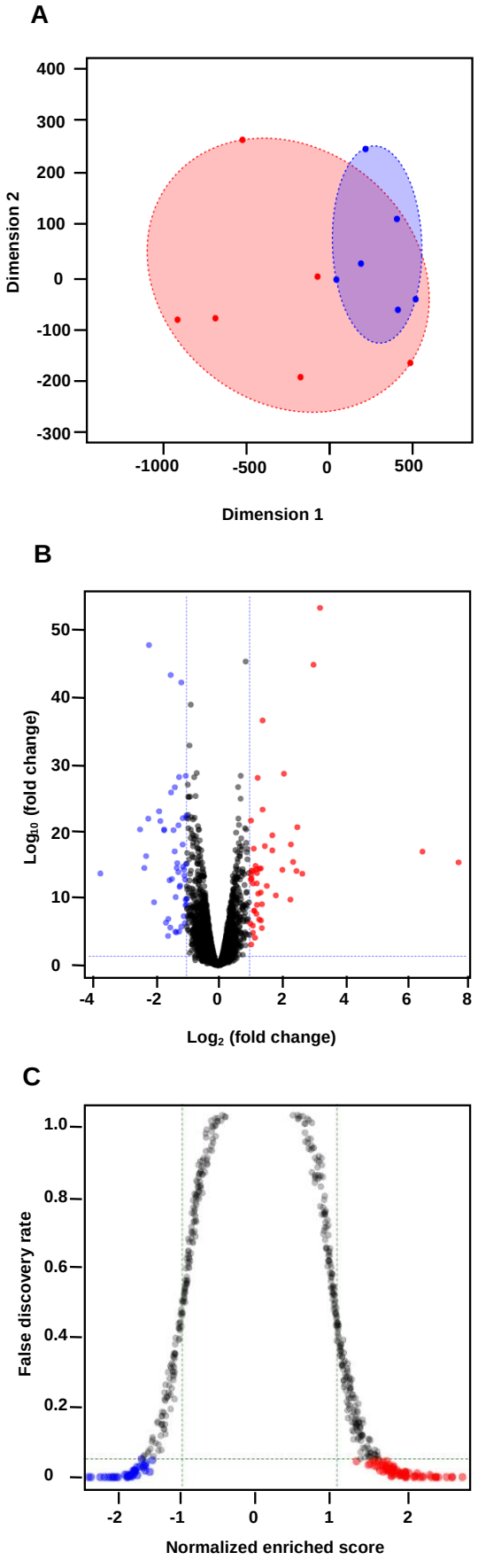
A
400
300
200
100
0
-100
-200
-300
Dimension 2
-1000
-500
0
500
Dimension 1
B
50
40
30
20
10
0
Log10 (fold change)
-4
-2
0
2
4
6
8
Log2 (fold change)
C
1.0
0.8
0.6
0.4
0.2
0
False discovery rate
-2
-1
0
1
2
Normalized enriched score

Figure 4

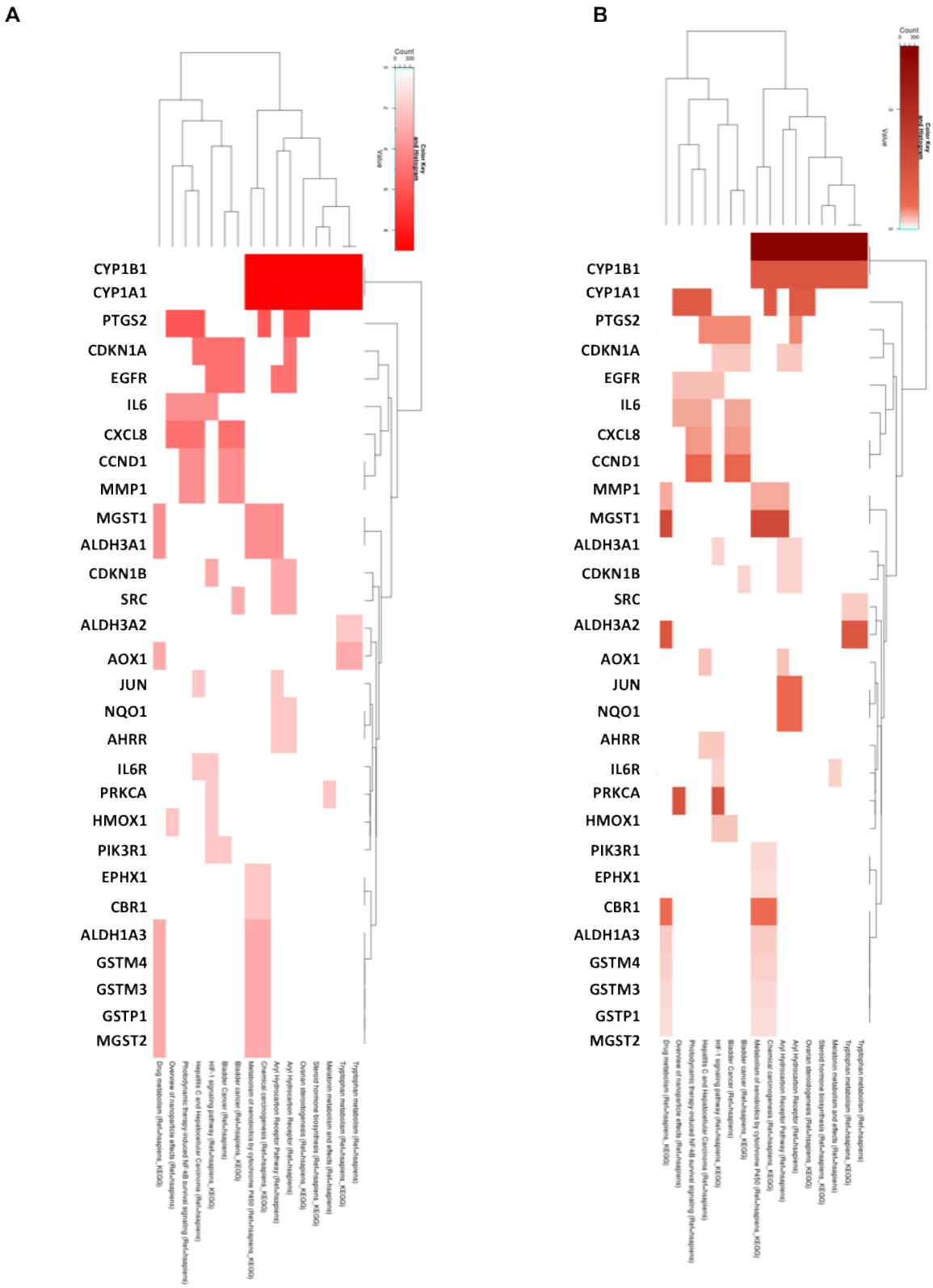
A
B
CYP1B1
CYP1A1
PTGS2
CDKN1A
EGFR
IL6
CXCL8
CCND1
MMP1
MGST1
ALDH3A1
CDKN1B
SRC
ALDH3A2
AOX1
JUN
NQO1
AHRR
IL6R
PRKCA
HMOX1
PIK3R1
EPHX1
CBR1
ALDH1A3
GSTM4
GSTM3
GSTP1
MGST2

Figure 5

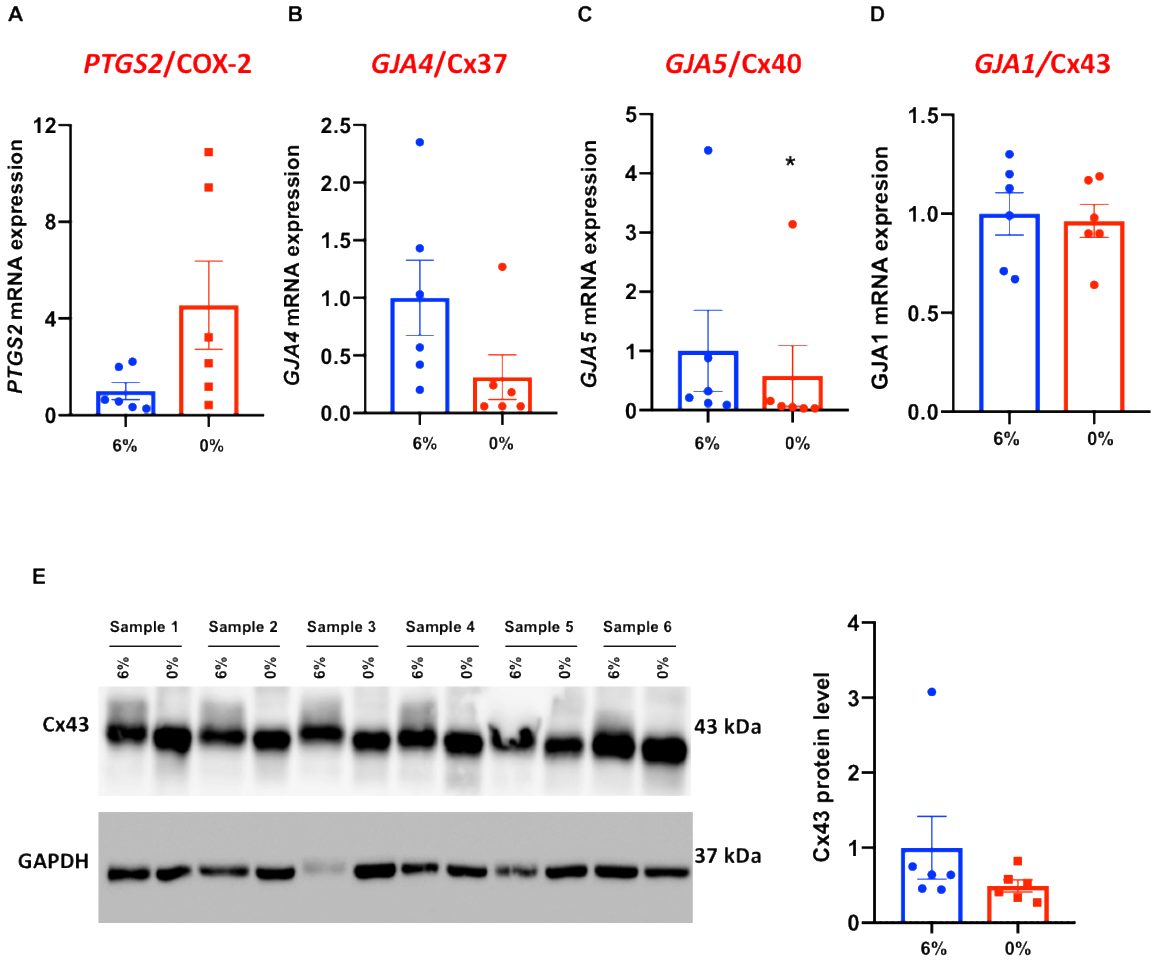
A
PTGS2/COX-2
PTGS2 mRNA expression
12
8
4
0
6%
0%
B
GJA4/Cx37
GJA4 mRNA expression
2.5
2.0
1.5
1.0
0.5
0.0
6%
0%
C
GJA5/Cx40
GJA5 mRNA expression
5
4
3
2
1
0
*
6%
0%
D
GJA1/Cx43
GJA1 mRNA expresion
1.5
1.0
0.5
0.0
6%
0%
E
Sample 1
Sample 2
Sample 3
Sample 4
Sample 5
Sample 6
6%
0%
Cx43
43 kDa
GAPDH
37 kDa
Cx43 protein level
4
3
2
1
0
6%
0%

Chapter 5: General discussion

1. Overview

The goal of my thesis was to get more insight into the mechanisms of IA disease. Firstly, we studied histopathological aspects of R-IA and UR-IA domes and we looked at how the typical characteristics would correlate with clinical risk factors (Chapter 2). To this end, we created a biobank of human IA domes obtained from the Geneva University Hospitals, and detailed patient history was documented. Specific immunostainings and colorations allowed us to identify markers of vulnerable IA. Indeed, we observed that the loss of SMCs and ECM were more pronounced in the wall of R-IAs. Increased macrophage content, pointing to ongoing inflammation, was also observed in R-IAs. In the third chapter, we investigated how aneurysmal LWSS would affect EC gene expression and how primary cilia impact on the EC response to flow. We used ECs from control WT mice or from a PKD mouse model (*Tg737*$^{orpk/orpk}$) to assess the effects of physiological flow or aneurysmal low flow. We observed changes in the specific gene expression pattern in response to LWSS that were enhanced in PKD ECs. We further showed that in absence of primary cilia, ZO-1 expression levels were reduced, leading to disorganization of cell-cell junctions and increased endothelial permeability. ECs in IA domes from PKD patients appeared to have lower ZO-1 levels compared to ECs in aneurysm domes of non-PKD patients, which further supports our findings in the *in vitro* model. Based on these results, we postulated that the mechano-sensory role of endothelial primary cilia is to limit variations induced by LWSS. In the fourth chapter, we looked at how CCS could affect EC behavior. We determined transcriptomic profiles of ECs under physiological or aneurysmal CCS. Differentially expressed genes were involved in signaling pathways related to oxidative stress, inflammation, ECM regulation and cell proliferation. These results clearly show that gene expression modulation by CCS can influence EC function, and absence of CCS may contribute to IA disease. The insights provided by these studies will be discussed in detail below.

2. Histology of human IA domes

IAs are mostly quiescent and asymptomatic until the rupture occurs. Rupture leads to subarachnoid hemorrhage that is associated with life-threatening complications [1]. The mechanisms leading to IA rupture are not yet fully elucidated. Studies using animal models have helped to understand the role of hemodynamic forces in the initiation and progression of the disease [2-4]. The combination of SWSS and positive WSSG is at the basis of IA initiation as it triggers EC dysfunction and subsequent vascular remodeling [2-4]. The early histological changes in IA disease comprise loss of IEL, media thinning, leukocyte infiltration and ECM degradation, which results in bulging of the vascular wall under blood pressure load [3-8]. Collagen, which is the major constituent of ECM, limits IA growth due to its poor distensibility properties. Collagen degradation by macrophages further enhances bulging of the IA and progressively leads to a degenerated IA wall with high risk to rupture [9]. The theory on the growth of IAs proposes the requirement of an active SMC population coupled with an active collagen synthesis [9]. When the balance tilts in favor of proteolytic injury, the remodeling will lead to rupture instead of growth [9, 10]. This theory is now relatively well accepted and is in agreement with our results as well as the findings of others [11, 12]. We observed in R-IAs a concomitant loss of SMCs and collagen as compared to UR-IAs. As expected, the macrophage content was higher in R-IA than in UR-IA. Findings from our histological study support the association between the grade of IA wall degeneration and the rupture status [11, 12]. R-IA domes were generally thinner with hypocellular walls. On the other hand, while UR-IA displayed generally hyperplastic thick walls, they included some weak points with same histological organisation as R-IAs. The hyperplastic remodeling has been described as an adaptive mechanism to the increase in wall tension in the growing aneurysm. This increase in wall thickness reduces intramural stress and maintains a stable state. However, thin walls have low resistance to wall tension and are more likely to rupture [9, 13]. Future work should focus

on determining the threshold of the media thickness under which IA rupture. In addition, it is also important to determine the extent of the medial thinning that triggers the rupture. The total collagen content in the vessel wall and a good balance of type I/type III collagen is important for the vascular homeostasis. In ageing or in diseases, the collagen ratio is disturbed, facilitating vascular failure [14]. It has been shown that type III collagen is required for type I collagen fibrillogenesis [15]. In addition, presence of type III collagen in the vessel wall increases the flexibility of the collagen fibrils [16]. Interestingly, we found that total collagen content, and the ratio type I/type III collagen was different depending on the thickness of UR-IA wall. However, no differences were found in R-IAs. These data suggest that even though the general wall characteristics of UR-IAs were stable, wall remodeling was progressively underway, increasing their likelihood to rupture, and collagen could be a good indicator of IA status.

Furthermore, we found some correlations between IA wall characteristics and clinical/radiological risk factors. Increased size of UR-IAs correlated with a higher content of CD68-positive cells and total collagen, more particularly with type III collagen. UR-IA domes with a rough appearance displayed a lower ratio type I/type III collagen in comparison to IAs with a smooth appearance due to an increase in type III collagen content. In addition, it appears that IA walls of smokers contained less SMCs in comparison to the walls of non-smokers, and was similar to the content of SMCs measured in R-IAs. We and others have shown [11, 17-19] that the inflammatory status in IAs correlates with poor disease outcomes. In addition, previous studies found that inhibiting monocytic MCP-1 or using immunomodulatory drugs reduced macrophage infiltration and IA progression [20, 21]. Based on these observations, we believe that macrophage presence in the IA wall is potentially a good marker for rupture risk stratification. Indeed, a non-invasive imaging of macrophages in lesions is achievable by the use of contrasting agents such as gadolinium or ferumoxytol [22]. Similarly, SMC content in IA media may also serve as a good marker of IA stability. To this end, it will first be required

to identify a specific marker of the "healthy" contractile SMCs, which promote ECM component formation, contrarily to dedifferentiated SMCs that show a more pro-inflammatory phenotype. The reduced SMC content in IA wall of smokers may be attributed to increased oxidative stress. Indeed, exposure of cerebral SMC to cigarette smoke upregulated the expression of NOX-1, and pro-inflammatory and ECM regulating genes [23]. Interestingly, we found that ECs exposed to aneurysmal CCS revealed an increased expression of genes involved in oxidative stress, inflammation et ECM remodeling. ROS produced by ECs can further amplify the expression of inflammatory genes and promote leukocyte recruitment in the IA wall. In addition, ROS diffusion can alter the contractile properties of SMCs and induce a switch towards a proliferative, synthetic phenotype. Moreover, we also found that aneurysmal CCS induces MMP expression, which may alter ECM content and further impair EC and SMC communication. Basically, these results demonstrate that lack of cyclic stretch stimuli can contribute to IA disease.

The management of UR-IA is still a clinical dilemma for physicians. The decision to treat or not an UR-IA is balanced between the risk of intervention on one hand and the risk of rupture, which is associated with severe brain damage and/or death on the other hand [24]. Scoring systems have been developed based on patient- and IA-specific characteristics to assist on UR-IA management. However, the scoring predictions do not always fit with clinical observations, probably due to the selection bias in the prospective studies underlying this scoring system. In addition to the robust risk factors currently used to predict IA rupture risk, additional markers representative of wall biology could be considered to achieve a more individualized risk assessment for rupture, but could also help on the choice of treatment strategy. Histological studies will not only help in the understanding of IA disease mechanism and progression but also bring to light potential biomarkers. As discussed above, our present study on IAs from the

AneuX biobank demonstrated that histological features can discriminate between a vulnerable IA wall with high risk of rupture and more stable IAs. One of the limitations of our study is the finite numbers of samples available. Therefore, investigations on larger populations will be required and examination of post-mortem human IA samples may help to overcome the limitation of small sample number. Future studies should examine 3D histological characteristics of IA domes, which would provide more extensive knowledge on IA wall organization and risk of rupture.

3. Aneurysmal low WSS and endothelial fate/behavior

As already well described in the literature, vascular cells have the ability to respond to different stimuli and trigger signaling that would influence vascular function [25-28]. IA wall organization results from the interplay between vascular cells and hemodynamic forces and there is a reciprocal influence between IA shape and resulting forces. Computational fluid dynamics (CFD) analyses have increased the knowledge on the contribution of WSS hemodynamic parameters on IA disease outcome [29-32]. However, conflicting data exist concerning which parameter associates with IA risk of rupture [30, 31, 33-35]. The absence of standardized protocols for computational analysis, and the high range of assumptions and simplifications may justify the discrepancy between studies. Studying hemodynamic forces in *in vivo* models is challenging as it is difficult to distinguish between the distinct flow parameters. To this end, the use of *in vitro* models is useful for understanding the processes stimulated by each distinct force. Laboratory devices that allow the application of well-defined hemodynamic stresses are of good help in decrypting molecular and cellular mechanisms associated with vascular wall dysfunction. In this way, using primary ECs, Dolan *et al.* were able to describe the effect of SWSS known to induce IAs [36]. In this study, SWSS induced a gene expression profile indicative of an anticoagulant, anti-inflammatory, proliferative, and

matrix remodeling phenotype in cultured bovine aortic ECs. Various *in vitro* studies have also investigated the effect of LWSS on ECs. These studies were mostly performed in an atherosclerosis disease context and involved higher levels of WSS (≈ 5 dynes/cm^2) [28, 37] compared to aneurysmal LWSS (≈ 2 dynes/cm^2). However, the mechanisms involved in the effects of aneurysmal LWSS have been poorly elucidated so far. We therefore used the Ibidi flow system to compare the effects of physiological and aneurysmal low WSS on ECs and to understand the implication of primary cilia in the response to LWSS. We used ECs from WT mice or from PKD mice lacking primary cilia.

The mechano-sensing through primary cilia is essential for the normal development and function of blood vessels [25, 38, 39]. Primary cilia mediate Ca^{2+} entry into the cell and regulate NO signaling. Previous studies have shown that in blood vessels, primary cilia distribution varies according to flow intensity. Primary cilia are abundant and longer in low and disturbed flow areas while in high flow areas they are either very short or absent [37, 40]. In our *in vitro* model, we observed no difference in primary cilia incidence between aneurysmal low flow and physiological flow indicating that our EC culture model was suitable to decipher the role of primary cilia in response to flow. Next, we performed an RNA-seq and subsequent gene expression analysis revealing that 296 genes were differentially expressed between aneurysmal and physiological WSS conditions in PKD ECs against 52 in WT ECs. In general, LWSS-induced differentially expressed genes generated an enrichment gene ontology terms that are known to be linked with EC function including cell cycle proliferation, EndoMT transition, response to stress, SMC regulation, and blood pressure regulation. However, we observed a different distribution of the differentially expressed genes functional classes, between PKD and WT ECs. For instance, 10%, 3.3%, 6.7% and 3.3% of genes in wild-type cells were involved in cell junctions, ECM, cytoskeletal regulation and immunity defense, respectively, as compared to 0.6%, 6.5%, 1.8% and 1.2% in *Tg737$^{orpk/orpk}$* cells. These results emphasize the

implication of cellular integrity, inflammation and matrix remodeling in IA remodeling involving LWSS.

Loss of endothelial integrity is commonly reported in vascular disease including IAs [8, 41]. We compared the barrier property of PKD and non-PKD EC monolayers using two permeability assays, and we found that PKD ECs had lower TEER and higher permeability to 4 kDa FITC-dextran. This goes along with the findings that junction protein expression and organization are perturbed in PKD ECs. The expression level of the junction proteins ZO-1, ZO-2, Catenin α-1, Catenin β-1, Claudin-3 was lower in PKD ECs, while Cx43 was upregulated. We hypothesize that there is a competition for the ZO-1 PDZ domain, since all the changed proteins are known to interact with ZO-1. Moreover, ZO-1 downregulation perturbed the organization of other junction proteins similarly to what was observed in PKD ECs. Since ZO-1 can also regulate gene expression the exact mechanism by which ZO-1 knockdown disturbed other junctional proteins remain to be uncovered. To this end, the investigation of ZO-2, Catenin α-1, Catenin β-1, Claudin-3 and Cx43 gene and protein expression levels will provide some clues on the mechanism by which ZO-1 regulates the junctional organization.

In the light of our findings, we concluded that endothelial primary cilia dampen the pathological response to aneurysmal LWSS by controlling gene expression. Accordingly, it has been shown that primary cilia percentage increases at predilected locations of atherosclerotic lesions in mice [40], and that primary cilia deficiency in apolipoprotein-E-deficient mice promotes atherogenesis [42]. Nevertheless, more experiments are required to rule out cilia-independent effects. Indeed, IFT88, the protein mutated in our PKD model, is not only involved in ciliogenesis but also in cell-cycle progression during G1-S transition [43], mitotic spindle alignment [44] as well as endocytosis recycling machinery [45, 46]. We have tried to exclude such non-canonical IFT88 effects as much as possible from our experiments by performing the WSS experiments in low serum conditions. Investigations using other PKD EC models will

provide more insight in the specific role of primary cilia in endothelium. Alternatively, studies could be performed using an opposite approach, *i.e.* by promoting ciliogenesis using pharmacological drugs such as aphidicolin [47].

Considerable work has been done in the past with respect to the role of Cxs in endothelial function, arterial remodelling, and atherosclerotic disease [28, 48, 49]. The regulation of vascular Cxs by mechanical forces is well established [48, 50, 51]. Yet, the contribution of Cxs in IA is not known. We observed in this study that absence of primary cilia resulted in Cx43 relocation from the membrane towards a more intracellular location. Since the distribution of primary cilia on the endothelium is not homogeneous, indirect intercellular communication through paracrine signalling or direct communication through gap junctions should be of great importance for a uniform EC response to LWSS. Additional investigations may help to uncover the role of Cxs in IA disease. Moreover, future research may look at primary cilia expression in the IA domes and compare cilia incidence in R-IAs and UR-IAs. IAs normally initiate at sites experiencing HWSS, thus where primary cilia expression is supposed to be low. From our data, one may hypothesize that IAs with more endothelial primary cilia may be more stable than IAs devoid of primary cilia. To support this hypothesis, we observed that IA domes from PKD patients exhibit more degenerated walls (thinner with less collagen) compared to IA walls of non-PKD patients.

4. Aneurysmal CCS and endothelial behavior: potential role in IAs

The pulsatile nature of blood flow exposes arteries to CCS. A physiological level of CCS is an important stimulus for the maintenance of vascular integrity [52-54]. The level of IA volume fluctuation related to cardiac cycle is not well defined. Previous studies based on 2-dimensional images from magnetic resonance angiography reported respectively 51% and 17.6% increase in volume during 1 cardiac cycle in R-IAs and UR-IAs [55]. Another study using 4-dimensional

CT angiography compared IA stretch percentage (5.40%±4.07%) during one cardiac cycle to normal vessel (4.20%±2.51%,) and found no difference, suggesting that IA wall integrity was similar to that of normal arteries [56]. However, these data contrast with clinical observations of neurosurgeons who often cannot visually detect pulsatility/wall deflection of an IA during an intervention. In addition, IA wall characterization by us [57] and others [11] revealed more degenerated walls. In addition, recent studies reported that calcification was highly prevalent in IAs [58]. These vascular wall changes would likely increase the stiffness of IA walls and results in a lower or even a lack of CCS. Nevertheless, future investigations are necessary to get more relevant values on the magnitude of cyclic stretch experienced by IA walls, which is likely influenced by IA location, shape and wall composition. Such information will be valuable for CFD analysis and will help to correlate IA wall phenotype in regards to CCS.

In the fourth chapter of my thesis, I investigated how CCS could affect EC behavior. The original project involved comparison between ECs with and without primary cilia. It turned out however impossible to culture these WT and PKD ECs on the flexible membrane, even with different coatings. As HUVECs readily adhered to the flexible membranes and grew nicely into monolayers, we decided to change the project to these primary cells. Thus, HUVECs were submitted to physiological (6%) or aneurysmal (0%) CCS and we performed transcriptomic analyses by RNA-seq. Multidimensional scale representation displaying transcriptome diversity between samples confirmed that ECs are sensitive to CCS. In addition, we noticed that stretching "homogenized" the HUVECs transcriptomic response as stretched ECs clustered on the MDS plot while non-stretched ECs were more spread out, indicating a more diverse response. We hypothesize that physiological CCS prevents large deviation in ECs, hence preventing disease.

Differentially expressed gene analyses (fold change≥2; $p<0.05$) revealed that 51 genes were upregulated and 49 genes were downregulated. The GSEA analysis indicated that under

aneurysmal CCS upregulated pathways were involved in oxidative stress, angiogenic and inflammatory pathways and downregulated pathways involved in proliferation and ECM-receptor interaction. In addition, we provide a full data set of genes sensitive to CCS, which will improve our understanding of the effect of cyclic stretch on EC function and IA disease. For instance, we confirmed that in absence of CCS the phosphorylation of eNOS on Serine 1177 was decreased, indicating that the activity of eNOS and subsequent availability of NO was reduced. These data suggest that under aneurysmal conditions ECs have reduced capacity to regulate vascular tone and blood pressure. Additionally, the inflammatory mediator COX-2 was identified as a leading-edge upregulated gene in ECs under aneurysmal CCS. Therefore, we can assume that in IA disease, absence of CCS participates in endothelial injury by promoting an inflammatory loop through COX-2 upregulation. Moreover, we have described that CCS is a regulator of Cxs. Indeed, Cx37 and Cx40 gene expression was reduced in ECs under aneurysmal CCS. Previous studies have shown increased Cx43 expression in response to cyclic stretch [51]. However, this study was performed using another device (tubes in which flow was simultaneously applied), other EC type and shorter periods of cyclic stretch. Although we did not find a difference in Cx43 gene expression, physiological CCS was associated to a shift in electrophoretic mobility of Cx43 on Western blots, indicative for a change in phosphorylation state of the protein. Altogether, the obtained results demonstrate that CCS not only controls gene expression in ECs, but also regulates the post-translational modifications of essential proteins and in this manner could participate in vascular homeostasis and disease. Aneurysmal CCS regulated pathways correlate with features of IA wall remodeling such as inflammation, oxidative stress and ECM remodeling.

5. WSS and CCS *in vitro* exploration

In vivo, WSS and CCS are 2 hemodynamic forces that cannot be dissociated. We showed that each force controls the expression of genes that are important for EC function and endothelial-mediated regulation of vascular functions. WSS and CCS may have opposite, cumulative or exclusive regulation for the expression and function of certain genes. It is therefore important to verify the findings from *in vitro* studies in more realistic models such as *ex vivo* perfusion models or *in vivo* animal models. In addition, other factors such as ECM and SMCs can shape the response of ECs to hemodynamic factors.

Nevertheless, one force may out-weight the other one in certain pathological conditions. For instance, in aging arteries, physiological flow would result in physiological HWSS and low CCS. In contrast, in genetic diseases like Ehlers–Danlos syndrome where collagen is mutated and arteries are highly distensible, physiological flow would likely result in physiological HWSS and elevated CCS. These different cases show the importance of studying these forces distinctly and knowing the consequences that each force could have on the vascular cells and therefore on the vascular function in general.

6. Conclusion

IA rupture is a leading cause of hemorrhagic stroke. Due to modern imaging modalities, the prevalence of UR-IAs is increasing and urge on the understanding of IA pathogenesis for a better clinical management. Vascular wall degenerative remodeling is prerequisite for IA growth and rupture of IAs. The implication of hemodynamic forces in IA initiation and growth has been related in several studies. However, there are missing data on the correlation between flow conditions and vascular wall histological features. We demonstrated in this thesis that physiological levels of WSS and CCS are critical for EC homeostasis. In addition, we show that primary cilia on ECs are essential for a suitable response to disturbed flow and to prevent large deviations in EC function. Moreover, aneurysmal flow conditions can promote vascular wall

remodeling through EC dysfunction, which involves processes such as oxidative stress, ECM degradation and inflammation. Transcriptomic analyses have led to the identification of several WSS and CCS responsive genes that can potentially mediate IA vascular wall remodeling towards rupture. Future investigations on the significance of differentially expressed genes may lead to the development of modulators to promote vascular stability and prevent IA growth and rupture. Furthermore, the results of these studies may help in the future to identify targets/markers for molecular imaging discriminating between stable and vulnerable IAs.

References

1. Brisman, J.L., J.K. Song, and D.W. Newell, *Cerebral aneurysms.* N Engl J Med, 2006. **355**(9): p. 928-39.
2. Alfano, J.M., et al., *Intracranial aneurysms occur more frequently at bifurcation sites that typically experience higher hemodynamic stresses.* Neurosurgery, 2013. **73**(3): p. 497-505.
3. Meng, H., et al., *Complex hemodynamics at the apex of an arterial bifurcation induces vascular remodeling resembling cerebral aneurysm initiation.* Stroke, 2007. **38**(6): p. 1924-31.
4. Metaxa, E., et al., *Characterization of critical hemodynamics contributing to aneurysmal remodeling at the basilar terminus in a rabbit model.* Stroke, 2010. **41**(8): p. 1774-82.
5. Aoki, T., et al., *Macrophage-derived matrix metalloproteinase-2 and -9 promote the progression of cerebral aneurysms in rats.* Stroke, 2007. **38**(1): p. 162-9.
6. Coutard, M., *Experimental cerebral aneurysms in the female heterozygous Blotchy mouse.* Int J Exp Pathol, 1999. **80**(6): p. 357-67.
7. Liu, M., et al., *Primary Cilia Deficiency Induces Intracranial Aneurysm.* Shock, 2018. **49**(5): p. 604-611.
8. Wang, S., et al., *Rabbit aneurysm models mimic histologic wall types identified in human intracranial aneurysms.* J Neurointerv Surg, 2018. **10**(4): p. 411-415.
9. Frosen, J., et al., *Flow-induced, inflammation-mediated arterial wall remodeling in the formation and progression of intracranial aneurysms.* Neurosurg Focus, 2019. **47**(1): p. E21.
10. Frosen, J. and A. Joutel, *Smooth muscle cells of intracranial vessels: from development to disease.* Cardiovasc Res, 2018. **114**(4): p. 501-512.
11. Frosen, J., et al., *Remodeling of saccular cerebral artery aneurysm wall is associated with rupture: histological analysis of 24 unruptured and 42 ruptured cases.* Stroke, 2004. **35**(10): p. 2287-93.
12. Marbacher, S., et al., *Loss of mural cells leads to wall degeneration, aneurysm growth, and eventual rupture in a rat aneurysm model.* Stroke, 2014. **45**(1): p. 248-54.
13. Robertson, A.M., et al., *Diversity in the Strength and Structure of Unruptured Cerebral Aneurysms.* Ann Biomed Eng, 2015. **43**(7): p. 1502-15.
14. Berillis, P., *The Role of Collagen in the Aorta's Structure.* The Open Circulation & Vascular Journal, 2013. **6**.
15. Liu, X., et al., *Type III collagen is crucial for collagen I fibrillogenesis and for normal cardiovascular development.* Proc Natl Acad Sci U S A, 1997. **94**(5): p. 1852-6.
16. Silver, F.H., I. Horvath, and D.J. Foran, *Viscoelasticity of the vessel wall: the role of collagen and elastic fibers.* Crit Rev Biomed Eng, 2001. **29**(3): p. 279-301.
17. Kataoka, K., et al., *Structural fragility and inflammatory response of ruptured cerebral aneurysms. A comparative study between ruptured and unruptured cerebral aneurysms.* Stroke, 1999. **30**(7): p. 1396-401.
18. Tulamo, R., et al., *Complement activation associates with saccular cerebral artery aneurysm wall degeneration and rupture.* Neurosurgery, 2006. **59**(5): p. 1069-76; discussion 1076-7.
19. Ollikainen, E., et al., *Mast cells, neovascularization, and microhemorrhages are associated with saccular intracranial artery aneurysm wall remodeling.* J Neuropathol Exp Neurol, 2014. **73**(9): p. 855-64.
20. Aoki, T., et al., *Impact of monocyte chemoattractant protein-1 deficiency on cerebral aneurysm formation.* Stroke, 2009. **40**(3): p. 942-51.
21. Shimada, K., et al., *Protective Role of Peroxisome Proliferator-Activated Receptor-gamma in the Development of Intracranial Aneurysm Rupture.* Stroke, 2015. **46**(6): p. 1664-72.
22. Shimizu, K., M. Kushamae, and T. Aoki, *Macrophage Imaging of Intracranial Aneurysms.* Neurol Med Chir (Tokyo), 2019. **59**(7): p. 257-263.
23. Starke, R.M., et al., *Cigarette Smoke Initiates Oxidative Stress-Induced Cellular Phenotypic Modulation Leading to Cerebral Aneurysm Pathogenesis.* Arterioscler Thromb Vasc Biol, 2018. **38**(3): p. 610-621.

24. Marbacher, S., et al., *Interdisciplinary decision-making and treatment of intracranial aneurysms in the era of complementary microsurgical and endovascular techniques.* Swiss Med Wkly, 2016. **146**: p. w14372.
25. Diagbouga, M.R., et al., *Role of hemodynamics in initiation/growth of intracranial aneurysms.* Eur J Clin Invest, 2018. **48**(9): p. e12992.
26. Davies, P.F., *Hemodynamic shear stress and the endothelium in cardiovascular pathophysiology.* Nat Clin Pract Cardiovasc Med, 2009. **6**(1): p. 16-26.
27. Givens, C. and E. Tzima, *Endothelial Mechanosignaling: Does One Sensor Fit All?* Antioxid Redox Signal, 2016. **25**(7): p. 373-88.
28. Kwak, B.R., et al., *Biomechanical factors in atherosclerosis: mechanisms and clinical implications.* Eur Heart J, 2014. **35**(43): p. 3013-20, 3020a-3020d.
29. Murayama, Y., et al., *Computational fluid dynamics as a risk assessment tool for aneurysm rupture.* Neurosurg Focus, 2019. **47**(1): p. E12.
30. Cebral, J.R., et al., *Quantitative characterization of the hemodynamic environment in ruptured and unruptured brain aneurysms.* AJNR Am J Neuroradiol, 2011. **32**(1): p. 145-51.
31. Cebral, J.R., et al., *Hemodynamics in Normal Cerebral Arteries: Qualitative Comparison of 4D Phase-Contrast Magnetic Resonance and Image-Based Computational Fluid Dynamics.* J Eng Math, 2009. **64**(4): p. 367-378.
32. Cebral, J.R., M. Sheridan, and C.M. Putman, *Hemodynamics and bleb formation in intracranial aneurysms.* AJNR Am J Neuroradiol, 2010. **31**(2): p. 304-10.
33. Cebral, J., et al., *Flow Conditions in the Intracranial Aneurysm Lumen Are Associated with Inflammation and Degenerative Changes of the Aneurysm Wall.* AJNR Am J Neuroradiol, 2017. **38**(1): p. 119-126.
34. Meng, H., et al., *High WSS or low WSS? Complex interactions of hemodynamics with intracranial aneurysm initiation, growth, and rupture: toward a unifying hypothesis.* AJNR Am J Neuroradiol, 2014. **35**(7): p. 1254-62.
35. Xiang, J., et al., *Hemodynamic-morphologic discriminants for intracranial aneurysm rupture.* Stroke, 2011. **42**(1): p. 144-52.
36. Dolan, J.M., et al., *Endothelial cells express a unique transcriptional profile under very high wall shear stress known to induce expansive arterial remodeling.* Am J Physiol Cell Physiol, 2012. **302**(8): p. C1109-18.
37. Pala, R., et al., *The Roles of Primary Cilia in Cardiovascular Diseases.* Cells, 2018. **7**(12).
38. Nauli, S.M., et al., *Endothelial cilia are fluid shear sensors that regulate calcium signaling and nitric oxide production through polycystin-1.* Circulation, 2008. **117**(9): p. 1161-71.
39. Van der Heiden, K., et al., *Role for primary cilia as flow detectors in the cardiovascular system.* Int Rev Cell Mol Biol, 2011. **290**: p. 87-119.
40. Van der Heiden, K., et al., *Endothelial primary cilia in areas of disturbed flow are at the base of atherosclerosis.* Atherosclerosis, 2008. **196**(2): p. 542-50.
41. Aoki, T., et al., *NF-kappaB is a key mediator of cerebral aneurysm formation.* Circulation, 2007. **116**(24): p. 2830-40.
42. Dinsmore, C. and J.F. Reiter, *Endothelial primary cilia inhibit atherosclerosis.* EMBO Rep, 2016. **17**(2): p. 156-66.
43. Robert, A., et al., *The intraflagellar transport component IFT88/polaris is a centrosomal protein regulating G1-S transition in non-ciliated cells.* J Cell Sci, 2007. **120**(Pt 4): p. 628-37.
44. Delaval, B., et al., *The cilia protein IFT88 is required for spindle orientation in mitosis.* Nat Cell Biol, 2011. **13**(4): p. 461-8.
45. Finetti, F., et al., *Intraflagellar transport is required for polarized recycling of the TCR/CD3 complex to the immune synapse.* Nat Cell Biol, 2009. **11**(11): p. 1332-9.
46. Schermer, B. and T. Benzing, *Endothelial cilia protect against atherosclerosis.* EMBO Rep, 2016. **17**(2): p. 125-6.
47. May-Simera, H.L., et al., *Primary Cilium-Mediated Retinal Pigment Epithelium Maturation Is Disrupted in Ciliopathy Patient Cells.* Cell Rep, 2018. **22**(1): p. 189-205.

48. Leybaert, L., et al., *Connexins in Cardiovascular and Neurovascular Health and Disease: Pharmacological Implications.* Pharmacol Rev, 2017. **69**(4): p. 396-478.
49. Molica, F., et al., *Connexins and Pannexins in Vascular Function and Disease.* Int J Mol Sci, 2018. **19**(6).
50. Meens, M.J., et al., *Regulation of cardiovascular connexins by mechanical forces and junctions.* Cardiovasc Res, 2013. **99**(2): p. 304-14.
51. Kwak, B.R., et al., *Shear stress and cyclic circumferential stretch, but not pressure, alter connexin43 expression in endothelial cells.* Cell Commun Adhes, 2005. **12**(5-6): p. 261-70.
52. Lu, D. and G.S. Kassab, *Role of shear stress and stretch in vascular mechanobiology.* J R Soc Interface, 2011. **8**(63): p. 1379-85.
53. Lacolley, P., *Mechanical influence of cyclic stretch on vascular endothelial cells.* Cardiovasc Res, 2004. **63**(4): p. 577-9.
54. Jufri, N.F., et al., *Mechanical stretch: physiological and pathological implications for human vascular endothelial cells.* Vasc Cell, 2015. **7**: p. 8.
55. Meyer, F.B., J. Huston, 3rd, and S.S. Riederer, *Pulsatile increases in aneurysm size determined by cine phase-contrast MR angiography.* J Neurosurg, 1993. **78**(6): p. 879-83.
56. Kuroda, J., et al., *Cardiac cycle-related volume change in unruptured cerebral aneurysms: a detailed volume quantification study using 4-dimensional CT angiography.* Stroke, 2012. **43**(1): p. 61-6.
57. Morel, S., et al., *Correlating Clinical Risk Factors and Histological Features in Ruptured and Unruptured Human Intracranial Aneurysms: The Swiss AneuX Study.* J Neuropathol Exp Neurol, 2018. **77**(7): p. 555-566.
58. Gade, P.S., et al., *Calcification in Human Intracranial Aneurysms Is Highly Prevalent and Displays Both Atherosclerotic and Nonatherosclerotic Types.* Arterioscler Thromb Vasc Biol, 2019. **39**(10): p. 2157-2167.

Mannekomba Roxane DIAGBOUGA

PhD student in Biomedical Sciences
Life Science PhD school, University of Geneva, Switzerland

mannekombaroxane.diagbouga@unige.ch
diagbouga.mannekomba@gmail.com

EDUCATION

04.2015– 12.2019: **Doctoral thesis**
- The Role of hemodynamics in the initiation, growth and rupture of intracranial aneurysms
- Under supervision of Prof. Brenda Kwak - Department of Pathology and Immunology - University of Geneva, Switzerland

09.2012 – 06.2014: **Master studies**
- Genetic and Cell Biology, Specialty Fundamental Infectiology - Claude Bernard Lyon 1 University, France
- With honors

09.2010 – 06.2012: **Bachelor studies**
- Graduated in Biology - Claude Bernard Lyon 1 University, France

09.2008 – 06.2010: **Medical studies** at Claude Bernard Lyon 1 University, France

SCIENTIFIC INTERNSHIPS

10.2013 – 06.2014: Characterization of the molecular interactions between translation initiation factors and genomic RNA of HIV-1
Ecole Normale Supérieure, Lyon, INSERM U1111, France

07.2013: The different types of biological materials, analysis and storage in biobanks
International Agency for Research on Cancer, Lyon, France

01.2013 - 03.2013 Hepatitis B Virus variability among African population
Centre de Recherche en Cancérologie de Lyon, INSERM U1052, France

SKILLS

Cell culture: Primary endothelial and smooth muscle cells, endothelial cell lines, application of wall shear stress (Ibidi), application of circumferential stretch (FlexCell)

Biochemistry: SDS-Page electrophoresis, western blot, protein extraction, immuno(histo/cyto)chemistry

Molecular biology: DNA and RNA extraction and quantifiquation, quantitative PCR, conventional PCR, cloning techniques, lentivirus transduction (CRISPR cas9 editing gene)

Histology: Sample cryo-sectioning, paraffin embedding and sectioning

Software: Microsoft office, Graphpad, Image J, Endnote, Zen (Zeiss nicroscopy), Metacore

Microscopy: Conventional (fluorescence) microscopy, confocal microscopy, Mirax scanner, staining quantification

Bioinformatic: RNA sequencing data analysis (differentially expressed gene analysis, pathway analysis)

Languages: French (native), English (B2), Dioula, Dagara

TEACHING EXPERIENCE

2016 , 2018: Swiss Youth in Science
1 week/year

2017 – 2019: Practicals in Physiology. Topic: electrocardiogram; University of Geneva, 2nd year medical students
Approx. 10h/year

2018 – 2019: Practicals in Histology. Topic: Cardiovascular system; University of Geneva, 2nd year medical students
Approx. 4h/year

AWARDS

05.2017: **3rd prize** in oral communication at My thesis in 180 Seconds, final of University of Geneva

04.2017: **1st prize** in oral communication at the International Symposium on Biomechanics in Vascular Biology and Cardiovascular Disease, Rotterdam, The Netherlands

SCIENTIFIC PUBLICATIONS

2019:

Diagbouga MR, Morel S, Lemeille S, Hierck B, Bijlenga P, Kwak BR. Primary cilia control endothelial permeability by regulating expression and location of junction proteins. ***In preparation***

Baeriswyl D, Prionisti I, Tsolkas G, Chooi KY, Peach T, Vardakis J, Morel S, **Diagbouga MR**, Bijlenga P, Cuhlmann S, Evans PC, Kwak BR, Ventikos Y, Krams R. Disturbed flow induces a sustained, stochastic NF-κB activation which may support intracranial aneurysm growth in vivo. ***Scientific Reports*** **2019; 18;9(1):4738**

Denis JF, **Diagbouga MR**, Molica F, Hautefort A, Linnerz T, Vermot J, Watanabe M, Lemeille S, Bertrand JY, Kwak BR. Induced connexin40 expression contributes to arterial endothelial quiescence - ***Frontiers in Physiology*** **2019; 12;10:80**

2018:

Diagbouga MR, Morel S, Bijlenga P, Kwak BR - Role of hemodynamics in initiation / growth of intracranial aneurysms ***European Journal of Clinical Investigation*** **2018; 48:e12992** (review)

Morel S**, Diagbouga MR**, Dupuy N, Sutter E, Braunersreuther V, Pelli G, Corniola M, Gondar R, Jägersberg M, Isidor N, Schaller K, Bochaton Piallat ML, Bijlenga P, Kwak BR - Correlating Clinical Risk Factors and Histological Features in Ruptured and Unruptured Human Intracranial Aneurysms: The Swiss AneuX Study. ***Journal of Neuropathology & Experimental Neurology*** **2018;77:555-566**

CONFERENCES AND WORKSHOPS

2019:

Poster presentation: Primary cilia affects the endothelial response to aneurysmal wall shear stress
International Symposium on Biomechanics in Vascular Biology and Cardiovascular Disease, London, UK

2018:

Oral presentation: Review on intracranial aneurysm animal model
Towards standardization of studies onto human and animal intracranial aneurysm wall vulnerability, Geneva, Switzerland
Poster presentation: Primary cilia affects the endothelial response to aneurysmal wall shear stress
Geneva Medical School PhD retreat, Leysin, Switzerland
Poster presentation: Primary cilia affects the endothelial response to aneurysmal wall shear stress
LS2 - Swiss Physiology Annual Meeting, Fribourg, Switzerland
Poster presentation: Primary cilia affects the endothelial response to aneurysmal wall shear stress
International Vascular Biology Meeting, Helsinki, Finland

2017:

Oral presentation: Does polycystic kidney disease affect the endothelial response to aneurysmal wall shear stress
International Symposium on Biomechanics in Vascular Biology and Cardiovascular Disease, Rotterdam, The Netherlands
Poster presentation: the effect of biomechanical forces on structure and composition of the aneurysm wall
Geneva Medical School PhD retreat, Champéry, Switzerland
Poster presentation: Does primary cilium influence the endothelial response to aneurysmal wall shear stress
LS2 - Swiss Physiology Annual Meeting, Bern
Workshop: Social and Professional Interaction in English: face-to-face communication at conferences and events, Lausanne, Switzerland
Workshop: Posture, respiration, voix: vos atouts pour conquérir votre auditoire, Lausanne, Switzerland
Workshop: Une image pour 180 secondes: les clés de la communication visuelle pour scientifiques, Lausanne, Switzerland

2016:

Poster presentation: The role of biomechanical forces on intracranial aneurym growth and rupture
Printemps de la Cardiologie, Dijon, France

2015:

Poster presentation: Modelling shape as biomarker for instability of intracranial aneurysm
Geneva Medical School PhD retreat, Leysin, Switzerland

REFEREES

Prof. Brenda R Kwak, PhD; Dept. of Pathology and Immunology, Faculty of Medicine, University of Geneva
✉ Rue Michel-Servet 1, CH-1211 Geneva 4, Switzerland; ☎ +41 22 379 57 37; 💻 brenda.kwakchanson@unige.ch

Prof. Philippe Bijlenga, MD-PhD; Dept. of clinical neurosciences , Faculty of Medicine, University of Geneva
✉ Rue Gabrielle-Perret-Gentil 4, CH - 1211 Genève 14, Switzerland; ☎ +41 22 372 34 26; 💻 philippe.bijlenga@hcuge.ch

Dr Sandrine Morel, PhD: Dept. of Pathology and Immunology, Faculty of Medicine, University of Geneva
✉ Rue Michel-Servet 1, CH-1211 Geneva 4, Switzerland; ☎ +41 22 379 46 95 ; 💻 sandrine.morel@unige.ch